Quantum-Enhanced Two Photon Interactions

PhD Thesis

Thomas Dickinson

Department of Physics

University of Strathclyde, Glasgow

May 7, 2025

This thesis is the result of the author's original research. It has been composed by the author and has not been previously submitted for examination which has led to the award of a degree.

Abstract

Parametric down conversion (PDC) is a nonlinear optical process that is extensively used to produce photon pairs; when it does this, it is conventionally called the low gain of PDC. The same state is also used to produce squeezed sources, light which can have uncertainties below the standard quantum limit, but at the cost of increased uncertainties in other properties. Two photon interactions are the term I will use to refer to a class of processes in which two photons must be present at a given position in a short time frame. Principle and particularly, I investigate sum frequency generation (SFG), a nonlinear process in which two pump photons are destroyed, and a final photon is produced at the sum of the pump photons' energies. In this work, I look to observe sum frequency generation pumped with the down converted state as we transition from the low gain into the high gain of parametric down conversion. In doing so, I develop both theoretical models and experimental procedures to understand and quantify entangled two photon interactions. Specifically, I study the effects of gain on the down converted state and present an intuitive explanation with a new interpretation of previous theoretical work to help quantify the effects. I examine the effect of losses in the down converted state on entangled sum frequency generation (eSFG) and originate a model explaining these results. I finish by conducting a comparative study between eSFG and classical SFG as we transition from the low gain to the high gain of PDC. We show that there can be an enhancement to sum frequency generation by pumping with the down converted light above the low gain of parametric down conversion.

Contents

List of Figures

List of Tables

Preface/Acknowledgements

I would like to express my sincerest thanks to my supervisor, Dr. Lucia Caspani, for accepting me as a PhD student. I assuredly would have missed a substantial part of my life without her belief, patience, kindness, and guidance. Her enthusiasm and pragmatic approach to answering my questions and reviewing my work have encouraged me throughout these years.

The experimental work contained in this thesis was conducted at the University of Glasgow in the lab of Professor Daniele Faccio and Dr Matteo Clerici under the supervision of Matteo Clerici, for whom I have particular thanks for his steadfast support and instruction. Special recognition must be paid to Ivi Afxenti for countless illuminating discussions and support through moments of frustration and doubt.

Finally, I express my great thanks to my family for their support.

Chapter 0. Preface/Acknowledgements

Chapter 1

Introduction

The work presented herein aims to gain an understanding of the effects the entangled state (in this case, parametric down conversion) has on entangled two photon interactions. One of the principal and most distinctive class of states in quantum mechanics are the entangled states. It is this which made Einstein despise his creation [1] and rail against 'Spooky action at a distance'. Particles are said to be entangled when we cannot independently express their states; observables from the individual particles do not commute. These states can be created directly when the particles are produced or through their interactions after the fact. In this work, I attempt to exploit this phenomenon and realise 'spooky action at no distance'. Specifically, I aim to exploit the energy-time, space-momentum entanglement present in the state produced in parametric down conversion (a process where a pair of photons are emitted in a very small time frame and close together) to improve the efficiency of nonlinear processes which require multiple photons to interact.

The idea of using entangled photons to improve the efficiency of two photon processes was first suggested by Javanainen and Gould (1990) [2] pertaining to two photon absorption. Two photon absorption (TPA) is an interaction in which a molecular or atomic transition may be stimulated by a pair of photons whose combined energy equals the transition energy. When pumped with a classical state, this is a random, probabilistic process. Therefore, the rate of transition will have a second order dependence on incoming photon flux as the rate of transition is proportional to the probability that

two photons will arrive at the same position in space-time. When we have a random state, this probability will simply be the product of the individual probabilities which, assuming an even distributions of photons, will be proportional to the photon flux.

When pumped with a state produced by parametric down conversion (PDC), however, the rate of transition will reduce to a linear dependence as, at low fluxes, photons are produced in pairs of two. Therefore, with careful control of the down converted state and perfect transmission of the field, the probability of two photons arriving at the up conversion medium is the same as the probability of one. Because of this, exciting two photon processes will be more efficient at low photon fluxes with a PDC source than a classical one with the same average photon number. Independently from Javanainen and Gould, Gea-Banacloche (1989) reached the same conclusion when considering TPA pumped by an optical-parametric oscillator operating below threshold [3].

Two photon absorption was first described by Maria Goppert-Mayer in the late 1920s/ early 1930s and published in 1931 [4] and later realised with the development of maser and laser technologies by Kaiser and Garrett [5]. It has been found to be useful in both spectroscopy [6] and imaging of biological samples. The purpose of its use in spectroscopy is to probe electronic excited states that are forbidden in single photon absorption. It was first thought to have an application to imaging with C.J.R Sheppard and R. Kompfner in their 1978 paper [7] where they proposed a raster scanning microscope. The idea is essentially to pump a sample prepared with a fluorophore with a coherent field and focus the beam down to the diffraction limit onto a sample which can undergo a two photon process such as two photon absorption. The sample would absorb and emit light very close to the focus in proportion to the relative amount of absorption material present. Then, by moving the focus point, one can build up an image of the sample; each position of the focus is a pixel of the overall image. Because of the high intensities required to stimulate a two photon absorption event, light is only absorbed and emitted very close to the focal spot of the pump field and, therefore, in a very small volume, far smaller than with single photon absorption.

There are several advantages that TPA has over single photon absorption when imaging. First, it reduces the total amount of radiation that the sample absorbs because

light only interacts with the sample at or very close to its focus. Moreover, the tight locality set from the low two photon cross section allows for probing below the surface of the sample [8] as photons will only be absorbed close to the focal spot of the pump field. A TPA microscope was first experimentally demonstrated by Denk, Strickler and Webb in 1990 [9], and since then, it has become a workhorse for the medical field. As of late, deep tissue imaging [10] has caught much interest; however, in order to delve further into the sample, higher order absorption may need to be exploited [11] as the longer wavelengths of the pump increase the scattering length inside of the materials.

Despite their ubiquity, two photon fluorescent microscopes have issues. The deterioration of flurophores and reduction of their responsivity is a well documented phenomenon [12–15]. This is known as photo bleaching and has been explicitly studied by Patterson and Piston [16], who show that the rate of unresponsiveness of the fluorophores is dependent on the intensity of light used. In no case did they find a purely second order dependence between the rate of photo bleaching and the pump intensity. This result suggests that the mechanism causing the photon bleaching is not two photon absorption. However, photo bleaching is still not well understood. It is believed to in part to be caused by higher than second order absorption events in the fluorophores, resulting in the molecule getting 'trapped' in a long lived excited state [16].

A further issue with the two photon fluorescent microscope is the so called phototoxicity. This is when biological material starts to deteriorate and denature because of the radiation. Phototoxicity has been studied, and a rate equation was also attempted to be derived [17, 18]. In both cases, a second order dependence with intensity was found; however, the mechanism for this is also not understood. Both of these are ongoing problems with the technique, and mechanisms are still being developed to mitigate them [19]; however, there is no way to avoid them altogether. We could suppress their effect by pumping with a reduced flux whilst stimulating the same response which provides and invitation for our work.

The use of entangled photons in a microscope was first put forward by Teich and Saleh in 1997 [20]. They propose a reduction of pump flux due to the linear scaling from using an entangled source. Since then, there have been several theoretical and

experimental investigations into the process. Entangled two photon interaction has also drawn much interest for spectroscopy [21–23] however, the principal interest motivating my investigation is for imaging applications. The idea of applying it to imaging has not yet been realised, partially because of the difficulty in stimulating Entangled Two Photon Absorption (eTPA) and the inconsistency of the published results. One of the main conclusions of this thesis will be to explain why we see inconsistent experimental results. This author concludes that there is a variable which is poorly controlled for, upon which the rate of eTPA is entirely dependent.

We will review the current state of that literature later in this chapter. However, first, we will discuss two critical theoretical results. The first is from Fei et al. [24], in which they derive the eTPA cross section. Starting from a simple probabilistic rate equation for eTPA of the form:

$$R = \delta\phi + \sigma\phi^2, \tag{1.1}$$

where ϕ is the flux of the pump photons and R is the rate of two photon absorption. They argue that the expected relation between the classical coefficient, σ, and the entangled cross section, δ, will be:

$$\delta = \frac{\sigma}{2A_eT_e}, \tag{1.2}$$

where A_e and T_e are the entanglement area and time, respectively, defined as the width of the second order correlation function in space and time. Another way of saying this is that these are the length scales and time scales in which the entangled state is created/exists. When this is expanded into a more complete model of the process, the entangled coefficient, δ, has a dependence on the entanglement time, T_e, and could disappear for specific values. This introduces new parameters we need to have control over for eTPA experiments. However, to my knowledge, this has not been investigated experimentally.

The second is an analysis undertaken by Jagatap and Meath [25] into classical two photon absorption, where they discuss the possibility of an alternative mechanism for TPA. Conventionally, it is understood that during TPA, the molecule/atom is stimu-

lated to a virtual level; Jagatap and Meath provide a mechanism in which a molecule with a permanent dipole moment gets flipped by a single photon and the system stabilised by the second. This results in a change of the selection rules for TPA as well as energy dynamics, which, when combined with the insight of Fei et al., could result in an issue interpreting the results of any eTPA experiment as in [26].

1.1 Literature Review

Initial results displaying non-classical behaviour in TPA by pumping with a squeezed state were obtained in the 1990s. Georgiades et al. [27] pumped the $6S_{1/2} \rightarrow 6D_{5/2}$ transition of atomic Cesium with an OPO operating below threshold. They observe, at low photon fluxes, the beginning of a linear relationship between the incoming photon flux and excitation rate precisely as described by Gea-Banacloche [3]. Close to thirty years later, this result remains elusive. Several future reports struggle to replicate this key feature, and we will examine some of these reports in this section.

In the early 2000's two groups began to investigate and publish results regarding the eTPA phenomenon. The first group was led by Silberberg, based at the Weizmann Institute of Science, and Goodson led the second team at the University of Michigan. The group lead by Silberberg published first the paper Dayan et al. [28] in which they probe eTPA with PDC stimulated entirely in the high gain. It is not believed that the linear scaling between incoming photon flux and excitation rate will be present in the high gain of PDC as at sufficiently high fluxes, the second order term in Equation 1.1 will be orders of magnitude larger than the linear term. This study does, however, display non-classical behaviour. In Dayan et al. [28] the investigators pump the down conversion process with a pulse duration of 3 ns but show that by introducing a delay of approximately 23 fs between the signal and idler fields (daughter fields of the down conversion process), they reduce the rate of TPA by half. By doing this and measuring a substantially narrower absorption spectrum than one would expect from a pump field of the bandwidth of their PDC, they show that pump TPA with a high gain PDC source behaves differently to a similar thermal source for which the PDC has the same statistical properties. This is due to entanglement in the down converted state.

While Dayan et al. provided the first evidence that eTPA is truly an entangled process as they show that the resultant fluorescent field depends on both the relative delay of the entangled photons and the spectrum of the pump field and therefore depends on the time-energy entanglement present in the down converted field; we do not intend to investigate directly the effect that they show. We will however, revisit the theme of non-classical behaviour in entangled two photon interactions in the high gain of parametric down conversion which they clearly display in their report. We instead want to directly investigate the linear relationship between incoming photon flux and response. Lee and Goodson attempt this investigation in their 2006 paper [29]. In this paper, they study eTPA in a porphyrin dendrimer (H_2TPP) pumped by PDC from a type II BBO crystal. They find an entangled cross section of $\sim 10^{-17}\text{cm}^2$ which is only an order of magnitude lower than the molecule's classical single photon absorption cross section, a pleasing result. However, this report has several issues. The main problem, I believe, is how they detect the TPA response.

Once a fluorophore has undergone absorption, there is no special direction in which it will emit. Fluorescence will, therefore, be emitted symmetrically about molecules, which makes collecting it difficult. The expected response will be dim enough that, in most cases, it will not be sufficient to simply detect the response in a section of the expected emitted space. This may be alleviated with the use of an integration sphere. However, it could be easier to measure the number of entangled photons lost when transmitted through the sample, as this field has a known direction and can be easily collected, and this will be directly proportional to the rate of absorption. The loss of any pump photons could be attributed to the TPA effect. This is the method they chose to employ, and as far as I can tell, all of the losses measured are attributed to TPA events. It is not reasonable to assume that this is the case. However, with a novel interpretation of their results, we cannot wholly dismiss this study.

As they use type II down conversion, their signal and idler fields are polarised orthogonal to one another. They attempt to compensate for dispersion in their system with a birefringent quartz plate. Due to the orthogonal polarisation of the pairs of down converted photons, the refractive indices and group velocities of the down con-

verted photons will be different, and as such, the relative delay between the pairs of photons can be controlled. They vary the width of this plate and, in doing so, introduce a delay between the signal and idler photons. They call the relative delay between these two fields the entanglement time. I would dispute this terminology. The entanglement time is the width of the second order correlation function. When they delay the entangled photons, they do not increase the width but increase the delay between photons. Therefore, they have shifted the correlation function in time. Instead of the photons arriving approximately simultaneously, they will arrive with a relative delay, and as such, what they have really done is destroy the state's ability to undergo efficient eTPA. However, this is effectively the same effect shown in [28]: introducing a delay between the entangled photons. Furthermore, when they introduce the delay, they see a reduction in the efficiency of the measured absorption rate. This strong dependence on relative delay is expected for an entangled state. In [28], they also show a strong dependence on the relative delay with complete loss of TPA events with relative delays of less than 100 fs. However, I do not believe we would expect the same response from random linear losses, which should have no dependence on the delay between photons. Therefore, it is likely that the losses they see in their down converted state are in part from two photon interactions.

The Michigan group have since gone on to investigate eTPA in many molecules [26, 30–32]. Many of the molecules that they have investigated are rare, and therefore, these studies have proven difficult to replicate. In eTPA studies, there are two aspects to consider: the absorption process itself and the state used to drive it. In most reports, the focus is placed on the absorption process. By that, I mean they are focused on the molecule in use, the magnitude of the linear term and alternative mechanisms, which may result in the same observation. I believe that there has been a lack of focus on the down converted state and how to optimise this for entangled two photon processes. For that reason, most of the attention in this thesis will be on how properties of the down converted state affect entangled two photon processes.

In 2018, Villabona-Monsalve et al. [33] presented the first investigation into eTPA with common fluorophores ZnTPP and Rhodamine B. They do not mention the down

converted state beyond the type and crystal in use. Most studies appear to treat the PDC as, simply, any other pump field, which it very assuredly is not. This experimental design is also susceptible to another issue, as outlined by Hickam et al. [34]: single photon losses. The method they are using to measure the TPA rate is the change of coincident counts between the sample in place and not in place. They attribute the reduction of coincident counts to eTPA. However, any linear loss mechanism, such as single photon scattering, could lead to this reduction. This problem is unavoidable. However, if the method of measuring the number of entangled photons has no dependence on entanglement then we may still be able too measure the number of photons lost in the up converted state as a tool for determining the rate of eTPA.

I believe that we could quantify and eliminate the effect of linear losses on eTPA measurements by destroying entanglement in the down converted state and measuring the reduction of down converted photons after the sample when there is no entanglement present. This should entirely remove the linear term due to entanglement but a linear term due to losses would still be present. There are two methods that could be used for this. First, introduce a delay between the entangled photons as Dayan et al. [28] do and my interpretation of Lee and Goodson [29]. Alternatively, because the down converted photons are emitted symmetrically about the pump beam, by introducing a mask in the far field of the PDC, which is asymmetric with regards to the the pump beams propagation direction, we would deterministically remove single photons from an entangled pair. There may be other methods of destroying entanglement,it does not matter which methods is used, all we require is a detection scheme that is robust to this destruction. This means we cannot use coincident counts as done in Villabona-Monsalve et al. [33] and Hickam et al. [34]. Instead we should just measure the total number of photons before and after the sample.

To put this idea in the language of Villabona-Monsalve et al. [33] where R_{abs} is the rate of photon pairs absorbed by a molecular system, $R_{solvent}$ is the rate of photon pairs observed with just a solvent and R_{sample} is the rate of photon pairs observed when the sample is pumped with the down converted field. If we assume that the number of entangled pairs is exactly half the total number of photons (clearly not physically

realisable; however, that is not an issue here) and introduced $R_{classical}$, which is the rate of photon pairs observed when the system is pumped with the PDC state with its entanglement destroyed then:

$$R_{abs} = R_{classical} - R_{sample}.$$

If any eTPA is present then $R_{classical} > R_{sample}$ (note, R_{abs} is the rate of two photon absorption but both $R_{classical}$ and R_{Sample} are measured rates of photon pairs). We no longer need to measure the rate of absorption with just the solvent present ($R_{solvent}$) as this will be present with both the rate of absorption when the sample is pumped by the down converted field (R_{sample}) and the rate of absorption when the sample is pumped by the down converted field with the entanglement removed ($R_{classical}$) and therefore will already cancel in the above equation. This has not been done in any studies I am aware of. However, I believe it could alleviate the linear loss issue as we do not measure coincidences; instead, we simply measure the total number of photons.

Placing this aside, the idea of requiring better information and control of the down converted state is not a novel one; in fact, Hickam et al. [34] end their paper by stating, "Only by characterising the entangled state, instead of relying solely on intensity measurements, can a definitive conclusion be reached". More recently, there have been several studies where the down converted state is better discussed and considered, to varying success. Three recent studies investigate the same common fluorophore, Rhodamine 6G; Landes et al. [35], Tabakaev et al. [36], and Parzuchowski et al. [37] with all attempting to measure the fluorescent light directly. We will discuss these studies in a later chapter in more detail when we can use the results contained herein to help analyse them, but only one, Tabakaev et al. [36], see the expected linear scaling. They further showed that this linear scaling is due to the entangled property of the down converted state by measuring the resultant TPA rate when attenuating the down converted state directly. This displayed a quadratic scaling as opposed to a linear that was found when attenuating the PDC pump to reduce the PDC power. This is a robust method to show that entanglement is the fundamental cause of the linear scaling observed in eTPA, as

for a classical field and mechanism, both methods would produce the same response.

Difficulties in realising these results and reproducing these studies has led to a large amount of literature questioning and countering the claims of these eTPA experiments. Parzuchowski et al. [37] and Landes et al. [35] both say the cross section, if any quantum interaction occurs, is orders of magnitude smaller than previously published, which is generally where the discussion resides. In neither of these studies do they observe anything they could call eTPA. The strongest experimental work which directly rebuts previous claims has come from Corona-Aquino et al. [38]. In this study, they attempt to observe eTPA from Rhodamine B (RhB) and zinc tetraphenyl-porphirin (ZnTPP) via transmission of the PDC as in [33]. They manage to reproduce their result and show the linear scaling. However, upon further experimentation, they conclude categorically that this cannot be due to entanglement as when they delay one of the entangled photons with respect to its entangled partner, they observe no strong dependence on the relative delay of the two photons, unlike in [28]. They present this null result in a very clean and clear way with good reasoning and even show that the linear scaling they do see could be interpreted as having a cross section of the same order of magnitude of previous reported entangled two photon cross section.

The more important studies are those that suggest alternative interpretations and mechanisms for the observed results and place limits on the possible practical advantage we could see. One of these, we discussed earlier, Hickam et al. [34], which attributes an observed linear scaling due to single photon scattering. This is probably the cause of the result observed in Corona-Aquino et al. [38]. A second, Mikhaylov et al. [39], describes a mechanism where a single photon can stimulate an excitation, which we expect can only be stimulated by two photons if the electron inhabits a highly energetic ground state. They show that this hot band absorption process could have a cross section which is compatible in magnitude with the reported limits on the entangled two photon cross sections ($\sim 10^{-25}\text{cm}^2$). These criticisms cannot be ignored, and they present a worrying set of unknown mechanisms that may influence any eTPA experiments.

1.1.1 A New Approach

TPA offers a multitude of variables which are hard to control, such as various excitation pathways and loss mechanisms. These could result in an altered reason for the observed result as in [38] or various excuses for observing or missing the scaling as expected; investigating TPA introduced uncertainties in the interpretation of results. However, two photon absorption is not the only two photon process we can use. Instead, we could try to investigate the effect of pumping sum frequency generation (SFG) with PDC. SFG can be thought of as the reverse of PDC. PDC involves one field decaying into two daughter fields, SFG is the process of two fields combining to form one final field. For the same reason as TPA, this is expected to have a linear term when pumped with PDC; the space-momentum, time-energy entanglement present in PDC, this time without the complications of TPA.

As a physicist, my focus is on how the properties of the down converted state affect the efficacy of entangled two photon processes rather than on the chemistry of any particular fluorophore. Therefore, despite being primarily motivated by imaging applications, which are most commonly conducted with fluorophores, the work contained herein shall be investigating solely entangled sum frequency generation (eSFG). I believe that this is directly applicable to eTPA as the linear term is caused by the same phenomena in the down converted state and not anything in the up conversion process.

1.2 Classical Nonlinear optics

Nonlinear optics refers to a field of study in which the properties of a system change due to the strength of a light field illuminating it. We consider here only the simplest materials and provide a basic summary of how to describe nonlinear light-matter interactions sufficient to describe the processes we are interested in. I will also attempt to keep the notation as simple as possible and adopt the Einstein summation convention where the same indices are summed over.

Nonlinear optics is often understood by considering the polarisation vector, $\vec{P}$. Generically, this is some function of the electric field, $\vec{E}$. In the cases where the po-

larisation vector responds instantaneously by the electric field (that is, has no explicit, independent dependence on the time), $\vec{P}$ can be expressed as a power series of the E-field. In conventional optics, it is usually sufficient to limit the perturbative expansion of the polarisation in therms of the E-field to only one term:

$$P_i = \epsilon_0 \chi_{ij}^{(1)} E_j, \tag{1.3}$$

for the i^{th} component of the polarisation. $\chi^{(1)}$ is the linear susceptibility and ϵ_0 is the permittivity of free space. In nonlinear optics, the perturbative expansion of the polarisation continues:

$$P_i = \epsilon_0 \chi_{ij}^{(1)} E_j + \epsilon_0 \chi_{ijk}^{(2)} E_j E_k + \epsilon_0 \chi_{ijkl}^{(3)} E_j E_k E_l + ... \tag{1.4}$$

$\chi^{(2)}$ and $\chi^{(3)}$ are the second and third-order nonlinear optical susceptibilities. Note, centrosymmetric materials materials are prohibited from having a second order $\chi^{(2)}$ due to their rotational symmetry [1]. Therefore, the lowest order nonlinear effects can only occur in a special class of materials.

We will find it convenient to split the polarisation vector into two components:

$$\vec{P} = \vec{P}_0 + \vec{P}_{NL}, \tag{1.5}$$

where $\vec{P}_{NL}$ contains all the nonlinear components. In order to describe the evolution of the fields classically, we develop a wave equation description of the interaction as in [40]. The electric displacement field, D, is related to the electric field and polarisation through:

$$\vec{D} = \epsilon_0 \vec{E} + \vec{P}. \tag{1.6}$$

Remembering the definition $n^2 = 1 + \chi^{(1)}$ where n is the refractive index, we can express 1.6 as:

$$\vec{D} = \epsilon_0 n^2 \vec{E} + \vec{P}_{NL}. \tag{1.7}$$

[1] Consider what would happen in a centrosymmetric materials when the material is roated by 180 degrees. $\vec{P}$ should become $-\vec{P}$ as $\vec{E}$ becomes $-\vec{E}$ which is not possible with a second order term.

To write the wave equation, we start from Maxwell's equations, which, in a charge free, current free, non-magnetic material, are given by:

$$\nabla \cdot \vec{D} = 0 \tag{1.8}$$

$$\nabla \cdot \vec{B} = 0 \tag{1.9}$$

$$\nabla \times \vec{E} = -\frac{\partial \vec{B}}{\partial t} \tag{1.10}$$

$$\nabla \times \vec{B} = \mu_0 \frac{\partial \vec{D}}{\partial t} \tag{1.11}$$

Taking the curl of 1.10 and substituting in 1.11 and 1.7 we arrive at:

$$\nabla \times \nabla \times \vec{E} + \mu_0 \epsilon_0 n^2 \frac{\partial^2 \vec{E}}{\partial t^2} = -\mu_0 \frac{\partial^2 \vec{P}_{NL}}{\partial t^2}. \tag{1.12}$$

In order to simplify this further, we need two definitions. The first from electromagnetism for which $\mu_0 \epsilon_0 = 1/c^2$ defines the speed of light c, the second from calculus:

$$\nabla \times \nabla \times \vec{E} = \nabla(\nabla \cdot \vec{E}) - \nabla^2 \vec{E}.$$

We have already assumed there are no charges, so the first term on the right hand side is zero, and Equation 1.12 becomes:

$$\nabla^2 \vec{E} - \frac{n^2}{c^2} \frac{\partial^2 \vec{E}}{\partial t^2} = \frac{1}{\epsilon_0 c^2} \frac{\partial^2 \vec{P}_{NL}}{\partial t^2} \tag{1.13}$$

1.2.1 Sum Frequency Generation Wave Equation

Limiting ourselves to just the second order process of sum frequency generation, we can write the nonlinear polarisation:

$$P_i^{NL} = \epsilon_0 \chi_{ijk}^{(2)} E_j E_k. \tag{1.14}$$

Sum frequency generation is a process in which two fields with different frequencies stimulate an up conversion event. Considering a pump consisting of two monochromatic

waves, the electric field will take the form:

$$E = E_1 e^{-i\omega_1 t} + E_2 e^{-i\omega_2 t} + E_1^* e^{i\omega_1 t} + E_2^* e^{i\omega_2 t}, \tag{1.15}$$

where we have assumed the fields are propagating in the same direction and we have ignored polarisation for simplicity. All of the processes described in second order nonlinear optics have strong dependence on polarisation however, this can be easily considered at a later point of the derivation if required. Equation 1.14 becomes:

$$\begin{aligned} P_{NL} = \epsilon_0 \chi^{(2)} \big[& E_1^2 e^{-2i\omega_1 t} + E_2^2 e^{-2i\omega_2 t} + 2E_1 E_2 e^{-i(\omega_1+\omega_2)t} + 2E_1 E_2^* e^{-i(\omega_1-\omega_2)t} \\ & + \text{Complex Conjugate} \big] + 2\epsilon_0 \chi^{(2)} \left[E_1 E_1^* + E_2 E_2^* \right]. \end{aligned} \tag{1.16}$$

The different terms in this equation give rise to the different phenomena. The first two terms can be identified as second harmonic generation (SHG), which is when a field of one frequency up converts to a field at twice the frequency. The third term can be identified as sum frequency generation (SFG) and the term we will consider. The fourth can be identified as difference frequency generation (DFG), where the final field produced in the interaction is at the frequency difference of the two pump fields. The complex conjugate terms not explicitly written in 1.16 but can be identified as the reverse DFG process and varieties of parametric down conversion (PDC), which we will discuss later. The final two terms can be identified as optical reflection.

Concentrating on the SFG term:

$$P_{NL} = 2\epsilon_0 \chi^{(2)} E_1 E_2 e^{-i(\omega_1+\omega_2)t}. \tag{1.17}$$

It is implicitly assumed in the above equation is that the second order susceptibility is independent of frequency and time. This will be the case provided the frequencies of the fields are much smaller than the resonant frequencies of the material system [40]. For SFG, the nonlinear susceptibility is a tensor of the form:

$$P_i(\omega_1 + \omega_2) = \chi^{(2)}_{ijk}(\omega_1 + \omega_2, \omega_1, \omega_2) E_j(\omega_1) E_k(\omega_2). \tag{1.18}$$

It would not make any difference if we swap the indices 1 and 2. Therefore, there must be an intrinsic symmetry in this tensor where:

$$\chi^{(2)}_{ijk}(\omega_1 + \omega_2, \omega_1, \omega_2) = \chi^{(2)}_{ikj}(\omega_1 + \omega_2, \omega_2, \omega_1), \tag{1.19}$$

note that the Cartesian indices are also swapped. Suppose we can treat the medium with the nonlinear susceptibility tensor as lossless. In that case, we can extend this into the full permutation symmetry, where we can permutate any of the frequencies provided, and we can also permutate the indices in the same manner. However, we have also assumed previously that the second order susceptibility is independent of frequency; when this is taken, we can freely permutate the Cartesian indices. The purpose of this is to reduce the rank of the tensor, and when these assumptions are taken, a lossless medium and optical frequencies much smaller than the resonance frequency of the system; it is called the Kleinman symmetry condition, named after D.A. Kleinman, who first used it [41].

The reason for going through that brief overview is that the Kleinman symmetry condition is very often met for the nonlinear processes we will be investigating, and we will be assuming it throughout. It is also an attempt to motivate a bit of notation shenanigans. When these conditions are met, for historical reasons, the nonlinear susceptibility tensor is rewritten in the form:

$$d_{ijk} = \frac{1}{2}\chi^{(2)}_{ikj}. \tag{1.20}$$

Moreover, when, as in our case, we consider fixed polarisations and direction of the pumping field, this results in a scalar factor, and Equation 1.17 becomes:

$$P_{NL} = 4\epsilon_0 d_{eff} E_1 E_2 e^{-i(\omega_1+\omega_2)t}, \tag{1.21}$$

d_{eff} is known as the effective d coefficient and is one of the main properties discussed when comparing nonlinear crystals.

Returning to Equation 1.13, the E field in this equation is the final, up converted

field and, if propagating in the positive z direction, has the form:

$$E_3 = A_3 e^{i(k_3 z - \omega_3 t)} + \text{Complex Conjugate} \tag{1.22}$$

where A_3 is the amplitude, k_3 is the wave number of the up converted field, and ω_3 is its angular frequency, which is related to the pump field via the relationship:

$$\omega_3 = \omega_1 + \omega_2. \tag{1.23}$$

Note that the wave number and frequency are related by:

$$k_i = \frac{n_i \omega_i}{c}, \tag{1.24}$$

where we have used the notation $n_i = n(\omega_i)$. We can similarly remove the spatial dependence on the pump fields and write Equation 1.21 as:

$$P_{NL} = 4\epsilon_0 d_{eff} A_1 A_2 e^{i[(k_1+k_2)z - \omega_3 t]}. \tag{1.25}$$

Substituting this into 1.13 and performing some of the operations:

$$\begin{aligned} \left[\frac{\partial^2 A_3}{\partial z^2} + 2ik_3\frac{\partial A_3}{\partial z} - k_3^2 A_3 + \frac{n^2(\omega_3)\omega_3^2 A_3}{c^2}\right] e^{i(k_3 z - \omega_3 t)} \\ = \frac{-4 d_{eff}\omega_3^2}{c^2} A_1 A_2 e^{i[(k_1+k_2)z - \omega_3 t]} \end{aligned} \tag{1.26}$$

The third and fourth terms on the left hand side of the above cancel each other, and we are left with the following:

$$\left[\frac{\partial^2 A_3}{\partial z^2} + 2ik_3\frac{\partial A_3}{\partial z}\right] = \frac{-4 d_{eff}\omega_3^2}{c^2} A_1 A_2 e^{i[(k_1+k_2-k_3)z]}. \tag{1.27}$$

Provided that the amplitude A_3 varies at distances much larger than the wavelength, we can take the slowly varying amplitude approximation:

$$\left|\frac{\partial^2 A_3}{\partial z^2}\right| << \left|k_3\frac{\partial A_3}{\partial z}\right|,$$

and so Equation 1.27 becomes:

$$\frac{\partial A_3}{\partial z} = \frac{2id_{eff}\omega_3}{n_3 c} A_1 A_2 e^{i[(k_1+k_2-k_3)z]}, \tag{1.28}$$

we can simply integrate for propagating into a crystal of length L using the identity $\Delta k = k_1 + k_2 - k_3$

$$A_3(L) = \frac{2id_{eff}\omega_3 A_1 A_2}{n_3 c} L e^{i\Delta kL} \operatorname{sinc}(\Delta kL/2). \tag{1.29}$$

The intensity is given by [42]:

$$I_i = 2n_i\epsilon_0 c|A_i|^2. \tag{1.30}$$

Thus, the up converted intensity will be:

$$I_3 = \frac{2d_{eff}^2\omega_3^2 I_1 I_2}{n_1 n_2 n_3 \epsilon_0 c^3} L^2 \operatorname{sinc}^2\left(\frac{\Delta kL}{2}\right). \tag{1.31}$$

I want to highlight two properties of Equation 1.31, which will be relevant later: the dependence on the two input field intensities and the quadratic dependence on crystal length. Later in this dissertation, we will show and discuss the changing properties of the down-converted field, which will make a comparison to the appropriate classical field complicated. We will also briefly investigate the effects of crystal length on eSFG.

1.2.2 Parametric Down Conversion

We will not go through a formal description of parametric down conversion here. This is a quantum process and needs a quantum formulation to go through, which we will undertake in a later chapter. Hopefully, we can match this up in a coherent manner with a quantum theory of entangled sum frequency generation. However, there are some aspects we should discuss here. PDC is a second order nonlinear process and, in many ways, can be thought of as the reverse of SFG. SFG involves the destruction of two fields and the production of one at the sum of the destroyed fields' energy. PDC involves the destruction of one field and the production of two daughter fields, conventionally called signal and idler, whose energies sum to the energy of the original field. Because

of this similarity, the function restraining momentum mismatch in Equation 1.31 is also applicable to PDC. Explicitly in the plane wave, monochromatic pump approximation:

$$\mathrm{sinc}^2\left(\frac{\Delta kL}{2}\right) \tag{1.32}$$

also constrains parametric down conversion; maximising this quantity is called phase matching. Phase matching will also be discussed in future chapters. In order to stimulate PDC, we have to ensure two fundamentals of physics are conserved, that is, energy:

$$\omega_p = \omega_i + \omega_s, \tag{1.33}$$

and momentum:

$$\vec{k}_p = \vec{k}_i + \vec{k}_s. \tag{1.34}$$

In the plane wave, monochromatic pump approximation used throughout this description, the conservation of energy remains satisfied however, a certain momentum mismatch between the pump field and the down converted fields is permitted, described by the function 1.32.

There is one key difference between the rate of SFG and PDC, which we can understand without the need for a full quantum treatment. For sum frequency generation it is sufficient to describe the process as in Equation 1.31 and outlines in Section 1.2.1. For parametric down conversion, however, the down converted fields can stimulate their sister field. This process is often called parametric amplification and can be described semi-classically when pumping a nonlinear crystal with a pump field and a weak signal field [43]. Because of this amplification process, PDC grows exponentially with pump intensity. We will show that this is the case in a later chapter. There is no stimulation of the up converted field for SFG. Therefore, the behaviour will remain constant until sufficiently high intensities where pump depletion will occur. However, for PDC, we have two distinct behaviours. One where the down converted field is produced spontaneously and a second in which the down converted field is stimulated. Spontaneous parametric down conversion (SPDC) can only be described quantum mechanically and

will lead to the linear scaling in eTPA and eSFG. Often, throughout this dissertation, I will be describing SPDC as low gain parametric down conversion or PDC with less than one photon per mode. All of these ways of referring to SPDC are equivalent for our purposes. Similarly, the stimulated parametric down conversion will also be referred to as high gain parametric down conversion or PDC with more than one photon per mode. We will investigate how both of these regimes affect the scaling of eSFG throughout this work.

1.3 Quantum Optics Basics

We will not quantise the field; this is beyond the scope of this work, but there are some key ideas from quantum optics we should introduce at the beginning. The first is the canonical quantisation for the electric field of a single polarisation and spatial mode in a dielectric medium [44–46]:

$$E = E^{(+)} + E^{(-)} \tag{1.35}$$

$$E^{+}(z,t) = i\int_0^\infty d\omega \left(\frac{\hbar\omega}{4\pi n(\omega)\varepsilon_0 cS}\right)^{\frac{1}{2}} \hat{a}(\omega,z)\ exp\left[-i\omega(t-z/c)\right] = \left[\hat{E}^{-}(\vec{r},t)\right]^{\dagger}, \tag{1.36}$$

where S is the beam area, $n(\omega)$ the refractive index at the frequency ω, ε_0 the permeability of free space, and we have restricted the electric field to only propagate along the z-axis. The operator $\hat{a}(\omega,z)$ is the bosonic harmonic annihilation operator in the continuous mode limit defined so that:

$$[\hat{a}(\omega_i), \hat{a}^{\dagger}(\omega_j)] = \delta(\omega_i - \omega_j), \tag{1.37}$$

where [ ] denotes the commutation relation between these two operators. We will be expressing the derivations throughout the remainder of this thesis in the Heisenberg picture, where the observables evolve according to the Heisenberg equation of motion:

$$\frac{d\hat{O}(t)}{dt} = \frac{i}{\hbar}[H, \hat{O}] \tag{1.38}$$

where $\hat{O}$ is a Heisenberg observable and H is the Hamiltonian of the system.

1.4 Summary

This chapter has presented a comprehensive review of the existing research, which serves as the basis for our upcoming investigations. In the following chapters we will delve deeper into parametric down conversion and the down converted state utilised in our work. We will then present a plethora of findings related to eSFG, with a focus on high gain, and provide explanations for these results to gain a more intuitive understanding of the effect. Additionally, we will isolate the impact of losses in the down converted state on eSFG efficiency, which is one of the principal outcomes of this thesis. Our analysis will reveal some unexpected behaviour, and we will present a model to explain these results. Finally, we will compare our findings to an appropriate classical state and demonstrate a brighter response when pumping with entangled photons in the stimulated regime of parametric down conversion above the gain level previously believed to be achievable.

1.5 Publications

Conference Proceedings

Invited

T. Dickinson, I. Afxenti, G. Astrauskaite, L. Hirsch, S. Nerenberg, O. Jedrkiewicz, A. Gatti, D. Faccio, C. Müllenbroich, M. Clerici, and **L. Caspani**, "Towards quantum-enhanced nonlinear imaging", *Meta 2024*, 14th International Conference on Metamaterials, Photonic Crystals and Plasmonics, Toyama, Japan, 16-19 July, 2024, invited talk.

T. Dickinson, I. Afxenti, G. Astrauskaite, L. Hirsch, S. Nerenberg, O. Jedrkiewicz, A.

Gatti, D. Faccio, C. Müllenbroich, M. Clerici, and **L. Caspani**, "Towards quantum-enhanced nonlinear imaging", *13th Advanced Lasers and Photon Sources*, Yokohama, Japan, 22-26 April, 2024, invited talk.

I. Afxenti, T. Dickinson, G. Astrauskaite, S. K. Rajendran, L. Hirsch, S. Nerenberg, C. Müllenbroich, A. Gatti, D. Faccio, M. Clerici, L. Caspani, "Multimode, High-photon number, Quantum enhanced sum frequency generation", *ICTON 2023*, Bucharest, Romania, 2-6 July, 2023, invited talk.

L. Caspani, T. Dickinson, I. Afxenti, G. Astrauskaite, S. K. Rajendran, D. Faccio, C. Müllenbroich, M. Clerici, "Quantum-enhanced multiphoton fluorescence microscopy", BQIT:22, *Ninth Annual Bristol Quantum Information Technologies Workshop*, April 25-28, 2022, invited talk.

Regular Contributions

T. Dickinson, I. Afxenti, G. Astrauskaite, L. Hirsch, S. Nerenberg, O. Jedrkiewicz, A. Gatti, D. Faccio, C. Müllenbroich, M. Clerici, and L. Caspani, "Quantum-enhanced two-photon interactions beyond the photon pairs regime", *Frontiers in Optics + Laser Science*, Denver, Colorado, USA, September 23-26, 2024.

I. Afxenti, T. Dickinson, G. Astrauskaite, L. Hirsch, S. Nerenberg, C. Müllenbroich, D. Faccio, A. Gatti, M. Clerici, L. Caspani, "Multimode, high-photon number, quantum-enhanced sum frequency generation", *SPIE Photonex*, Glasgow, UK, 24-26 October, 2023.

T. Dickinson, I. Afxenti, G. Astrauskaite, L. Hirsch, S. Nerenberg, C. Müllenbroich, O. Jedriekiewicz, D Faccio, A. Gatti, M. Clerici, L. Caspani, "Entangled sum-frequency generation from bright twin beams", *Quantum, Atomic and Molecular Physics - QuAMP (Institute of Physics)*, Glasgow, UK, September 12-13, 2023, (poster).

T. Dickinson, I. Afxenti, G. Astrauskaite, S. K. Rajendran, D. Faccio, C. Müllenbroich,

M. Clerici, L. Caspani, “Towards enhanced nonlinear imaging with entangled photons”, *Photon2022*, Nottingham, UK, August 30-September 2, 2022 (poster).

Article

T Dickinson, I. Afxenti, G. Astrauskaite, L. Hirsch, S. Nerenberg, C. Müllenbroich, O. Jedriekiewicz, D Faccio, A. Gatti, M. Clerici, L. Caspani, ”Quantum-enhanced second harmonic generation beyond the photon pairs regime”, *Science Advances*, submitted, 2025

Chapter 2

Theory of Entangled Sum Frequency Generation

There have been many theoretical investigations into entangled two photon absorption. It was first investigated in two articles, one from Javanainen and Gould [2], and separably but simultaneously from Gea-Banacloche [3]. Recently, more complete theoretical investigations have been undertaken e.g. [21, 47–49]. However, few theoretical investigations have considered entangled sum frequency generation explicitly. This is largely because eSFG is less directly applicable to further research into fluorescent microscopes and entangled two-photon absorption spectroscopy which have been the primary motivations for these studies. As in this work we explicitly investigate eSFG, we will present a full quantum derivation of eSFG. This will closely follow the derivation from Dayan [50]. We will start by deriving the operators describing the down converted field after a pump field has passed through a crystal of length L and then apply this state to the up conversion process. In doing this, we will gain a greater understanding of the quantum nature of this process.

The analysis that will follow will assume the down converted state has a single spatial mode with multiple temporal modes. The down converted states used experimentally in this work contains multiple spatial modes and a more complex analysis is required to properly consider this fact [48, 51]. However, in order to capture the most prevalent features, the single mode treatment is sufficient.

2.1 Parametric Down Conversion

Parametric down conversion can only occur in media which permit a second order term in the polarisation vector. This is only possible in noncentrosymmetric materials, that is, materials which will not be invariant under spatial translations and rotations. Specifically, these materials will be not be invariant with the transformation $\vec{r} \to -\vec{r}$. In the Heisenberg representation, the spatial evolution of the electric field, $\hat{E}$, will be governed by the momentum operator $\hat{G}$. In the same way that the Hamiltonian generates time translation (Equation 1.38), the momentum operator generates spatial translations. As such the spatial evolution of the electric field is governed by the equation [52–54]:

$$\frac{\partial \hat{E}(\omega, z)}{\partial z} = \frac{i}{\hbar}\left[\hat{E}(\omega, z), \hat{G}(z)\right]. \tag{2.1}$$

Classically, the momentum density is given by [54]:

$$\vec{d}(z,t) = \vec{D}(z,t) \times \vec{B}(z,t), \tag{2.2}$$

where the field propagates along the z-axis. $\vec{D}(z,t)$ is the electric displacement field: $\vec{D}(z,t) = \varepsilon_0 \vec{E}(z,t) + \vec{P}(z,t)$, $\vec{E}(z,t)$ is the electric field, $\vec{B}(z,t)$ is the magnetic field and $\vec{P}(z,t)$ is the polarisation vector. We can separate the electric field into a forward and backward propagating component $E(z,t) = E^+(z,t) + E^-(z,t)$. Noting the canonical quantised electric field (Equation 1.36):

$$E^+(z,t) = i\int_0^\infty d\omega \left(\frac{\hbar\omega}{4\pi n(\omega)\varepsilon_0 cS}\right)^{\frac{1}{2}} \hat{a}(\omega, z)\exp\left[-i\omega(t - z/c)\right] = \left[\hat{E}^-(\vec{r}, t)\right]^\dagger, \tag{2.3}$$

and magnetic field:

$$B^+(z,t) = i\int_0^\infty d\omega \left(\frac{\hbar\omega n(\omega)}{4\pi\varepsilon_0 c^3 S}\right)^{\frac{1}{2}} \hat{a}(\omega, z)\exp\left[-i\omega(t - z/c)\right] = E^+(z,t)\times c/n(\omega). \tag{2.4}$$

where S is the beam area and the operator $\hat{a}(\omega, z)$ is the the bosonic harmonic annihilation operator in the continuous mode limit. The momentum flux operator, $\hat{g}$, is

simply rate of the momentum flow, $\vec{d}$ per unit area:

$$\hat{g}(z,t) = [\hat{D}^-(z,t)\hat{B}^+(z,t) + \text{h.c.}]v, \tag{2.5}$$

where v is the speed of light in the medium, $v = c/n$. By substituting Equation 2.4 we can write the momentum flux as:

$$\hat{g}(z,t) = [\hat{D}^-(z,t)\hat{E}^+(z,t) + \text{h.c.}]. \tag{2.6}$$

The momentum operator is then the integral over time, t, of this quantity:

$$\hat{G}(z) = \int_0^T \hat{g}(z,t)dt, \tag{2.7}$$

where T is the periodicity of the electromagnetic field. For a pulsed laser field this will be the pulse duration; for a continuous wave laser this will be infinity. In order to study PDC, we only need to consider the second order polarisation, which may be written as $P_{nl} = \chi E_s E_i$. Substituting this into Equation 2.6 and expanding the electric field terms, the nonlinear momentum flux operator will be:

$$\hat{g}_{nl}(z,t) = \chi \left[\hat{E}_s^-(z,t)\hat{E}_i^-(z,t)\hat{E}_p^+(z,t) + h.c.\right]. \tag{2.8}$$

Substituting in the definition 2.3 and taking the integral for the momentum operator:

$$\hat{G}_{nl}(z) = \int_0^\infty d\omega_p \int_0^\infty d\omega \hbar\beta(\omega_p,\omega)\left[\hat{a}_s(\omega,z)\hat{a}_i(\omega_p-\omega,z)\hat{a}_p^\dagger(\omega_p,z)e^{i\Delta k(\omega_p,\omega)z} + \text{h.c.}\right], \tag{2.9}$$

where $\beta(\omega_p,\omega)$ is:

$$\beta(\omega_p,\omega) = \chi(\omega_p,\omega)\sqrt{\frac{\hbar\omega_p\omega(\omega_p-\omega)}{16\pi\epsilon_0 c^2 S n_p(\omega_p)n_s(\omega)n_i(\omega_p-\omega)}}. \tag{2.10}$$

and Δk is given by:

$$\Delta k(\omega_p,\omega) = k_p(\omega_p) - k_s(\omega) - k_i(\omega_p-\omega). \tag{2.11}$$

The evolution of the signal operator as the field propagates through the medium will be given by:

$$\begin{aligned}\frac{\partial \hat{a}_s(\omega,z)}{\partial z} &= \frac{-i}{\hbar}\left[\hat{a}_s(\omega,z),\hat{G}(z)\right] \\ &= -i\int_0^\infty d\omega_p \beta(\omega_p,\omega)e^{-i\Delta k(\omega_p,\omega)z}\hat{a}_p(\omega_p,z)\hat{a}_i^\dagger(\omega_p-\omega,z).\end{aligned} \tag{2.12}$$

We can simplify this expression by taking two approximations. First, assume an undepleted pump. The pump operator, $\hat{a}_p$, can now be replaced by the classical amplitude, A_p. Second, we assume a broadband PDC so that the bandwidth of the down converted state is much larger than that of the pump. In that case, we can neglect the dependence on the pump frequency bandwidth in both of the coefficients related to the crystal properties (Δk and β) and only need to consider the central pump wavelength, ω_p, as crystal properties change on larger scales than a typical pump bandwidth. The evolution of the signal operator is thus:

$$\frac{\partial \hat{a}_s(\omega,z)}{\partial z} = -i\beta(\omega)e^{-i\Delta k(\omega)z}\int_0^\infty d\omega_p A_p(\omega_p)\hat{a}_i^\dagger(\omega_p-\omega,z), \tag{2.13}$$

and similarly the evolution of the idler operator $\hat{a}_i^\dagger$ is given by:

$$\frac{\partial \hat{a}_i^\dagger(\omega,z)}{\partial z} = i\beta(\omega)e^{i\Delta k(\omega)z}\int_0^\infty d\omega_p A_p^*(\omega_p)\hat{a}_s(\omega,z). \tag{2.14}$$

The classical amplitude is defined in such a way that:

$$\int_0^\infty d\omega_p A_p(\omega_p)A_p^*(\omega_p+\Delta\omega) = 2\pi P_p\delta(\Delta\omega), \tag{2.15}$$

P_p is proportional to the power of the pump field (photon flux). The solution to equations 2.13 and 2.14 is [50]:

$$\begin{aligned}\hat{a}_s(\omega,z) = &\left(\cosh(\Gamma(\omega)z)+\frac{i\Delta k(\omega)}{2\Gamma(\omega)}\sinh(\Gamma(\omega)z)\right)\hat{a}_s(\omega,0)e^{-i\Delta k(\omega)z/2} \\ &-\frac{i\beta(\omega)}{\Gamma(\omega)}\sinh(\Gamma(\omega)z)e^{-i\Delta k(\omega)z/2}\int_0^\infty d\omega_p A_p(\omega_p)\hat{a}_i^\dagger(\omega_p-\omega,0),\end{aligned} \tag{2.16}$$

with:

$$\Gamma(\omega) = \sqrt{2\pi P_p \beta(\omega)^2 - \Delta k(\omega)^2/4}. \tag{2.17}$$

Finally the average number of down converted photons per second after propagating through a distance L is then:

$$\begin{aligned} n_s(\omega, L) &= \int_0^\infty d\omega' \, \langle 0| \, \hat{a}_s^\dagger(\omega, L) \hat{a}_s(\omega', L) \, |0\rangle \\ &= \frac{2\pi P_p \beta(\omega)^2}{\Gamma(\omega)^2} \sinh^2(\Gamma(\omega) L) \end{aligned} \tag{2.18}$$

In the well phase matched limit, $\Delta k(\omega)^2/4 << 2\pi P_p \beta(\omega)^2$, this simplified to:

$$n_s(\omega, L) = \sinh^2\left(\sqrt{2\pi P_p \beta(\omega)^2 L^2}\right). \tag{2.19}$$

2.1.1 Gain

One concept which can be very useful to understand pertaining to the down converted state is the gain. This quantity dictates many properties of PDC but can have varying definitions in literature. When the low or high gain is discussed throughout this work, the quantity being referred to will be:

$$g = \chi(\omega_p, \omega) \sqrt{\frac{\hbar \omega_p \omega (\omega_p - \omega) P_p L^2}{8\epsilon_0 c^2 S n_p(\omega_p) n_s(\omega) n_i(\omega_p - \omega)}}, \tag{2.20}$$

which is simply the term inside of the sinh function in Equation 2.19 with Δk set to zero and β substituted from Equation 2.10:

$$\beta(\omega_p, \omega) = \chi(\omega_p, \omega) \sqrt{\frac{\hbar \omega_p \omega (\omega_p - \omega)}{16\pi\epsilon_0 c^2 S n_p(\omega_p) n_s(\omega) n_i(\omega_p - \omega)}}. \tag{2.21}$$

Throughout this work, the gain will often be discussed when the figures are plotted as a function of down converted power. This is because the gain is the parameter that sets the properties of the down converted state; there is no independent way to increase the PDC power without changing the gain. The gain however, does not directly reflect the measured, experimental, properties of the down converted state as it is solely a

function of the phase matching conditions and pump beam properties. For this reason, we have chosen not to present any of the data in this work in terms of the gain.

The gain however still provides a useful shorthand as the properties and much of the behaviour of the down converted state directly depends on it. We can easily understand this however by considering the unique relationship between gain and the number of down converted photons per second. To a good approximation for a multi mode state these are related through:

$$n_{pdc} = m \sinh^2(g), \tag{2.22}$$

where m is a measurement of the number of modes [55]. This is the form that will be taken throughout the remainder of this chapter. Equation 2.22 provides a convenient way of understanding low vs high gain. When $g << 1$, $n \approx m \times g^2 \propto P_p$, i.e. there will be a linear relation between pump power and PDC power, this is the low gain. Whereas when $g >> 1$ Equation 2.22 scales exponentially with pump power and this is the high gain. Therefore, the low vs high gain relationship can be understood entirely as the regimes where the down converted energy has a linear or non linear relation with the pump power.

2.2 Sum Frequency Generation

We can start from the same Hamiltonian and momentum operator as we found for parametric down conversion. This time, we consider the generation of one photon from the destruction of two, which equates to changing the operator $\hat{a}_p$ used previously by an operator $\hat{a}_{SFG}$, which describes the up converted field. The evolution of this operator as the pump beams travel through the crystal is:

$$\frac{\partial \hat{a}_{SFG}(\omega, z)}{\partial z} = -i \int_0^\infty d\omega' \beta(\omega, \omega') e^{i\Delta k(\omega,\omega')z} \hat{a}_s(\omega', z) \hat{a}_i(\omega - \omega', z), \tag{2.23}$$

where $\beta(\omega, \omega')$ is:

$$\beta(\omega, \omega') = \chi(\omega, \omega') \sqrt{\frac{\hbar\omega\omega'(\omega - \omega')}{16\pi\epsilon_0 c^2 S n_{SFG}(\omega) n_s(\omega') n_i(\omega - \omega')}}, \tag{2.24}$$

and Δk is given by:

$$\Delta k(\omega, \omega') = k_{SFG}(\omega) - k_s(\omega') - k_i(\omega - \omega'). \tag{2.25}$$

The operators $\hat{a}_s$ and $\hat{a}_i$ represent the pump fields. If we take the undepleted pump approximation, we can neglect the positional dependence on these operators and integrate Equation 2.23:

$$\begin{aligned}\hat{a}_{SFG}(\omega, z) = \hat{a}_{SFG}(\omega, 0) - iL \int_0^\infty d\omega' e^{i\Delta k(\omega,\omega')L/2} \operatorname{sinc}\left\{\Delta k(\omega, \omega')L/2\right\} \\ \times \beta(\omega, \omega')\hat{a}_s(\omega')\hat{a}_i(\omega - \omega').\end{aligned} \tag{2.26}$$

where L is the length of the crystal, and all other coefficients have been defined previously. The generated photon flux after propagating through a crystal of length L from a pump state $|\phi\rangle$ is then described by the equation:

$$N_{SFG}(t, L) = \int_0^\infty d\omega_1 \int_0^\infty d\omega_2 \, \langle\phi| \, \hat{a}^\dagger_{SFG}(\omega_1, L) e^{i\omega_1 t} \hat{a}_{SFG}(\omega_2, L) e^{-i\omega_2 t} \, |\phi\rangle \, . \tag{2.27}$$

2.2.1 Entangled Sum Frequency Generation

Equation 2.27 holds for any pump state $|\phi\rangle$, we will now explicitly consider the effect of pumping this process with the PDC state. The term inside of the integral in Equation 2.27 will be:

$$\begin{aligned}\hat{a}^\dagger_{SFG}(\omega_1, L) e^{i\omega_1 t} \hat{a}_{SFG}(\omega_2, L) e^{-i\omega_2 t} = L^2 \int_0^\infty d\omega' \int_0^\infty d\omega'' e^{i(\omega_1 - \omega_2)t} e^{i\{\Delta k(\omega_2, \omega'') - \Delta k(\omega_1, \omega')\}L/2} \\ \times \operatorname{sinc}[\Delta k(\omega_1, \omega')L/2] \operatorname{sinc}[\Delta k(\omega_2, \omega'')L/2] \beta(\omega_1, \omega')\beta(\omega_2, \omega'') \\ \times \hat{a}^\dagger_s(\omega')\hat{a}^\dagger_i(\omega_1 - \omega')\hat{a}_s(\omega'')\hat{a}_i(\omega_2 - \omega'').\end{aligned} \tag{2.28}$$

When the pump field is PDC generated by a crystal of length L', the pump operators $\hat{a}_s$ and $\hat{a}_i$ will be:

$$\begin{aligned}\hat{a}_s(\omega, L') = &\left(\cosh\big(\Gamma(\omega)L'\big) + \frac{i\Delta k(\omega)}{2\Gamma(\omega)}\sinh\big(\Gamma(\omega)L'\big)\right)\hat{a}_s(\omega,0)e^{-i\Delta k(\omega)L'/2} \\ &-\frac{i\beta(\omega)}{\Gamma(\omega)}\sinh\big(\Gamma(\omega)L'\big)e^{-i\Delta k(\omega)L'/2}\int_0^\infty d\omega_p A_p(\omega_p)\hat{a}_i^\dagger(\omega_p-\omega,0),\end{aligned} \tag{2.29}$$

$$\begin{aligned}\hat{a}_i(\omega_p-\omega, L') = &\left(\cosh\big(\Gamma(\omega)L'\big) + \frac{i\Delta k(\omega)}{2\Gamma(\omega)}\sinh\big(\Gamma(\omega)L'\big)\right)\hat{a}_i(\omega_p-\omega,0)e^{-i\Delta k(\omega)L'/2} \\ &-\frac{i\beta(\omega)}{\Gamma(\omega)}\sinh\big(\Gamma(\omega)L'\big)e^{-i\Delta k(\omega)L'/2}\int_0^\infty d\omega_p A_p(\omega_p)\hat{a}_s^\dagger(\omega,0).\end{aligned} \tag{2.30}$$

Throughout this work, we have chosen to examine interactions with the same phase matching conditions for the PDC and SFG processes. This simplification has been made when constructing Equation 2.28 as the phase matching information is contained within the β term (Equation 2.24) which is shared with the Γ terms in equations 2.29 and 2.30 (the full expression for Γ is shown in Equation 2.17). We could relax this by taking a new value for β, β', for the SFG interaction. However, we chose to examine the same crystal and therefore the same phase matching conditions in both down and up conversion crystals. Continuing, we will define two complex variables:

$$C(\omega, L') = \left(\cosh\big(\Gamma(\omega)L'\big) + \frac{i\Delta k(\omega)}{2\Gamma(\omega)}\sinh\big(\Gamma(\omega)L'\big)\right)e^{-i\Delta k(\omega)L'/2}, \tag{2.31}$$

$$D(\omega, L') = -\frac{i\beta(\omega)}{\Gamma(\omega)}\sinh\big(\Gamma(\omega)L'\big)e^{-i\Delta k(\omega)L'/2}. \tag{2.32}$$

The full expression contains 16 terms (attained by substituting Equations 2.29 and 2.30 into Equation 2.28). However we can reduce the number of terms if we recall that our intentions are to take the expectation value of this quantity and apply the vacuum state (i.e. $|\phi\rangle \rightarrow |0\rangle$). Therefore, any terms which contain an unbalanced number of creation or annulation operators (more or fewer creation operators than annihilation operators) and any term that applies an annihilation operator directly on the vacuum will definitely be zero. This also forces us to make the substitutions $\omega_1 = \omega_2 = \omega_p$ and

$\omega' = \omega'' = \omega$ in Equation 2.28 as these definitions contain the only non zero terms. Equations 2.28 becomes:

$$\begin{aligned}\hat{a}^\dagger_{SFG}(\omega_1, L)e^{i\omega_1 t}\hat{a}_{SFG}(\omega_2, L)e^{-i\omega_2 t} = L^2 \int_0^\infty d\omega \int_0^\infty d\omega_p \,\mathrm{sinc}^2\left[\Delta k(\omega_p, \omega)L/2\right] \beta^2(\omega_p, \omega) \\ \times \Big\{ |D(\omega, L')|^2 |C(\omega, L')|^2 |A_p(\omega_p)|^2 \hat{a}_i(\omega_p - \omega, 0)\hat{a}^\dagger_i(\omega_p - \omega, 0)\hat{a}_s(\omega, 0)\hat{a}^\dagger_s(\omega, 0) \\ + |D(\omega, L')|^4 |A_p(\omega_p)|^4 \hat{a}_s(\omega, 0)\hat{a}_i(\omega_p - \omega, 0)\hat{a}^\dagger_i(\omega_p - \omega, 0)\hat{a}^\dagger_s(\omega, 0) \Big\}.\end{aligned} \tag{2.33}$$

For simplicity these are the explicit expressions of $|C(\omega, L')|^2$ and $|D(\omega, L')|^2$:

$$|C(\omega, L')|^2 = \cosh^2(\Gamma(\omega)L') + \frac{\Delta k^2(\omega)}{4\Gamma^2(\omega)} \sinh^2(\Gamma(\omega)L'), \tag{2.34}$$

$$|D(\omega, L')|^2 = \frac{\beta^2(\omega)}{\Gamma^2(\omega)} \sinh^2(\Gamma(\omega)L'). \tag{2.35}$$

Note $\Gamma(\omega)$ is generically complex as if $\Delta k^2/4 > 2\pi P_p \beta^2(\omega)$ then Γ is imaginary however, it can only be purely real or purely imaginary. Therefore, in the limit where Γ is purely imaginary we may write:

$$\begin{aligned}\cosh\big(-i|\Gamma(\omega)|L'\big) &= \cosh\big(i|\Gamma(\omega)|L'\big), \\ \frac{\sinh(-i|\Gamma(\omega)|L')}{-i|\Gamma(\omega)|} &= \frac{\sinh(i|\Gamma(\omega)|L')}{i|\Gamma(\omega)|}.\end{aligned}$$

Therefore, $|C(\omega, L')|^2$ and $|D(\omega, L')|^2$ may take the form as in 2.34 and 2.35 without loss of generality.

2.2.2 Coherent vs Incoherent eSFG

There are two terms in Equation 2.33 which correspond to the down converted state interacting in different manors. The first is the term

$$\hat{a}_i(\omega_p - \omega, 0)\hat{a}^\dagger_i(\omega_p - \omega, 0)\hat{a}_s(\omega, 0)\hat{a}^\dagger_s(\omega, 0). \tag{2.36}$$

If we consider the operators acting on the vacuum state on the right, we produce a single photon which instantly gets destroyed and then produce a second photon which likewise

instantly gets destroyed. This corresponds to the vacuum state simply being multiplied by two scalars. In order for this to occur, the entire twin beam state must be present at the recombination event and so, we will refer to this as coherent recombination. The second term is

$$\hat{a}_s(\omega,0)\hat{a}_i(\omega_p-\omega,0)\hat{a}_i^\dagger(\omega_p-\omega,0)\hat{a}_s^\dagger(\omega,0). \tag{2.37}$$

This component does not require the entire down converted state to be present as two creation operators appear first on the right hand side of the expression therefore in principle, any down converted photons produced at the down converted crystal can stimulate this component and not just the twin beam state (the individual pairs of photons). As we are investigating entangled sum frequency generation, when two entangled photons interact, they will reconstruct the fundamental pump which, as we pump with a coherent laser, will be coherent as well. This is an alternative meaning to the coherent component, the component of eSFG which is a coherent field.

By taking the well phase matched limit, $\Delta k(\omega)^2/4 << 2\pi P_p\beta(\omega)^2$, $\Gamma \approx \sqrt{2\pi P_p\beta(\omega)^2}$ we can more easily see the relationship between PDC power and up converted power. In this limit, the term in Equation 2.33 which is proportional to 2.36 will be multiplied by the coefficient:

$$\frac{1}{2\pi\beta(\omega)^2}\cosh^2(\Gamma(\omega)L')\times\sinh^2(\Gamma(\omega)L'). \tag{2.38}$$

Remembering the number of down converted photons for PDC is proportional to $N_{pdc}\propto\sinh^2(\Gamma L')$, we can explicitly write this in terms of the number of PDC photon, N_{pdc}:

$$N^{Coherent}_{Up\ converted\ photons}\propto N_{pdc}+N_{pdc}^2. \tag{2.39}$$

This is the term in Equation 2.33 which corresponds to pairs of photons produced in the down conversion crystal coherently recombining at the up conversion crystal. This is the component of the up converted state which can be considered 'quantum' as it is only present because the down converted field is comprised of entangled pairs of photons. It is important to note that in the low photon limit ($N_{pdc} << 1$), this term is linearly proportional to the number of down converted photons, as expected, but also

contains a second order component. Generally, it has been said that a linear relationship between the number of down converted photons and number of up converted photons or rate of absorption displays quantum interactions. However, we can also see that the same interactions, between individual pairs of photons, also give rise to a second order relationship between the number of down converted photons and up converted photons which is typically thought of as the classical relationship. If we go on to consider the term in Equation 2.33 proportional to the term in Equation 2.37, in the well phase matched limit, this will be multiplied by a different coefficient:

$$\frac{1}{4\pi^2\beta(\omega)^4}\sinh^4(\Gamma(\omega)L') \tag{2.40}$$

or explicitly in terms of PDC photon number, N_{pdc}:

$$N^{Incoherent}_{Up\ converted\ photons} \propto N^2_{pdc}. \tag{2.41}$$

This component displays a pure second order relationship between number of PDC photons and up converted photons and therefore corresponds to purely classical behaviour. We shouldn't be surprised by this fact as the term which we have called the incoherent component is proportional to the second order correlation function which can be non zero for classical fields unlike the coherent component.

2.2.3 Experimental Design

In order to stimulate efficient eSFG, we have to preserve our down converted state and reconstruct it in time, space, and phase. This corresponds to imaging the down converted state inside the up conversion sample. The simplest way of doing this is with a 4f system, which we will exploit. However, we also have a broadband state, and we are therefore aware that chromatic dispersion has a detrimental effect on the efficiency of up conversion. For this reason, we forgo the use of lenses and instead utilise a pair of 204 mm effective focal length, one inch in diameter 45 degree parabolic mirrors to project the down converted state into the far field with respect to the down conversion crystal plane. For the same reasons, transmissive optics were avoided throughout the

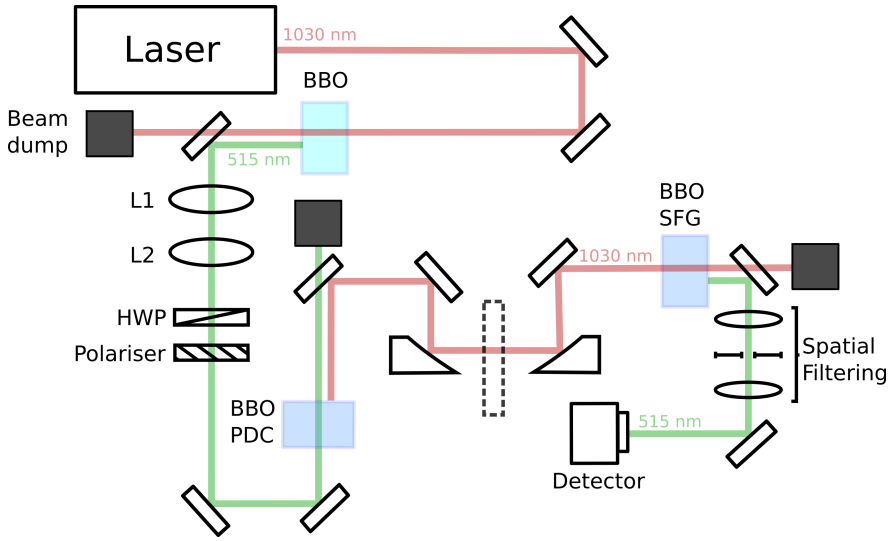

Figure 2.1: Experimental layout with parabolic mirrors used for imaging. L1 and L2 are a pair of lenses used to form a telescope to control the PDC pump beam size. The half wave plate (HWP) and polariser pair were the control mechanisms of the PDC gain, and the grey dashed box shows the approximate position of the PDC far field where additional filtering was placed.

design.

The experimental design is shown in Figure 2.1 slightly simplified. We employed a 40 W pulsed laser at 1030 nm with a pulse duration of 245 fs and a variable repetition rate, operating at both 200 kHz and 500 kHz throughout the experiments (Light Conversion Carbide CB3-40 W), for our fundamental beam. We frequency doubled the beam in a 1 mm long type I BBO crystal to produce our PDC pump at 515 nm. In order to maximise the efficiency of this up conversion process, we have a telescope before the up conversion crystal (not shown in Figure 2.1) formed by a focal length 300 mm UVSF thin lens and a negative 100 mm focal length UVSF lens (Eksma optics) both anti reflected coated for 1030 nm wavelength. This telescope ensures that the maximum efficiency of the up conversion process is $\sim$ 60 %.

The PDC pump beam size is controlled with a non focusing telescope increasing the beam size after the beam is frequency doubled formed by a negative lens, L1 (-100 mm focal length UVSF thin lens from Eksma Optics) and a positive lens, L2 (+200 mm focal length UVSF thin lens from Eksma Optics). The PDC pump power is varied with a half wave plate and polariser prior to the down conversion crystal. Because we

utilise a very high intensity pump, we struggled to reduce the pump leakage through the system below any potential signal which will be emitted around the same wavelength and, therefore, can unintentionally become mistaken for one another. We also want to avoid absorptive optics as they will burn if placed directly in the pump path and introduce unwanted dispersion in the down converted state. We require the pump to be well below the power of the down converted field. The highest the pump power can reach is of the order of magnitude of $\sim$ 10 W, and the highest PDC power this can generate is in the order of magnitude of $\sim$ 100 nW. Therefore, we require more than eight orders of magnitude of filtering to be confident in the signal we see. The majority of this filtering is done with the use of dielectric mirrors (Layertec custom made) with $\sim$ 1% reflection at 515 nm (optical density of 2). There are four of these mirrors in the far field (not depicted in Figure 2.1) as well as a total of three routing the field before and after the parabolic mirrors. These are supplemented with the use of long pass filters (usually Thorlabs FELH0700 with an optical density $\sim$ 5 at 515 nm) in the PDC far field necessary to remove scattered pump not directly along the beam path and further filtered with a bandpass filter (Brightline FF01-1055/70-25, optical density of $\sim$ 6 at 515 nm) which removes unwanted components of the down converted state.

After the field has been up converted in a 2 mm long type I BBO crystal, the eSFG is sent through a telescope with an iris in the far field. In this plane, the two components of the down converted field, coherent and incoherent, are seen as a bright spot containing the coherent contribution and a large diffuse area containing the incoherent component. This is because the geometry of the two components differ. The coherent component reconstructs the pump field, and therefore, as we pump the PDC crystal with a collimated beam, it will also be collimated. The incoherent component, however, does not have any such constraints and will therefore be emitted in the geometry of the down converted field, which in this case is a cone around the coherent component. By closing the iris in the far field of the eSFG, we can select for coherent eSFG only, allowing us to focus our attention on the quantum component we want to investigate. Often, after this filtering, the field is focused to increase the signal-to-noise ratio or ensure the whole field fits on the detector, not shown in Figure 2.1.

Chapter 3

PDC Characterisation

Parametric down conversion (PDC) is a second order nonlinear process in which a single pump photon is annihilated and two daughter photons, conventionally called signal and idler, are produced. This process can be seeded from the vacuum and it is then referred to as spontaneous parametric down conversion. In this case, the final state is referred to as a squeezed vacuum and composed of entangled pairs of photons. The squeezed vacuum is a useful resource in quantum experiments. The focus of this thesis is to explore the potential of this state. Before delving into this, we will explore some of the nuances of PDCs behaviour. In particular, we will attempt to experimentally determine the phase matching constraints of the down converted interaction in a BBO crystal, the crystal that we will be using throughout this thesis. This is important as these constraints determine the spatial and temporal properties of the down converted state. We will consider the simple case of type I parametric down conversion in BBO and comment on the spatial properties of the down converted state by analysing an image of the far-field emission pattern acquired after filtering the PDC with a narrow band filter (Thorlabs FLH1030-10). Furthermore, we will describe the spectral properties of the down converted state in the near field. We will outline a physical understanding of the down converted modes and give an overview of two distinct methods of determining the number of down converted modes experimentally, weighing the pros and cons of both methods. Finally, the chapter resolves with a novel discussion of the effects of gain on the PDC near field and its clear consequences on entangled two photon interaction.

The remaining chapter will be primarily experimental. During this process I worked closely with several contributors. For the data presented in this chapter, I worked closely with a lab partner to mount the experiments and collect the data. The analysis was done by me with scrutiny from my collaborators. The model presented in Section 3.4.1 for the PDC near field size in the high gain limit was developed solely by me.

3.1 PDC Phase Matching

Parametric down conversion must fulfil both conservations of energy and momentum. We can see from Equation 2.17 that some momentum mismatch is permissible. The effects of phase mismatch can be characterised by the following function when pumped with a continuous wave laser:

$$\Phi(L, \omega_p, \omega_s, \omega_i) = \mathrm{sinc}^2\left(\frac{\Delta k(\omega_p, \omega_s, \omega_i)L}{2}\right), \tag{3.1}$$

which is the $\sinh^2(\Gamma L)$ term in the weak phase matched limit, $\Delta k(\omega)^2/4 >> 2\pi P_p \beta(\omega)^2$ as this will permit the largest possible bandwidth. By solving Equation 3.1 and conserving energy:

$$\omega_p = \omega_s + \omega_i, \tag{3.2}$$

we can build up the expected relationship between transverse momentum and frequency of the down converted field. Even though we stimulated the down conversion with a short pulsed laser, we can still use these phase matching conditions as a good approximation for ours as phase matching is mostly a property of the crystal used to preform parametric down conversion rather then the pump field. Note, Equation 3.1 only considers the longitudinal momentum (momentum mismatch along the pump's propagation direction). We can trivially include the transverse momentum in the phase matching as in [56] by considering the finite transverse size of the pump. However, in this work we are only considering short crystals, operating in the low gain and, pump beams with large transverse sizes. All of these properties mean that large momentum bandwidths are possible and this reduces the dependence on the transverse momentum

to the point that it does not have a noticeable effect when tuning the phase matching curve. Calculating phase matching characteristics can be a handy tool when designing bulk experiments with short crystals where the weak phase-matched limit largely holds.

Solving these equations simultaneously is a challenging task, however. Parametric down conversion is stimulated in crystal structures, which allow for a none zero second order component of the polarisation operator; however, by the very nature of these crystals, the refractive index must have a dependence not only on the wavelength of light but also on the light polarisation, propagation direction and, the temperature of the crystal however, BBO does not have a strong dependence on temperature and therefore I will ignore this dependence in the following. Therefore Δk has a dependence in all three spatial dimensions, wavelength and polarisation:

$$\Delta\vec{k} = \vec{k}_p - \vec{k}_s - \vec{k}_i = \left[\frac{n(\lambda_p, \hat{s}_p)}{\lambda_p}\hat{s}_p - \frac{n(\lambda_s, \hat{s}_s)}{\lambda_s}\hat{s}_s - \frac{n(\lambda_i, \hat{s}_i)}{\lambda_i}\hat{s}_i\right] c, \tag{3.3}$$

where $\hat{s}_m$ are unit vectors in the m^{th} field propagation direction and, λ_m and $n(\lambda_m, \hat{s}_m)$ are the wavelength in vacuum and refractive index of the m^{th} field respectively. The polarisation and propagation properties of the field allow for the phase matching conditions to be met inside of the crystals. When phase matching is achieved with only the use of propagation direction of the pump field in the crystal and the polarisation of the fields, this is called critical phase matching. This is the method we will be using to phase match crystals throughout this work. Phase matching is split into three different types encapsulating the polarisation relationship between the pump and down converted field. In type 0, all of the down converted fields are polarised parallel to one another. For type I, the down converted fields are parallel but orthogonal to the pump and type II, the two down converted fields are orthogonal to one another. We will focus on type I which is the type used throughout this work. Even with this decision made, we still have three spatial dimensions to consider and three reference frames: the lab frame where the experiment is conducted, the crystal frame where the refractive indices are known and the pump frame where $\Delta\vec{k}$ is most simply understood (note, we can however trivially combine the lab frame and pump beam frame by deciding the beam propagates along the Z axis in the lab). A good explanation of how to deal with many

of the issues with solving these equations is given in [57]. We can create a program with the following procedure in order to solve for the phase matching conditions:

1. Select the pump wavelength (λ_p), polarisation, pump propagation direction with respect to the crystal axis (θ_p,ϕ_p) and temperature if the crystal has a strong dependence. Calculate the refractive index of the pump field (n_p). With this, we have all of the information to determine the pump field's angular wave vector, $\vec{k_p}$, inside of the crystal. It is convenient to rotate $\vec{k_p}$ so the pump propagates along the z-axis; this is the pump propagation direction (PPD).

2. Define a range of down converted wavelengths (λ_s) and, using conservation of energy between the pump and two down converted fields, calculate the corresponding partner wavelength (λ_i). The polarisations of the down converted fields should also be set here.

3. Define a search range of down converted angles (θ_s) in the PPD (from zero to some, usually small, value). This is done in the PPD as we can trivially set this to be the lab frame. In this reference frame, we only need to define one angle as the down converted fields are, to a good approximation, emitted symmetrically.

4. Start a parameter search by calculating the refractive index for each wavelength (λ_s) and angle (θ_s), we can either repeat this process for all the partner wavelengths (λ_i) or take [57]:

$$\theta_i = \arcsin\left(\frac{n_s \sin(\theta_s)}{\sqrt{n_s^2 + n_p^2 \frac{\lambda_s^2}{\lambda_p^2} - 2n_s n_p \frac{\lambda_s}{\lambda_p}\cos(\theta_s)}}\right) \tag{3.4}$$

   as an approximation. This equation assumes perfect phase matching, i.e. $\delta k = 0$. It is not correct to do so as there is no perfect phase matching for all wavelengths, and this could reduce the number of solutions found for which $\delta k \neq 0$ however, practically, little difference has been found between the results obtained by manually cycling through both down conversion angles and using Equation

3.4. The computation time is significantly reduced with the use of Equation 3.4, and therefore, I would suggest using this.

5. Project all $\vec{k}$ vectors into the PPD and calculate $\Delta\vec{k}$, we could consider all dimensions by modifying Equation 3.1 however, we can essentially get the same result by selecting for the z-component in this frame and substitute this into the current Equation 3.1. We can either take this to be the result itself, the perfect phase matched solutions will give a value of 1. By saving the values found and θ_i's calculated, one can use this data to create colour plots such as in Figure 3.2 or be used as a launching point for a searching algorithm.

6. If we want to carry on, the angle and wavelengths which maximise Equation 3.1 can be used as a first guess for a two-dimensional Newton-Raphson method to find the exact solution for minimising $\Delta\vec{k}$. Care must be taken to ensure the correct reference frames are maintained. It is possible to do this in order to speed up the program; however, if the initial angle space is already finely sampled, the results will not be appreciably better and this may considerably increase computation time.

The program outlined above is very general and can be incredibly powerful, provided we are able to find the refractive indices of the field propagating in a general direction through a crystal. For my program, I collected the required crystal information from 'Nonlinear Optical Crystals: A Complete Survey' [58] and developed the capability to find the refractive index in a general direction of a large group of crystals using the work of Dmitriev and Nikogosyan [59]. Modifications can be made to calculate critically phase matched angles, temperature dependence, and poling lengths for quasi-phase matched crystals [60], and the results are made more accurate by taking into account spatial and temporal walk-off [61] by modifying the phase mismatch equation, $\Delta\vec{k}$.

Examples of the graphics produced by this program are shown in Figures 3.1 and 3.2. Both are calculated for a BBO crystal pumped with a 515 nm field cut for type I phase matching, the crystal that will be used throughout this work. In figure 3.1 we show

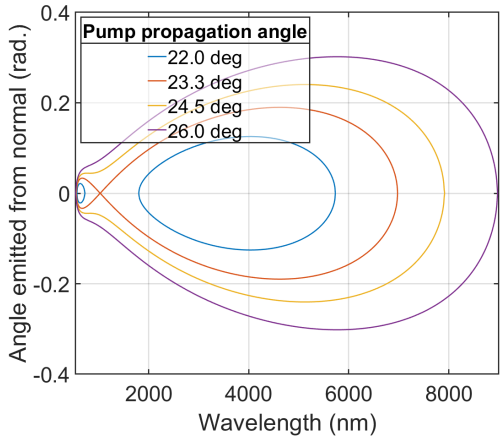

Figure 3.1: Phase matching curved for Barium borate (BBO) crystals for increasing angle between crystal axis and PDC pump propagation direction.

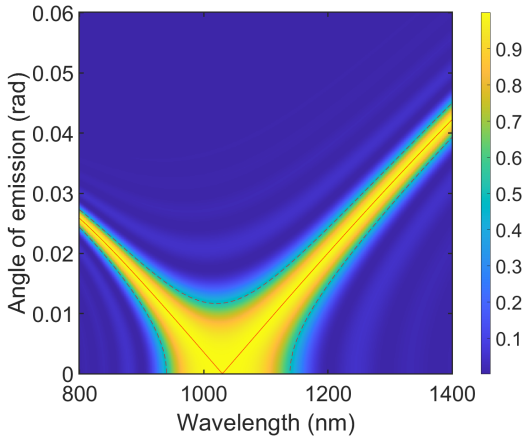

Figure 3.2: Phase matching around degeneracy density plot. Yellow shows the highest probability of down conversion, blue shows no probability of down conversion.

the perfect phase matching angles found from a Newton-Raphson method to minimise $\Delta\vec{k}$ at varying angles between the pump propagation direction and the crystal axis. The blue curve displays the phase matching found with the smallest angle between the pump and crystal axis (0.401 rad), and the angles increase through to the purple curve. From this figure, we can gain some intuition on the phase matching characteristics of BBO. As the angle is increased, a larger proportion of the down converted field is emitted at an angle to the pump beam and therefore, the field is seen as a ring around the pump far from the crystal. The orange curve is a special case where the degenerate down converted fields (both fields with equal energies, of half the pump) are emitted collinearly with the pump field. This arrangement conventionally maximises overlap between all three fields and, therefore, offers the greatest chance for highly efficient down conversion. The program found that collinear degenerate emission occurs in a type I BBO crystal for a 515 nm pump at an angle of 0.407 radians between the crystal axis and pump beam. Figure 3.2 shows the case close to the degenerate wavelength with the solid red curve showing perfect phase matching and the red dashed line showing the point at where half of the maximum intensity is reached. The background is a density plot where Equation 3.1 is evaluated at each point.

3.1.1 Experimentally Determining Phase Matching

As the bulk of the work to determine the phase matching conditions theoretically has been done by developing the program outlined in the previous section, it makes sense to think about how these affect the field seen in the lab. The angles of emission plotted in Figures 3.1 and 3.2 are defined from the pump beam. When we do not have, or may neglect walk off, there is a rotational symmetry around this point, and therefore, for type I down conversion, the PDC will be emitted in a cone with entangled pairs on opposite sides of the pump beam. As such, in the far field of the crystal, the PDC will either be seen as a spot or a ring depending on the phase matching condition of the crystal and filtering of the down converted field. Figure 3.3 shows a typical view of the PDC far field in use throughout this work. This field is produced by a 2 mm BBO crystal pumped by a 515 nm pump with a 10 nm band-pass filter (Thorlabs FLH1030-10) centred at 1030 nm filtering the down converted field.

We can use the program above to attempt to determine the angle between the crystal axis and pump propagation direction with only a calibrated (in momentum, k, space or angle of emission) image of the far field as our experimental data point. From the calibrated image, we can determine the centre of emission (as in Figure 3.3) and calculate the intensity of light emitted in annuli of constant width radiating out from

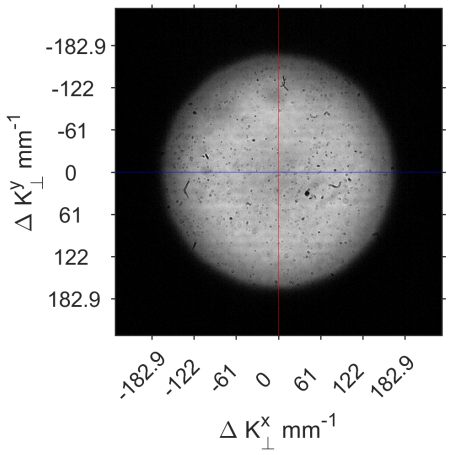

Figure 3.3: PDC far field with a 10 nm bandpass filter on camera centred on 1030 nm.

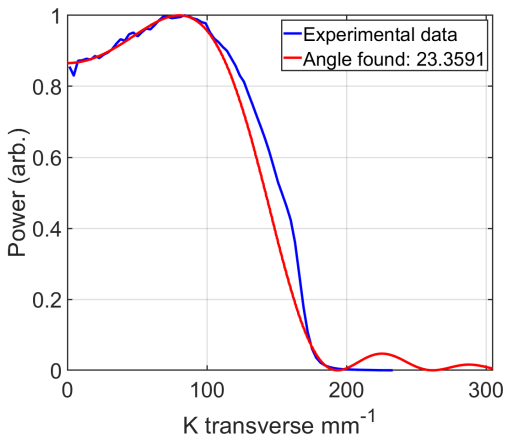

Figure 3.4: Intensity of PDC emitted at angle from pump propagation direction.

that centre. This provides us with a new calibration where we can see the intensity of radiation emitted at each angle relative to the pump propagation direction. The result of this can be seen in the blue line of Figure 3.4, which is normalised into transverse momentum space (assuming that the light emitted is purely 1030 nm). The purpose of this procedure is to make it possible to compare the data from the image to the output of the program. The program provides us with the lab frame angle of emission between the pump beam propagation and down converted radiation. Suppose we produce the full density plots as in Figure 3.2, we can then also find the relative intensity of the generated radiation across the full spectrum of the down converted field. This can be compared to our intensity data from the image once we factor in the filtering present when the image was taken, which can be done by applying the spectral response of the filter to the density plot. Then, as there is no way to distinguish between different wavelengths on our camera, which has a very flat response profile around 1030 nm, we need to reduce the density plot so we only consider the relative intensity emitted at each angle. In Figure 3.2, the wavelength-angle space is split into pixels, and each is ascribed a value. These values correspond to the maximum value of Equations 3.1, which can be found for a down converted field at that angle and wavelength. Once the filter is applied, we can remove any wavelength dependence by adding up the values found at each angle, and finally, we have a data set that can be compared precisely with the intensity data from the image. Finally, in order to determine the angle between the crystal axis and pump propagation direction, we tune this angle in the program to maximise the R squared value between the data sets from the image and program. The result of this procedure is shown in Figure 3.4 with a theoretical phase matching angle of approximately 23.4 degrees.

3.2 Spectrum of Down Converted field

We expect that the spectrum of our down converted field to be very broad. In order to control this spectrum, we intend to filter the down converted field with a bandpass filter. In order to understand the effect that the other components have on the down converted field, we should take a full spectrum of the PDC, which reaches the up

conversion crystal. This will also allow us to identify any issues with our experimental design. As a reminder, we have a BBO crystal pumped by a pulsed 245 fs laser at a repetition rate of 200 kHz. The pump is separated from the down converted field with the use of 7 dielectric mirrors with less than 1 % reflection at 515 nm and greater than 99.9 % reflection between 900 nm and 1200 nm placed after the down conversion and before the sample position and in order to exclude scattering of the pump field close to the crystal, a 850 nm long pass filter is placed in the far field of the PDC. The PDC is projected into the far field for the crystal by an off-axis parabolic mirror and re-imaged with a second in a 4-f configuration. We do not need to resolve the spectrum in space and, therefore, take the spectrum of the near field where that information is absent. The alteration to the experimental design is shown in Figure 3.5. The PDC was rerouted after where the second crystal would be placed, though nothing was present. It was re-projected into the near field by two 100 mm lenses and routed with a silver mirror to ensure minimal effect on the final spectrum. The spectrum was taken with an Andor Shamrock 163, a Czerny-Turner spectrometer. With this kind of spectrometer, the spectral information is encoded in the plane orthogonal to the diffraction grating, which, when in the orientation we have during this measurement, translates to the horizontal spatial dimension. Due to the wavelengths of interest, we

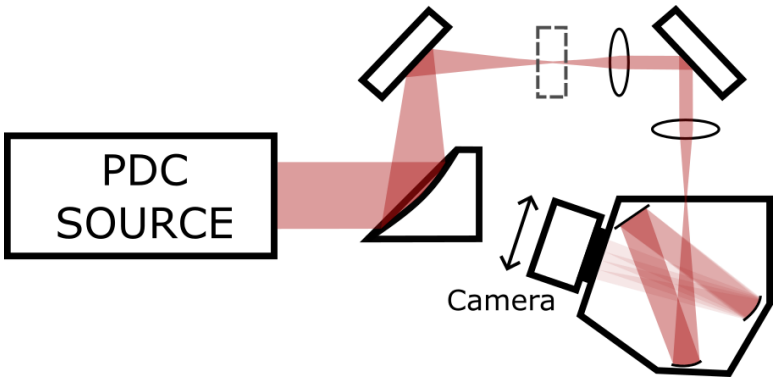

Figure 3.5: Arrangement for taking near field PDC spectrum. The Shamrock 163 from Andor instruments was used to produced the spectrum. It uses 163 mm focal length spherical mirrors and a 600 lines per mm grating (SR1-GRT-0600-1200). The CCD camera (LUCID vision labs Atlas SWIR) had to be placed on a translation stage perpendicular to the spectrum's exit propagation direction in order to take the full spectrum.

chose to use a non-standard camera for this spectrometer, a LUCID vision labs Atlas SWIR camera that includes a Sony IMX990 InGaAs sensor with a broadband response in the NIR region of the spectrum. This is a physically small sensor that cannot fit the entire spectrum. Therefore, this camera was placed on a translation stage orientated orthogonally to the output facet of the spectrometer. This allows us to take the full spectrum but requires manual calibration and post-processing.

To this end, spectra at each camera position was taken with reference wavelengths produced by a mixture of laser lines and known calibrated filters. The camera was then translated, and it was ensured that one of these reference lines was still present on the sensor, and the process repeated. After all of these spectra were collected, we could stitch the data together with the use of the common reference lines. These reference lines are re-normalised to be on the longer, stitched-together sensor and are fitted with a second order polynomial to generate the pixel vs wavelength calibration. The final spectrum is shown in Figure 3.6.

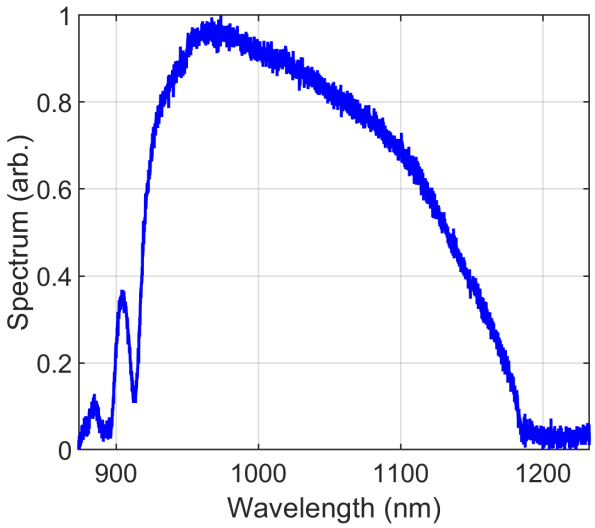

Figure 3.6: PDC spectrum in wavelength space, corrected for the spectral response of both the camera and grating.

3.2.1 Features of the PDC Spectrum

The short wavelength components which appear to oscillate are a consequence of the mirrors used to filter out the pump. The long wavelength cut off is due to the spatial filtering introduced by the size of the optics in use. The main feature present is the asymmetry of the spectrum around the degenerate condition. This is expected due to the asymmetry present in wavelength space from the conservation of energy condition. The down converted photons are emitted on either side of the pump wavelength; however, the range of wavelengths they are emitted over differs (see Figure 3.1, note the same number of photons are emitted either side of the degenerate wavelength, 1030 nm). In frequency space however, we expect the spectrum to be symmetric. We therefore will recalibrate this spectrum into frequency space to ensure this is the case. When doing this, we have to take care to normalise the spectrum appropriately. The spectrum in wavelength space, $S(\lambda)$, is defined such that:

$$\int^{\infty} S(\lambda)\, d\lambda = E, \tag{3.5}$$

where E is a measurement of the energy present in the spectrum. We need to define an equation in frequency space, $S'(\omega)$, which preserves this relationship:

$$\int^{\infty} S(\lambda)\, d\lambda = \int^{\infty} S'(\omega)\, d\omega. \tag{3.6}$$

Starting from the left hand side of Equation 3.6 and remembering

$$\omega = \frac{2\pi c}{\lambda}, \tag{3.7}$$

we substitute $d\omega / d\omega$:

$$\int^{\infty} S(\lambda) \frac{d\lambda}{d\omega}\, d\omega = \int^{\infty} \frac{2\pi c}{\omega^2} S(\lambda(\omega))\, d\omega = \int^{\infty} S'(\omega)\, d\omega. \tag{3.8}$$

Simply reading off

$$S'(\omega) = \frac{2\pi c}{\omega^2} S(\lambda). \tag{3.9}$$

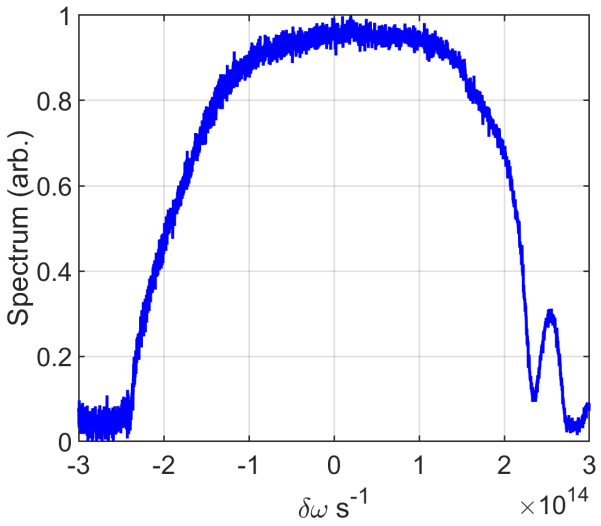

Figure 3.7: PDC spectrum in frequency space centred on the central wavelength of the pdc, 1030nm.

This calibration of the spectrum ensures that the interpretation of the spectrum as the intensity of light remains consistent between wavelength and frequency. The result of this re-calibration is seen in Figure 3.7 with the frequencies centred on the degenerate frequency. From this, we can see the expected symmetry of the down converted spectrum. We can also see that this symmetry appears to fall away at frequencies greater than 1×10^{14} rad Hz different from the central frequencies, which correspond to wavelengths of $\sim$ 1090 nm and $\sim$ 975 nm. This range also corresponds well to the range over which it is expected that the group delay dispersion of the optics we use to filter is low enough to ensure the preservation of the temporal overlap between conjugate frequency modes as calculated by the manufacturer. For these reasons, it appears necessary to filter the down converted field as a large proportion of the measured PDC field will not be able to under go entangled two photon interactions, either due to one of the entangled photons getting scattered or through dispersion preventing temporal overlap between entangled photons.

3.2.2 Spectrum Calibration

By the nature of the field we are interested in, we require to calibrate the spectrum over a large range of wavelengths and we do not have reference lines for the entire spectrum. The conventional way of calibration is to acquire several values of pixel positions and wavelengths with the use of known frequency reference lasers and fit these values with a first, second or third order polynomial. Inside the range for which calibration values are obtained, this is an efficient and accurate method, however, it quickly succumbs to high error outside of this region. Liu and Hennelly [62] presented a method which involved modelling the spectrometer and derive equations for the relationship between pixel position and wavelength [62]:

$$\lambda = -d' \left[\sin\left(\tan^{-1}\left(\frac{xT - C}{f} \right) + \alpha - \theta \right) + \sin(-\alpha - \theta) \right], \tag{3.10}$$

where d' is a measure of the grating period, T is the pixel pitch (distance between pixels), C is the camera centre position (should be zero), f is the focal lengths of the Czerny-Turner spectrometer, α is half the deviation angle of the spectrometer and θ is the grating angle, these are all fitting parameters, x is the pixel position and the variable we are attempting to fit.

When using the model the root mean squared error (RMSE) between the fit and the calibration data points we have is 4.37×10^{-18} meters per pixel whereas the RMSE between the data and the second order fit was found to be 4.67×10^{-18} meters per pixel between fit and data, these fits along with the calibration data can been seen in Figure 3.8 where the green line is the second order fit and the blue the model. The difference does not appear to be significant with just a $\sim 7\%$ decrease in RMSE between using a second order fit and Equation 3.10. However, the difference becomes more evident when moving out of this region. Figure 3.9 displays the difference in the observed spectrum due to the different calibrations, and Figure 3.10 is a direct measurement of the difference between the wavelengths obtained with the polynomial fit and those obtained with the grating model. In the region where calibration data was available (between the red lines) the two fitting methods do not vary by more than 1.3 nm

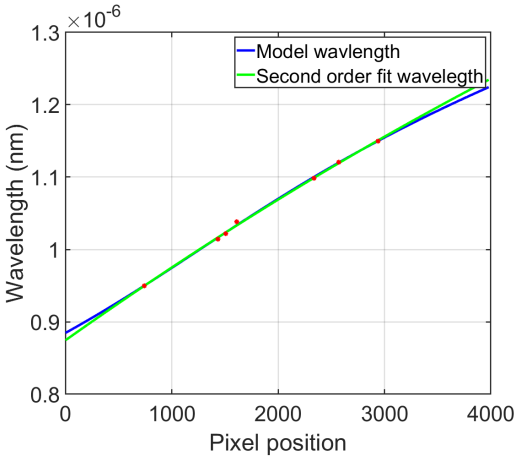

Figure 3.8: The two calibration methods, second order fit in green and model in blue with the data point to fit shown in red.

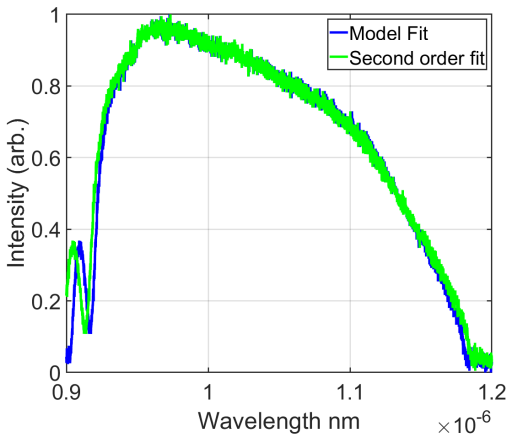

Figure 3.9: Comparison of the spectrum found for second order fit versus a model.

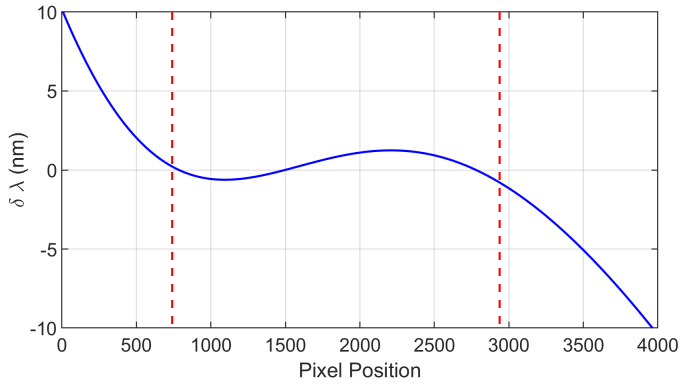

Figure 3.10: In blue the difference between the second order fit and the model fit over the complete range of pixel positions we required. The red dashed lines show the lower and upper limit of the range over which we have calibration data.

however, outside of this region we quickly get a difference close to 10 nm.

Ultimately, in the range of wavelengths which are important to our experiment, the difference is negligible between the two methods and only becomes significant far from degeneracy, which will be filtered away for most measurements and, therefore, can be ignored. Nevertheless, this exercise does raise questions about how we should calibrate spectrometer, particularly for large wavelength ranges.

3.3 Determining the Number of Modes

It should be understood that the behaviour of the down converted state changes between the low and high gain regimes. In the low gain regime, the majority of the down converted photons are produced via spontaneous parametric down conversion, which is stimulated by vacuum fluctuations. Therefore, each mode in the generated field is composed of two photons that can undergo single photon interactions. In the high gain, the down converted field is stimulated from an already present field, whether that be the spontaneous field or an injected one. The down converted field will still have quantum properties, often exploited to get sub shot noise measurements, i.e. for imaging applications [63]. However, the field will contain not only two-photons states but four-photons, six-photons and higher even-photon number states. Therefore, much of the field will not undergo entangled interactions. If we consider the spatial-temporal modes, the difference between the low and high gain can be thought of as having less or more than one photon per mode in the far field of the PDC. Below an average of one photon per mode, most of the near field states will be composed of the two photons and above one, we have introduced $2n$, $n \in \mathbb{Z}^+$, $n > 1$ states into the near field.

For the purposes of this thesis, we will equate modes to the speckles in the PDC near field. Each speckle corresponds to the area in the PDC near field where the down converted pair of photons are generated. As such, in the near field of the down converted crystal, these speckles will be orthogonal as we cannot preform an interference measurement between them and therefore, they can be characterised as a complete set of modes. It will be convenient to have an idea of the number of modes we have present in the down converted field. Ideally, we would take a picture of the far field and count

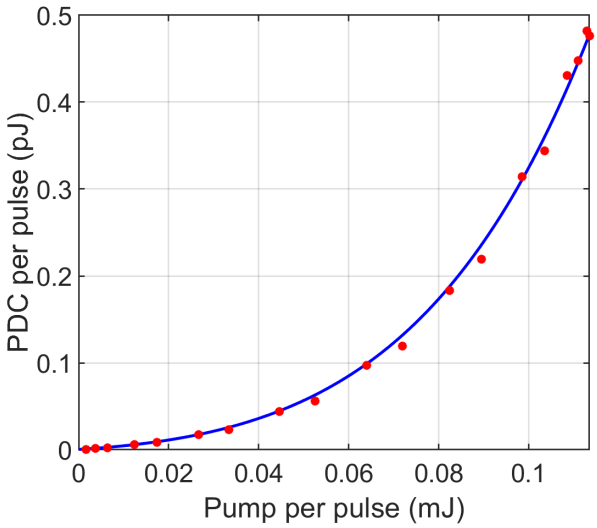

Figure 3.11: PDC energy scaling with incoming pump energy. Data fitted with equation 2.22.

the speckles to estimate the number of spatial modes. However, due to the broadband nature of the down converted field, the modes are small and, therefore, we are unable to resolve them the far field. Furthermore, owing to the gain levels we are interested in, close or at one photon per mode, it takes multiple laser pulses to build up a field we can see with the camera, at which point the mode information is lost. We therefore need a less direct method for determining the number of modes. There are two methods that we use to determine the number of modes experimentally, and these will be outlined below. It should be noted that this is a random process and any value placed on the number of modes can only be considered an average.

3.3.1 Power Law

The first method is by fitting Equation 2.22 to a set of PDC pulse energy vs pump pulse energy data as in Figure 3.11. We can gain some confidence in the validity of Equation 2.22 by considering the derivation in Section 2.1 and in particulate the Equation 2.19 reached at the end. During this derivation, we have assumed a single mode; let us consider what physically happens when we relax this constraint. The spatial-temporal modes that we have been discussing are speckles in the down converted field. They exist

in regions of space-time that cannot interact at the moment of the down-converted field production, i.e. when a twin beam state sits in a mode it cannot be influenced by or influence a different mode. Therefore if we relax the single mode constraint, each mode should scale independently according to Equation 2.19 and the total number of down converted photons will be approximately the number of modes times this or precisely Equation 2.22.

We have to be careful with the calibration of the PDC power, as this is a broadband field. The data was collected with a 70 nm filter (Brightline FF01-1055/70-25) in the far field of the PDC. By rotating this filter, the central wavelength shifts. We orientated the filter in such a way as to maximise the counts of SFG on our detector, which equated to symmetrically cutting the frequency spectrum (Figure 3.7) around the central frequency. This occurs at approximately 23 degrees to normal. The PDC was recorded with a Ge photodiode (Thorlabs s132c), which has a relatively flat response over the range of wavelengths of interest. This photodiode is calibrated to display the incident power in Watts. We need to change this normalisation from power to number of photons. Due to the flat response profile of the detector we can simply divide the reported power by the energy of the central photon (assumed to be 1030 nm) to give an estimation of the number of photons. Once calibrated appropriately, the number of modes can be identified as the coefficient m in the equation used for the fit (eq. 2.22) and is found to be $\sim 1.7 \times 10^4$ modes per pulse which contains both the spatial and temporal modes.

3.3.2 Phase Matching

The second method involves a more robust understanding of the origins of the modes. If we take the modes as the regions of space-time over which the down converted state is produced, we have to consider the characteristic lengths that define this scale. If we have an idea of how large each mode will be, then the number of them will approximately be the number of times we can fit this into the pump dimensions [64]. If we approximate all the modes as only containing degenerate photons, we can separate the number of modes spatially and temporally and consider these separately; the total

number of modes will be the product of these values. The region of space in which the down converted state will be emitted in will be approximately inversely proportional to the uncertainty in the momentum of the down converted state. The reason for this can be understood from Heisenberg's uncertainty principle:

$$\Delta x \Delta p \geqslant \frac{\hbar}{2}.$$

When we have a known uncertainty in momentum p, the uncertainty in position, x, will be $\Delta x \sim 1/\Delta p$, note for a photon $p = \hbar k$. We can directly measure the momentum uncertainty in the down converted state for a given bandwidth by calibrating the far field images in momentum space instead of real space as done in Figure 3.3. The approximate momentum uncertainty we found by doing this was ~ 154 rad/mm^{-1}, with an appropriate pump beam size estimation of ~ 1.4 mm. This equates to a total number of far field spatial modes of $\sim 1.2 \times 10^4$ per pulse. As in the near field, two photons must overlap in one mode, ideally, the number of near field modes should be half the number of far field spatial modes, so we should have approximately $\sim 6.0 \times 10^3$ near field modes. The same argument can be made for the temporal-energy uncertainty. The bandwidth of the down converted state has been set by the 70 nm filter, and the frequency uncertainty is thus $\Delta\omega = 19.8 \times 10^{12}$ rad Hz. The PDC pump has a duration of 180 fs, and therefore, the number of temporal modes is approximately ~ 3.5 per pulse. The total number of modes with this method is thus $\sim 2.1 \times 10^4$ per pulse.

3.3.3 Mode Justification

These two methods give slightly different values for the number of modes, differing by almost 4000 modes per pulse. This equates to about a 20% discrepancy between the values, which, considering the methods are entirely different, it is satisfactory. The sanguine point we can derive is that we have around 10000 modes per pulse, which includes a few thousand spatial modes. From this value, we can estimate the expected PDC pulse energy at which we approach a single photon per mode per pulse. We find it to be ~ 2 fJ per pulse. We should, however, decide between these two values

for calibrating further data. Both methods have shortcomings. The problem with the power fit is the calibration and ensuring we have the correct value for PDC energy per pulse, particularly in the low gain regime. There are, however, many problems determining the number of modes through phase matching due to the more complicated nature of this measurement. We have to factor in uncertainties in the wavelength, beam size, pulse duration and focal length of the lens projecting the field into the far field. If any of these are wrong, this has a direct impact on the value found. Because of this, the power law approach, and the resultant value of 1.7×10^4 modes per pulse will be taken as the number of modes throughout the remainder of this work.

3.4 Effects of Gain on the PDC Near Field

The phenomenon we want to investigate (sum frequency generation) is classically dependent on the intensity of the incoming field. However, so far, we have only discussed the pulse energy. In order to observe entangled sum frequency generation, we want to bring the photons back together in both space and time and, therefore, need to consider the near field properties of the down converted state. With a bit of thought, it becomes evident that the near field size will not be constant but will have a dependence on the gain as the function that governs the down conversion, Equation 2.19, is exponential with respect to power. Therefore, when pumped with a Gaussian field, the centre of the pump will down convert more than the edges. This will lead to a narrowing of the down converted field that will shrink with increasing pulse energy. In the low gain where the down converted energy is directly proportional to the pump energy, we expect the PDC near field to be the same shape as the pump field. The changing properties of the PDC near field is a simple phenomenon to observe by placing a camera in the near field and changing the gain of the down conversion. We can then fit this data to an expected Gaussian. However, it will be helpful to have a deeper understanding of this effect.

3.4.1 High Gain Limit

We should be able to characterise much of the behaviour by relaxing the plane wave pump approximation in Equation 2.19 and consider this equation only in the high gain of parametric down conversion. In the high gain, the 'sinh' function [Noting the relationship $\sinh^2(x) = \frac{\cosh(2x)}{2} - \frac{1}{2} = \frac{e^{2x}+e^{-2x}}{4} - \frac{1}{2}$] will simplify to:

$$n^{\text{high gain}} \approx \exp\left[2\Lambda\sqrt{P}\right], \tag{3.11}$$

where $\Lambda = g/\sqrt{P}$. Relaxing the plane wave pump approximation means we can consider a finite size pump with some spatial distribution i.e. $P = P(x)$. Let us explicitly consider a Gaussian pump:

$$P(x) = P_0 \exp\left(\frac{-x^2}{2\sigma^2}\right),$$

the spatial dependence on the number of photons will be:

$$n^{\text{high gain}}(x) \sim \exp\left[2\Lambda\sqrt{P_0}\exp\left(\frac{-x^2}{4\sigma^2}\right)\right]. \tag{3.12}$$

In the high gain regime, we only need to consider down conversion in the centre of

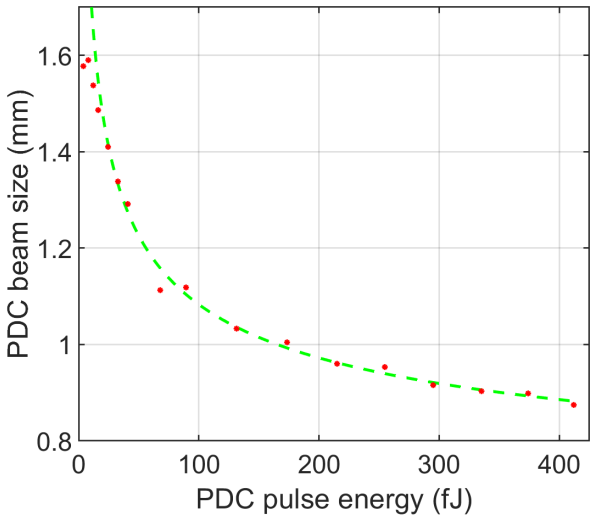

Figure 3.12: PDC near field evolution due to the effects of gain.

the pump ($x << \sigma$) as this will convert exponentially more than the edge. Therefore, we are able to expand the Gaussian:

$$\exp\left(-\frac{x^2}{4\sigma^2}\right) \approx 1 - \frac{x^2}{4\sigma^2}, \tag{3.13}$$

substituting this into Equation 3.12 we get the relation

$$n^{\text{high gain}}(x) \approx \exp\left[2\Lambda\sqrt{P_0}\left(1 - \frac{x^2}{4\sigma^2}\right)\right] = \exp\left(2\Lambda\sqrt{P_0}\right)\exp\left[-2\Lambda\sqrt{P_0}\left(\frac{x^2}{4\sigma^2}\right)\right]. \tag{3.14}$$

Therefore, in the high gain of PDC, the final field should be a Gaussian beam with a new σ, σ':

$$\sigma' = \frac{\sigma}{\sqrt{\Lambda\sqrt{P_0}}}. \tag{3.15}$$

Note that the power in equation 3.15 is the pump power. We can convert between this and the PDC power using Equation 2.22 to plot this in terms of PDC power which we find a more convenient measurment (see section 2.1.1). Equation 3.15 (rescaled for PDC power) is used to fit the data in Figure 3.12 and shows good agreement with the experimental data over an extensive range of powers. We can see the data and fit deviate at the low pulse energies as expected, where the high gain approximation cannot be taken. The equation will also fail when the undepleted pump approximation can no longer be taken, which Equation 2.19 requires.

3.4.2 Quasi-Stationary Model

The previous section provides us with an intuitive derivation for the changing near field. However, it cannot describe the behaviour in the low gain, which is the region we want to investigate. Therefore, a more complicated theory has to be derived. In [49], Gatti et al. investigate this problem and derive an equation which should hold in both the low and high gain. Using a model they call the 'Quasi-Stationary' model, they found that the distribution of the down converted momentum for a finite sized pump can be

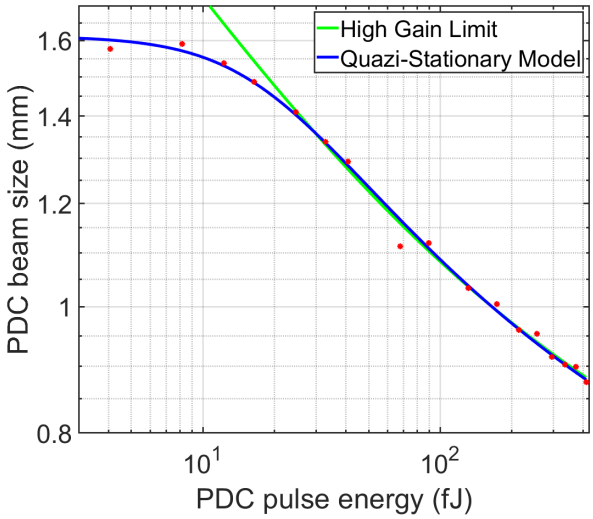

Figure 3.13: PDC near field evolution due to the effects of gain fitted with fitted both Equations 3.15 and 3.17.

described by the equations:

$$\Delta k_x' = \sqrt{\frac{4g}{\tanh(g)}}\frac{1}{\Delta x_0}, \tag{3.16}$$

where g is the gain and Δx_0 is the standard deviation in the spatially transverse, x, dimension. In order to estimate the standard deviation of the down converted spatial dimension, $\Delta x'$ we can take the inverse of the above equation:

$$\Delta x' = \sqrt{\frac{\tanh(g)}{4g}}\Delta x_0. \tag{3.17}$$

Remembering $g \propto \sqrt{P}$ where P is the PDC pump power and therefore, we can use Equation 2.22 to recalibrate for PDC power. This equation has been used to fit the same data in Figure 3.12 presented in log-log space to more easily see the difference between the two fits. We can see that the high gain both relax to the same behaviour. As we approach the low gain, however, the Quasi-Stationary model captures the behaviour well, whereas the high gain limit does not. We are unable to observe the size of the near field in the low gain due to the weakness of the signal. However, the data and

model both indicate that the size is beginning to level off as expected. The value that the Quasi-Stationary model reaches at what should be the low gain is approximately 1.65 mm, which coincides with the upper bounds of the pump beam size.

3.5 Conclusion

This has been an overview of the work we have completed in characterising and understanding the down converted state before undertaking any sum frequency generation measurements. This is an important step as we attempt to exploit many spatial-temporal modes and operate at a gain level where it is challenging to make any direct measurements of the down converted structure. We produce PDC with a 2 mm BBO crystal cut for type I phase matching with a 515 nm pump operating slightly non-collinear-degenerate as described in Section 3.1.1. This field is filtered to remove unwanted components of the spectrum (outlined in Section 3.2) and reimaged in an attempt to recombine the entangled photons in both space and time. The most pertinent sections for future chapters are Sections 3.3 and 3.4 outlining the methods undertaken to determine the number of modes and near field size, respectively. In particular, the scaling behaviour of the near field will reemerge throughout this thesis as we investigate the properties and behaviour of entangled sum frequency generation when transitioning from the low to high gain of parametric down conversion.

Chapter 4

Properties of PDC and eSFG

The principal property we want to investigate is the rate of sum frequency generation when pumped with parametric down conversion. There are, however, a variety of other relationships we may find interesting to probe. The investigations that follow in this Chapter occur primarily in the mid and high gain of parametric down conversion, as much of the information we want to gather is available at this gain level. Moreover, it is far easier to take measurements outside of the low PDC powers of the low gain. We do, however, attempt to observe the linear relationship with a sCMOS camera to examine how far we can take this technology in probing that property. We also investigate the dependence eSFG has on pump pulse duration, the effects gain has on the up converted spectrum and how the position of the up conversion crystal and dispersion in the far field of the down converted field affects the efficiency of up conversion. It is worth noting that some of these are better thought of as investigations into properties of the down converted state instead of the eSFG directly. The results will, therefore, help further the discussion in Section 3.4. The data presented in this chapter was collected by myself and a lab partner. I undertook the data analysis and subsequent reflections.

4.1 Limits of detecting eSFG with a sCMOS Camera

Ideally, we would be able to see the effects of an increased SFG signal from the use of an entangled pump with cameras to facilitate the use of this technique for imaging

applications. To this end, we started our investigation with the use of an sCMOS camera for our detector. Many of the investigations in this Chapter will utilise sCMOS and CCD cameras; therefore, a better understanding of their limitations will be beneficial.

4.1.1 Method

The design is precisely that in Figure 2.1 and detailed in Section 2.2.3 with a lens to focus the eSFG onto the camera. There was no bandpass filter in the PDC as, while this makes interpretation of the data simpler, it reduced the overall eSFG counts substantially. For this initial measurement, we are not attempting to understand anything further than if we can observe a linear relationship between PDC and eSFG flux with a camera as a detector. For the camera, we used an Andor Zylar 5.5 with a quantum efficiency of $\sim 55\%$ at 515 nm.

When evaluating a camera for scientific purposes, it is important to take into account the inherent noise. sCMOS cameras have several noise characteristics, but for our purposes, we only need to focus on two: dark current and read out noise. Dark current is caused by charge build-up in the sensor, leading to heating and thermal emission. Read out noise is introduced when amplifying the signal on each picture upon the values being read. While neither of these can be eliminated entirely, there are measures we can take to mitigate their effect. For example, we can cool the camera to reduce the dark counts. While we only had access to native air cooling, we made sure that the camera had reached a steady state before capturing any data. Additionally, we can take background images with no signal present to help characterise the dark currents and remove them from the signal image.

The measurement was made by adjusting the PDC pump energy, thereby changing the PDC energy at the second, up conversion crystal. The PDC energy was measured by a power meter (Thor labs s132c), and the eSFG signal was collected and filtered with a short pass 600 nm filter and a 10 nm bandpass filter centred on 515 nm, approximately the central wavelength of the PDC pump field. For each gain level, we took background images by rotating the SFG crystal, thereby destroying phase matching and recording an exposure for the same duration as when the signal was present. Natively, the camera

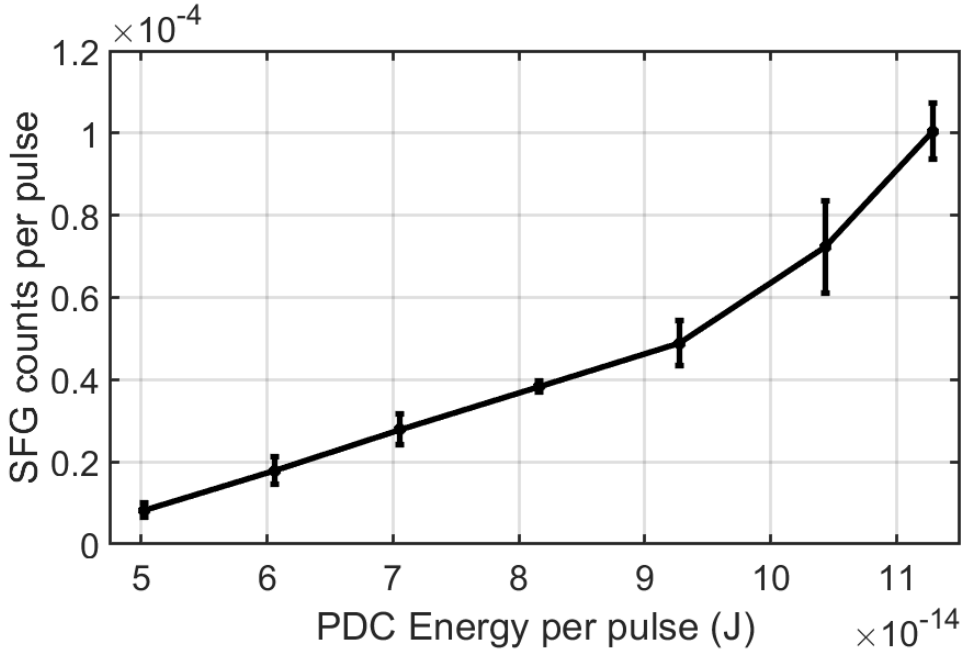

Figure 4.1: PDC vs SFG with the Zylar camera.

had a maximum exposure time of 30 seconds. However, this can be overcome by taking several images and summing the resultant signals. This increases the amount of read out noise per image but was necessary for several of the points collected.

4.1.2 Result: 200 kHz repetition rate

The result of this investigation is shown in Figure 4.1, the laser is operated at a 200 kHz repetition rate, and this appears to show a robust linear term. However, we need to be careful when interpreting this linear term as evidence of eSFG. If we try fitting this data with the expected linear plus second order, $y = a + bx + cx^2$, the fit appears to cross the x-axis, $y = 0$, at approximately $x = 2.6$ fJ per pulse $>> 0$ contrary to what we expect. If, on the other hand, we follow the apparent linear trend, it appears to cross at about 4.1 fJ per pulse. These could be due to poor background removal; however, we are still well above the single photon per mode regime, and therefore, we would not expect to see the relationship so linear. As this data was collected for unfiltered PDC radiation, we do not have a robust estimation of the total number of modes. However, the smallest PDC energy corresponded to around ~ 2 photons per mode.

We cannot make a strong claim based on this outcome. As well as error in the measurement, the result in Figure 4.1 may be a consequence of the detector behaving unexpectedly at these power levels or merely a consequence of looking too closely at the curved lines and thereby seeing the approximate flat region; the flat earther's paradox. We do not have the sensitivity to carry on this measurement to lower PDC energies, which would allow us to investigate the x-axis crossing, y=0, which would allow us to eliminate any issues with background correction. All we can conclude confidentially is that the Zylar camera cannot discriminate with sufficient confidence in the trend of the SFG process at the low energies required for our investigation. At a minimum, we require the sensitivity to approach the zero PDC energy point. We will address this in future measurements.

4.2 eSFG Dependence on Pump Pulse Duration

Classically, SFG is dependent on the intensity of the field pumping the process described by the equation (Equation 1.31):

$$I_{\mathrm{SFG}} = \sigma I_{\mathrm{Pump}}^2. \tag{4.1}$$

Equation 4.1 implies a relationship between the pulse duration of the up converted field, Δt_{SFG}, and the pulse duration of the pump field, Δt_{Pump} when pumped by a Gaussian beam:

$$\Delta t_{\mathrm{SFG}} = \frac{\Delta t_{\mathrm{Pump}}}{\sqrt{2}}. \tag{4.2}$$

This can be seen by substituting a Gaussian pump into Equation 4.1. We do not measure the intensity directly, instead we measure the energy of the pumping field. Therefore, ignoring the spatial dimension, if we restate Equation 4.1 in terms of measured energy we can see that the energy of the generated up converted field is inversely proportional to the pump pulse duration:

$$E_{\mathrm{SFG}} = \frac{\sigma}{\sqrt{2}\Delta t_{\mathrm{Pump}}} E^2_{\mathrm{Pump}}. \tag{4.3}$$

In the case of entangled sum frequency generation, it's not entirely clear what this relationship will be. We can develop an intuitive understanding of how the pulse duration will affect the intensity of eSFG by considering Equation 1.1:

$$R = \delta\phi + \sigma\phi^2. \tag{4.4}$$

In the low gain of PDC, where the linear term dominates, the pulse duration of the up converted field will be precisely that of the field used to pump it. In this regime, all interactions are between individual photons and the probability of conversion will be proportional to the photon flux density, hence the temporal profiled of the pump intensity. In the high gain, however, where the second order term of Equation 1.1 dominates, the duration of the up converted field will be shorter by a factor $1/\sqrt{2}$ as in the classical case. Therefore, at a general gain level, the temporal profile of the up converted field should be some combination of the two.

The entangled case has another deciding factor however. If we wish to preserve entanglement in our down converted field, the only way to alter the down converted energy is by reducing the PDC pump energy. This will increase the down converted pulse duration, which should be reflected in our up converted, eSFG, field but also effect the efficiency of up conversion. While the effect of the linear term in Equation 4.4 is easy to describe and understand, the effect of changing gain on the down converted pulse duration and how that impacts eSFG is less obvious. The changing properties of the PDC pulse duration are important to understand as we do not have a way of measuring this directly and we expect that eSFG efficiency will strongly depend on this property. Therefore, the change in eSFG efficiency due to the changing pulse duration with gain is the property we wish to investigate, which will be done in the high gain of PDC as this will facilitate easier detection.

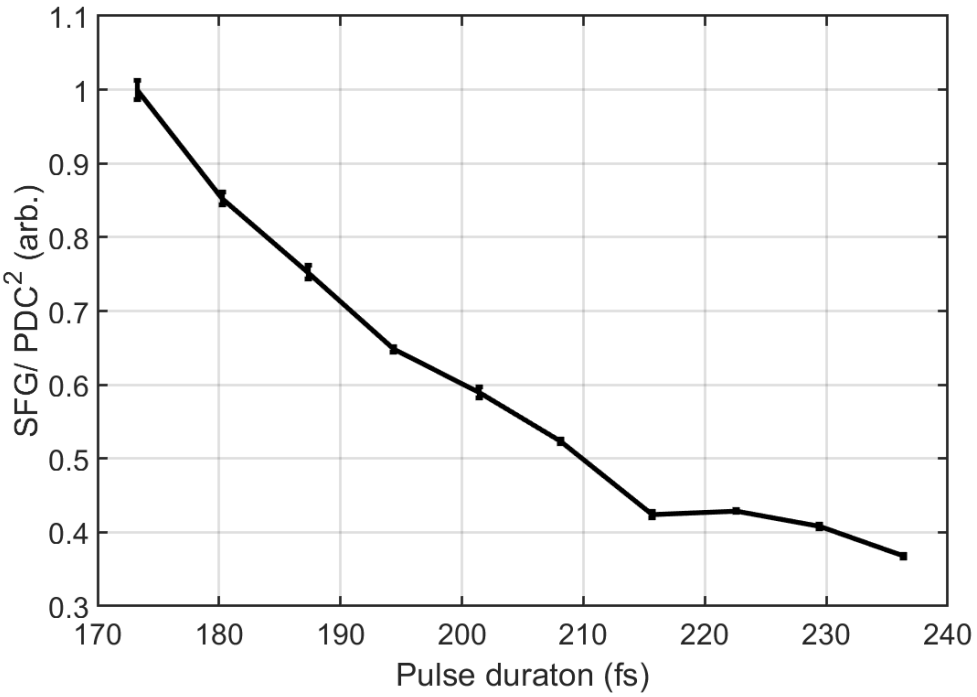

Figure 4.2: eSFG coefficient vs PDC pumps pulse duration.

4.2.1 Measurement

As in the previous section, a Zyla 5.5 is used as a detector. The pulse duration of the fundamental laser is altered by chirping the pulse. This duration is not measured directly, instead we relied on pulse compressor built into the laser and the calibration provided by the manufacturer. In Figure 4.2, the pulse duration on the x-axis is the pulse duration of the PDC pump, as the PDC pump is simply the frequency doubled fundamental, this was calculated by dividing the set fundamental pulse duration by $\sqrt{2}$. As we operate in the high gain of parametric down conversion, we expect the SFG to scale classically according to Equation 4.3. Consequentially, by dividing the measured SFG counts by the average PDC energy to the power of two, we should be able to isolate the dependence on the pulse duration on the eSFG efficiency. The SFG energy divided by the PDC energy squared is the value that is plotted on the y-axis of Figure 4.2.

Similarly to the argument for the near field size in Section 3.4.2, the PDC pulse

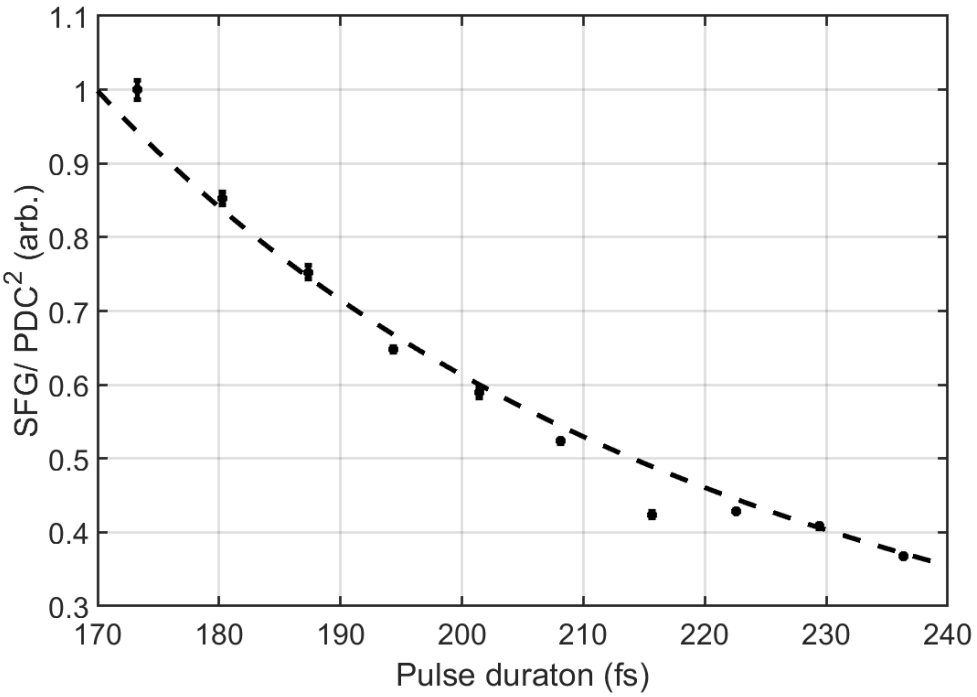

Figure 4.3: eSFG coefficient vs PDC pumps pulse duration fitted with Equation 4.8.

duration dependence on gain will be given by the Equation [49]:

$$\Delta t = \sqrt{\frac{\Delta t_0^2 \tanh(g)}{4g}}, \tag{4.5}$$

where Δt_0 is the pulse duration of the pump. The gain, g, is proportional to the square root of the pump power, $g = \Lambda\sqrt{P}$. We must consider the peak power of a pump pulse. Therefore, P will depend on the pulse duration:

$$P = \frac{E}{\Delta t_0},$$

where E is the energy per pulse. One final correction to make is that because of how we conducted this measurement, the energy E is not constant. The fundamental beam energy per pulse is constant. Fortunately, these are simply related as the PDC pump

is the second harmonic of this:

$$\frac{E}{\Delta t_0} = \frac{\eta}{2}\left(\frac{E'}{\Delta t_0}\right)^2, \tag{4.6}$$

where E' is the energy of the fundamental field, η is the SHG coefficient, and the pulse duration of the fundamental field is $\sqrt{2}\Delta t_0$. Therefore, the relationship between the PDC pump pulse duration and the PDC pulse duration follows:

$$\Delta t = \sqrt{\frac{\Delta t_0^3 \tanh\left(\frac{\Lambda\sqrt{\eta E'/2}}{\Delta t_0}\right)}{\Lambda\sqrt{\eta E'/2}}}. \tag{4.7}$$

We expect the relationship SFG Counts/ PDC energy^2, which isolates the pulse duration dependence on this interaction, to be:

$$\mathrm{SFG/PDC^2} \propto \sqrt{\frac{\Lambda\sqrt{\eta E'/2}}{\Delta t_0^3 \tanh\left(\frac{\Lambda\sqrt{\eta E'/2}}{\Delta t_0}\right)}}. \tag{4.8}$$

Equation 4.8 was used to fit the data from Figure 4.2 by taking the coefficient $\Lambda\sqrt{\eta E'/2}$ as a fitting parameter. The result of this fit is shown in Figure 4.3 and shows good agreement with the data. We have shown how the efficiency of eSFG depends on the pump beam pulse duration in the high gain of parametric down conversion and provided a model explaining this result. Importantly, this result provides direct evidence that the pulse duration of the down converted field can be described by Equation 4.5, a relationship that will be used later in this work.

4.3 Translating the Crystal Through the PDC Focus

In order to get efficient entangled two photon interaction, we must recombine the twin photon state we produce in the down conversion crystal in the up conversion crystal (or sample). The simplest way of maximising this property is to ensure we are imaging the down converted field, which is why our experimental design comprises of two parabolic mirrors in a 4-f configuration. When aligning the experiment, we attempt to image

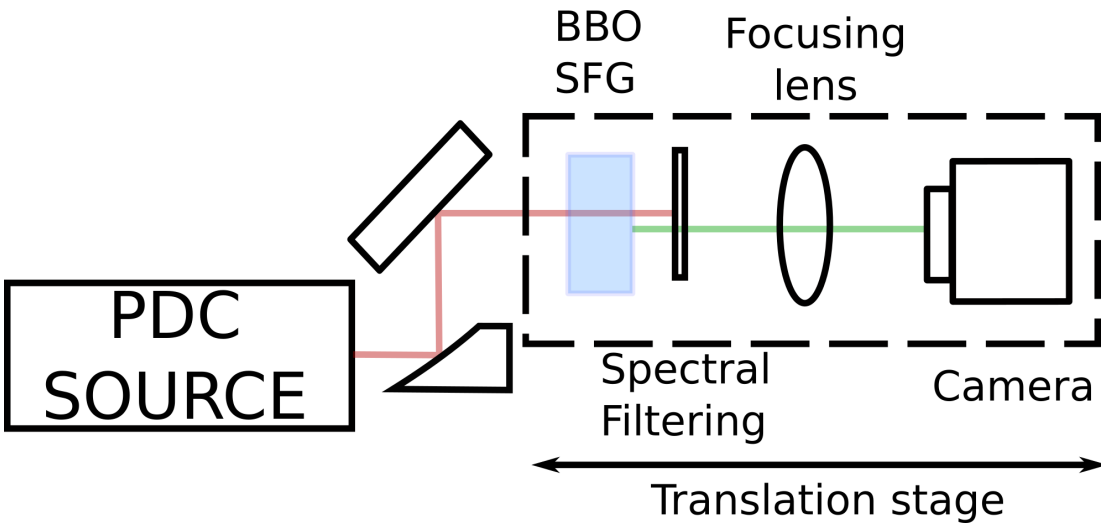

Figure 4.4: Experimental design for measuring the changing efficiency as the up conversion crystal is translated through the focal point of the PDC.

the second face of the down converted crystal (face closest to the parabolic mirror) at the position the second crystal will be placed. We have observed a strong dependence on crystal position for efficient eSFG. We believe this is due to the requirement to recombine the entangled modes for eSFG. To thoroughly investigate this property, we conducted a systematic study. We positioned the crystal, imaging objective, and camera on a single translation stage and recorded the up-converted counts at various points along the focusing beam (as depicted in Figure 4.4). By positioning the detector in this manner, we ensured that the up conversion crystal remained in the imaging plane of the camera, enabling easy identification of any up-converted photons that were focused on the camera. This study was carried out in the high gain of PDC, capturing only the coherent component, the component where we expect to observe any 'entangled' interactions. Because we are considering the coherent component only, the lens is placed 1-f away from the back face of the up conversion crystal, and the camera is placed 1-f away from this in order to focus the coherent component, which is emitted in a collimated beam. This is done to increase the signal-to-noise ratio on the camera; the SFG data will consist of the total number of counts we observe on the camera. It is worth noting that the coherent and incoherent components may demonstrate different behaviour when the crystal is translated. The incoherent component of eSFG is purely

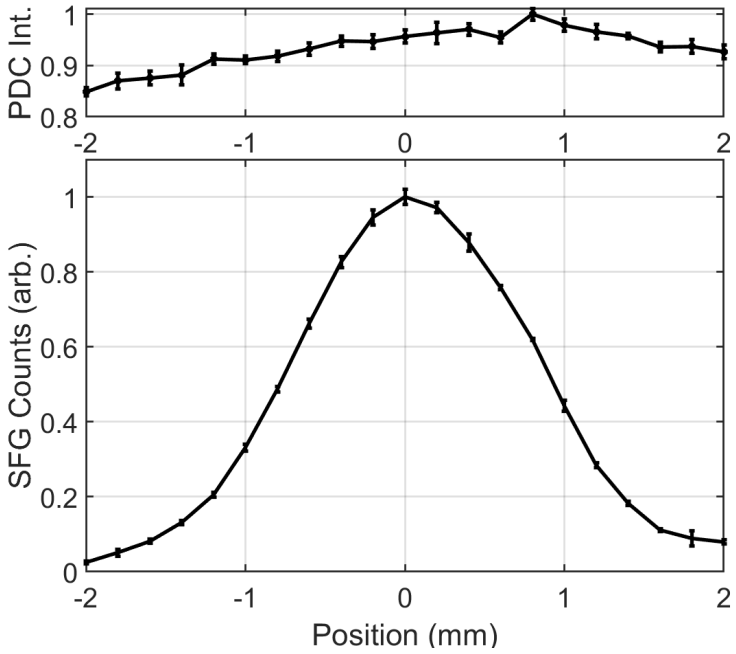

Figure 4.5: The effects of translating the crystal through the focal point of PDC with upper plot showing measured average intensity of PDC over same range of positions.

classical. Therefore, its efficiency is proportional to the average intensity squared. We expect to observe a different relationship for the coherent component.

The result of this study is shown in Figure 4.5. We can see that the dependence is approximately Gaussian but slightly lopsided towards the positive position when the crystal is closer to the parabolic mirror. We also recorded the changing PDC size by replacing a filter which blocked the PDC, depicted in Figure 4.4, with one that blocked the SFG and swapping the lens for one that is half the focal length. This way, the new lens on the translation stage is placed 2-f away from the back face of the up conversion crystal, and the camera is placed 2-f away from it. Therefore, this lens should produce an image of the near field PDC at that position. As the power of the PDC does not change during this measurement, the inverse of this size will provide a measure of the intensity of the PDC field, and this is shown in the upper diagram of Figure 4.5. It does not appear that the peak of the PDC intensity and the peak of SFG occur at the same point. However, I believe this is a consequence of imaging the rear face of the up conversion crystal. The up conversion crystal is 2 mm in thickness, and the PDC near

field intensity maximises approximately 1 mm after the eSFG, i.e. it appears at the back face 1 mm after we maximise the SFG. Therefore, when the PDC is maximised, it will be approximately at the centre of the up conversion crystal as expected.

In the high gain regime, we can approximate the near field of the down converted field as a Gaussian (shown in Section 3.4.1). For a Gaussian beam, the spot size, w, of a propagating beam increases with distance from the focal point according to the equation [65]:

$$w(z) = w_0\sqrt{1 + \left(\frac{z}{z_R}\right)^2}, \tag{4.9}$$

where z_R is the Rayleigh range defined as:

$$z_R = \frac{\pi w_0^2}{\lambda} \tag{4.10}$$

w_0 is the beam waist (smallest possible spot size), and λ is the wavelength of the radiation in a vacuum. The PDC intensity data (top of Figure 4.5) should follow the trend of $1/w(z)^2$. If we attempt to fit this data to Equation 4.9 then we find a Rayleigh range of approximately 6.8 mm. The Rayleigh range is defined as the point at which the area of the beam has doubled in size. After one Rayleigh range, we would, therefore, expect the intensity of the beam to halve and the resultant SFG to drop to a quarter it's peak value. However, we can see in Figure 4.5 that the measured coherent component of eSFG drops to approximately a quarter of its peak value just 1.2 mm from this peak. From this, we can conclude that either the coherent component of eSFG behaves as if a tighter focused Gaussian beam pumps it or that even in the high gain, this component is still dependent on recombining the entangled modes of PDC, which can only occur close to the focal plane of the parabolic mirror.

4.4 Effects of Dispersion on eSFG

Our final study of this chapter is into the effects of dispersion in the down converted field on the efficiency of eSFG. This is a complex property to quantify. The significance

of the effect will depend on several factors: the bandwidth of the down-converted field and the materials used. However, dispersion will affect any experiment in the field. In our specific system, we utilise a broadband field, which will magnify the effects of dispersion.

The experimental design is the same as in Figure 2.1 with a 70 nm band pass filter centred on 1030 nm placed in the far field of the PDC. Our goal was to shift the gain level towards the low end, so we utilised a PMT as the SFG detector (Hamamatsu H7422P-40 photon counting head). In the photon starved regime, where we do not see a pile-up in the signal from the PMT, this operates as a single photon counting device with an efficiency of approximately 40%. A 10 nm band pass filter centred on 515 nm is placed in front to exclude other visible signals. The data from this detector is passed through a device which ascribes time stamps to the signal (HydraHarp 400). The trigger for this device is taken directly from the laser. The data consists of a series of time binned histograms, with a bin width of 1024 ps. The value of each bin corresponds to the number of photons detected at the corresponding time from the detection of the

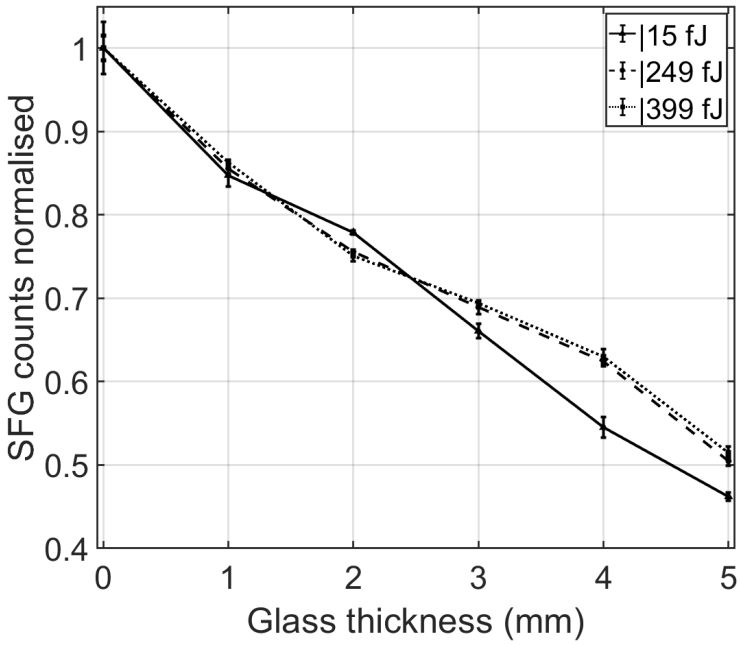

Figure 4.6: The effects of additional thickness of CaF_2 glass on the efficiency of eSFG at varying PDC energy per pulse.

trigger. This enables us to eliminate a significant portion of the background noise as we know the signal will only appear at or close to the PDC pump pulse and, therefore, in a very small time frame (hundreds of femtoseconds for the pulse vs microseconds between pulses).

We selected three values of PDC power to investigate, from high gain through to very close to low gain, and measured the coherent eSFG response as we added varying thicknesses, from 1 to 5 mm, of CaF_2 glass in the far field of the PDC. This glass was chosen as it has relatively low chromatic dispersion and, therefore, is a common material used for lenses and filters.

The result is shown in Figure 4.6. We chose to normalise the SFG counts as the absolute value of SFG is not the question we wanted to investigate. Dispersion is clearly detrimental to the overall efficiency of eSFG. The addition of just 5 mm of excess glass reduces the efficiency by half. There does not appear to be any dependence on the gain. As will become clear in later chapters, the lowest gain data are taken in a regime where the linear dependence of eSFG is visible. Even in this case, we do not see a significant deviation with respect to the high gain cases. In conclusion, it is clear that additional dispersion negatively impacts the eSFG efficiency, reinforcing the idea that for entangled sum frequency generation and entangled two-photon absorption experiments, dispersive optics should be avoided entirely.

4.5 Conclusion

This section has comprised of short studies on various effects and phenomena related to entangled sum frequency generation. Our findings indicate that the low gain regime is not detectable with an sCMOS. This suggests the necessity of more sensitive camera technology, such as an EMCCD or scanning with a PMT, for any imaging application. We have investigated how the PDC gain affects the down converted states' pulse duration and shown how this is reflected in the eSFG efficiency. We went on to show the strong dependence the position of the focal plane has on coherent eSFG, which implies that this component does not just depend on the intensity of the pumping field but also on our ability to recombine the down converted fields spatial-temporal modes.

Finally, we have presented evidence supporting our belief that the dispersed nature of the experimental components will significantly affect eSFG efficiency and, therefore, should be avoided in experiments intended to investigate this phenomena.

Chapter 5

The Effects of Losses in the Down Converted Field on eSFG

Entangled sum frequency generation (eSFG) has been investigated before [66,67] and it is starting to be used as a diagnosis stage for entangled two photon absorption (eTPA) experiments [35]. We believe that we can use the eSFG process to understand better the two photon interaction process and the struggle with experimental realisation of eTPA [34, 35, 39, 68] as the linear term in both cases originates from the same source, the energy-time and position-momentum correlations in the down converted state. By studying these properties through sum frequency generation (SFG) instead of two photon absorption (TPA), we can better understand the effect the quantum nature of the state has on efficient up conversion and avoid potential complications such as hot band absorption which can be present in eTPA [39]. Hot band absorption occurs when photons have sufficient energy to stimulate electrons in high energy 'ground states' to an excited state through single photon absorption and this can be mistaken for two photon absorption. In this Chapter, we will outline our investigation into the effect of losses in the down converted field as we transition from the low to the high gain of parametric down conversion. While doing this, we will derive a simple toy model to explain the scaling of eSFG with losses and examine the consequence of this relationship. We will finish by scrutinising the relationship as we progress into the high gain of PDC and provide an intuitive understanding of the experimental result. The results in this

section have potentially far reaching implications in the study of entangled two photon interactions and quantum imaging more generally. The data presented in this chapter was collected by myself and a lab partner. We worked together on the explanation of the results presented in Section 5.2. I undertook the initial data analysis and the conclusions are my own.

5.1 The Effects of Losses in the Down Converted Field on eSFG

It has become conventional to 'prove' the quantum nature of eSFG and eTPA by showing the linear relationship between incoming photon power and up converted power when the power is reduced by reducing the PDC pump and then showing a second order relation when the PDC power is reduced by increasing random losses in the PDC state (e.g. [66] for eSFG and [36] for eTPA). If the down converted state were not entangled, there would be no difference in these two methods of reducing the pump power. Whilst this is a convenient way to show the difference in scaling, it does not inform us about what would happen if we pumped the process with a lossy field. This is a pertinent question because, as a practical matter, all systems will be somewhat lossy. Therefore, in order to be able to compare studies, we must understand how losses will affect eSFG and quantify the losses we have in our system appropriately. We plan on discovering the effects of losses on the down converted field on eSFG by placing fixed, known losses in the form of neutral density (ND) filters in the down converted field. We will adjust the gain (by altering the PDC pump energy) in order to match the measured range of powers at the up conversion crystal with and without losses, and perform power scans where we measure the PDC energy at the second, SFG, crystal versus the number of SFG counts. This way, we keep a physically meaningful quantity constant, the number of photons incident on the sample, while isolating the effects of the losses.

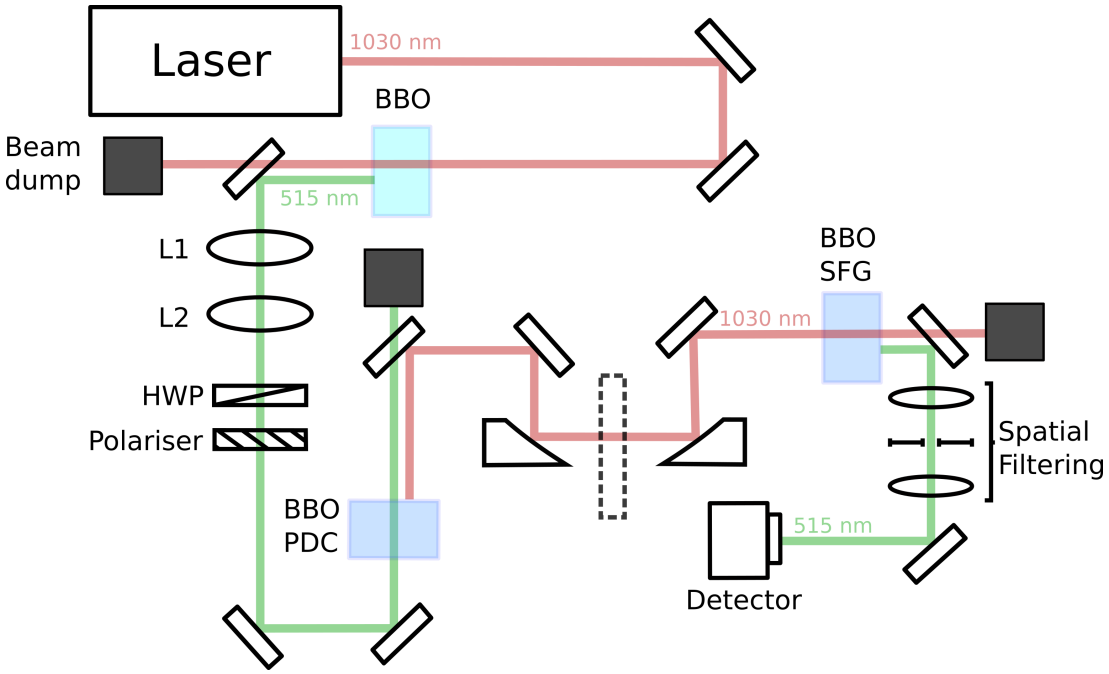

Figure 5.1: Experimental layout with parabolic mirrors used for imaging.

5.1.1 Method

The experimental design has been detailed in previous Chapters and is reproduced in Figure 5.1 only for the reader's convenience. The down converted state is filtered and losses are introduced by placing neutral density filters in the far field of the down converted beam (grey box on Figure 5.1). For the detector, we required a low noise, high sensitivity device. We decided to use a PMT, which will operate in the photon counting regime at the expected up converted power. We used a Hamamatsu H7422P-40 photon counting head, which has a quantum efficiency of ≈ 40 % at 515 nm, filtered with a 10 nm band pass filter around 515 nm and a shortpass 600 nm to ensure exclusion of the PDC. The amplified output of this is connected to a HydraHarp 400, a time-correlated single photon counting (TCSPC) module, which we used to time gate the response of the PMT. Due to this, we can consider only the signal stimulated from the laser pulse passing through the up conversion crystal, removing much of the background noise. The rise time of the PMT (length of time it takes the output pulse to raise from 10 % of its peak value to 90 %) is reported to be 1 ns. This suggests a time scale over which

we should time bin the PMT response as we require one pulse from the PMT to equate to one count from the Hydraharp; the discrepancy voltage (voltage below which the HydraHarp will ignore the response) was also selected to ensure that only the peak of any output was registered. The data consisted of time-binned histograms with a bin width of approximately 1 ns where the laser reference provided a start signal for the TCSPC.

Due to the highly delicate nature of the measurement, we wanted to limit our presence in the lab. When we initially took these measurements, our presence in the lab appeared to introduce a source of noise and, particularly, appeared to diminish our ability to reproduce the result. Therefore, most of the measurement was automated. First we placed an ND filter in the far field of the PDC, and created a calibration curve between the half wave plate (HWP) angle (the angle of the HWP placed before the down conversion crystal in Figure 5.1) and the PDC energy at the SFG crystal with either a photodiode (Thor labs S132C) or a photoreceiver for very low energies (Femtowatt

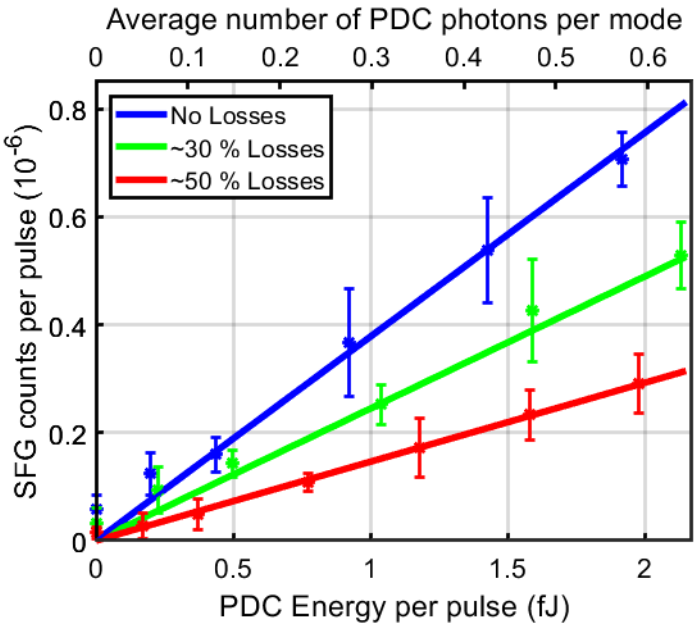

Figure 5.2: PDC energy per pulse and eSFG counts in the less than one photon per mode regime. Data collected at 500 kHz, each data point was exposed for 5 minutes and we took 5 samples with background samples obtained by rotating the second SFG crystal by $\pi/2$ to destroy phase matching.

Photoreceiver FWPR-20-IN). This is the extent of the necessary human interaction. We then created a script that can rotate the HWP to set a PDC energy, records the PMT response from the SFG crystal and acquires a background by rotating the SFG crystal to 90 degrees, thereby destroying the phase matching in this crystal without any further human interaction. We repeated this procedure for a variety of induced losses (ND filters) and at a variety of gain levels (maximum PDC pump energy).

5.1.2 Results

Starting from the low gain of parametric down conversion, we can see the linear scaling expected in Figure 5.2. This linear scaling is present for all loss levels, and we have already revealed something important to understand. The critical feature of entangled two photon interactions, the linear relationship between pump and up conversion, will be present with any entangled field, no matter the purity. Previous studies have shown a quadratic relationship between the PDC energy and SFG energy when the

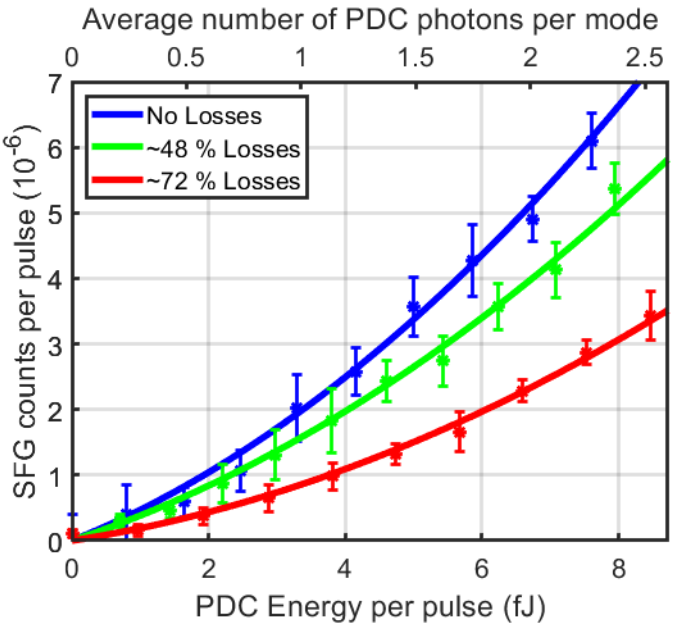

Figure 5.3: PDC energy per pulse versus eSFG counts greater than one photon per mode. Data collected at 500 kHz, each data point was exposed for 2 minutes and we took 5 samples with background samples obtained by rotating the second SFG crystal by $\pi/2$ to destroy phase matching.

PDC energy is reduced by increasing losses in the far field. From Figure 5.2, we can see this is clearly due to the increase of losses reducing the efficiency of eSFG whilst simultaneously reducing the number of photons at the SFG crystal (a quantity we are matching), hence the second order relation. We can gain a physical intuition of the result by understanding that at these photon fluxes, the only photons that can recombine are entangled and scale linearly; if any photons are lost from the entangled pair, the remaining photon cannot contribute.

Moving beyond the low gain regime and into a regime we will call the 'mid' gain, we arrive at Figure 5.3. There are two takeaways from this. First, a non-lossy down converted field remains more efficient for pumping eSFG than a lossy one into the stimulated regime of PDC where the eSFG counts are no longer linear with the PDC energy. The linear term also appears to remain for all energy levels as shown by the simple fits reported in Table 5.1. This offers the possibility of the entangled case remaining superior even into the high gain of PDC because of the quantum nature

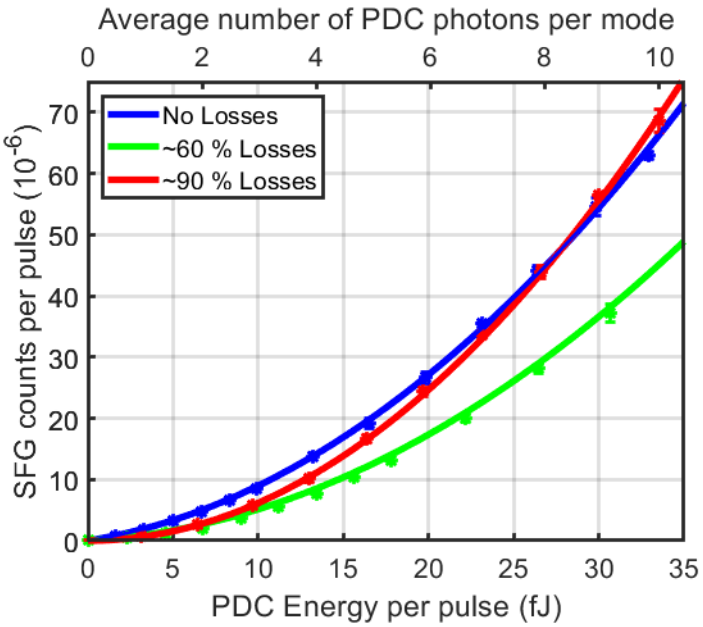

Figure 5.4: PDC energy per pulse versus eSFG counts much greater than one photon per mode. Data was collected at 200 kHz, each data point was exposed for 2 minutes and we took 5 samples with background samples obtained by rotating the second SFG crystal by $\pi/2$ to destroy phase matching.

of the down converted state, as the origin of this linear term is solely the pair-wise entanglement of the PDC.

Progressing into the high gain of parametric down conversion, we arrive at Figure 5.4. This has a surprising feature: it appears that at high gain and losses, the lossy field becomes not only as efficient as but more efficient than the no losses PDC field when pumping SFG. A summary of the fits used for the data in Figures 5.2, 5.3 and 5.4 can be found in Table 5.1. The data set ends here for these experiments, as we ran out of pulse energy to probe this phenomenon further. However, we have two further data sets showing the same effect taken in slightly different manners, which we will discuss later in this Chapter. From the data we have collected, it appears that crossing point between more and less 'pure' quantum states are characteristic of eSFG. Note, when I refer to less or more pure state here, I am not necessarily referring to the quantum understanding of purity but rather simply the idea that as we add losses into our down converted field, a portion of the photons we measure at the crystal will not have an entangled partner and therefore, the whole state can no longer drive eSFG. We will address this in the next section by developing a model for the relationship between a lossy down converted field and up converted photons.

5.2 Developing a Model for Losses in the Down Converted Field

We start with the expected rate of sum frequency generation pumped with an entangled source of photons:

$$R_e = \delta\phi_e + \sigma\phi_e^2, \tag{5.1}$$

where ϕ_e is the flux of entangled photons, δ is the entangled SFG coefficient and σ the classical SFG coefficient. When we add losses into our down converted field, the result is a mix of states. One component has its entangled pairs intact and undergoes SFG according to Equation 5.1, the other does not and therefore can only undergo SFG as a classical state. The rate from this component will be given by:

Figure	Fit	Measured Losses	Coefficients	
5.2	$R = \delta\phi$	∼0%	δ	3.77×10^8
		∼30%	δ	2.45×10^8
		∼50%	δ	1.46×10^8
5.3	$R = \delta\phi + \sigma\phi^2$	∼0%	δ	4.19×10^8
			σ	5.13×10^{22}
		∼48%	δ	3.46×10^8
			σ	3.68×10^{22}
		∼72%	δ	1.63×10^8
			σ	2.75×10^{22}
5.4	$R = \delta\phi + \sigma\phi^2$	∼0%	δ	4.40×10^8
			σ	4.58×10^{22}
		∼60%	δ	1.60×10^8
			σ	3.53×10^{22}
		∼90%	δ	0.00×10^8
			σ	6.16×10^{22}

Table 5.1: Summary of the coefficients found for Figures 5.2, 5.3 and 5.4.

$$R_{cl} = \sigma\phi_{cl}^2, \tag{5.2}$$

where ϕ_{cl} is the classical flux and the meaning of σ is maintained. When we have both of these components present, the total rate of sum frequency generation will be:

$$R_{tot} = R_e + R_{cl} = \delta\phi_e + \sigma\left(\phi_e^2 + \phi_{cl}^2\right), \tag{5.3}$$

and the measured flux of PDC at the SFG crystal will be:

$$\phi = \phi_e + \phi_{cl}. \tag{5.4}$$

If we start with a pure entangled state and the mixed nature is caused by a system of transmission T, then the measured photon flux ϕ, entangled photon flux ϕ_e and 'classical' photon flux ϕ_{cl} are related:

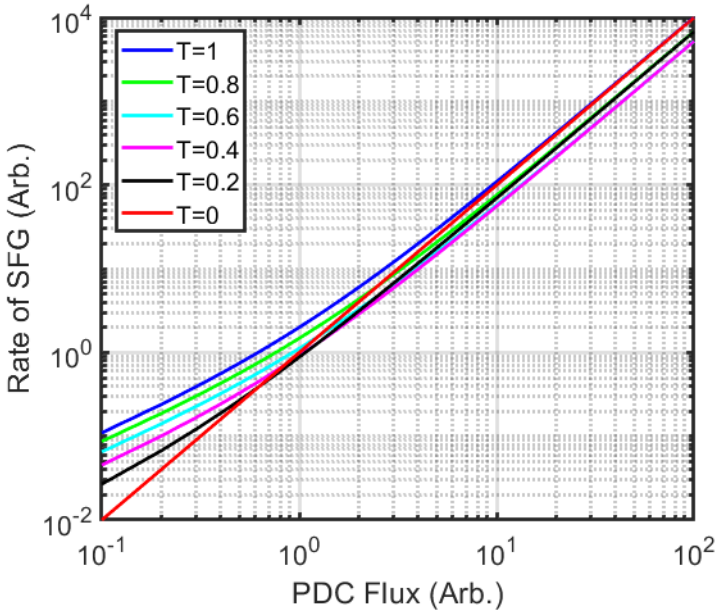

Figure 5.5: R_{tot} plotted for varying transmission coefficients (T). δ and σ are both set to one.

$$\begin{aligned} \phi_e &= T \times \phi, \\ \phi_{cl} &= (1-T) \times \phi. \end{aligned} \tag{5.5}$$

Substituting these definitions into Equation 5.3, the rate of eSFG in a system of transmission T will be given by:

$$R_{tot}(T,\phi) = T\delta\phi + \sigma\phi^2(2T^2 - 2T + 1). \tag{5.6}$$

Equation 5.6 is plotted for a variety of different transmissions T at a constant δ and σ in Figure 5.5. This is presented in log-log space to see the changing properties more efficiently. We can see that the most lossy case in red on the plot becomes more efficient than almost all of the alternatives at finite powers; it will only asymptotically reach the no losses case. The most lossy field is fitted with zero transmission. As we are adding losses with absorptive filters, this is not possible. However, we do not have to add losses in this manner. All we have assumed is that a proportion of the field has remained entangled; how that entanglement was preserved or destroyed is

Figure	Shared Coefficients		Measured Losses	Fitted T
5.3	δ	4.23×10^8	∼0%	0.9899
			∼48%	0.8185
	σ	5.24×10^{22}	∼72%	0.3855
5.4	δ	5.19×10^8	∼0%	0.8485
			∼60%	0.3083
	σ	6.16×10^{22}	∼90%	0

Table 5.2: Summary of the coefficients found for data in Figures 5.3 and 5.4 fitted with equation 5.6.

not important. Therefore, the zero transmission case can stand as a system that has destroyed the entanglement in the down converted field, and the up conversion therefore scales entirely classically. From this, we can see that if we have any losses in our down converted field, there will always exist a classical field that will be up converted more efficiently than this field at finite energies. Below these crossing points, the purer field remains more efficient, and an entirely pure down converted field should still be more efficient than any 'classical' field for all energies. This is the first evidence to my knowledge that there is any perceptible quantum effect of pumping entangled two photon interactions in the high gain of parametric down conversion.

5.2.1 Fitting Data with Model

We can fit the data in Figures 5.3 and 5.4 with Equation 5.6. We can only fit the data in Figures 5.3 and 5.4 as we need an observable second order term in order to fit to Equation 5.6. In the real world, we will always have losses in the down converted field. Therefore, the best fits are found if we assume that even the no losses case still has a transmission $T < 1$. We then can vary the transmission between the three fits in order to match the data best and maximise the found R^2 values of all three fits simultaneously. Alternatively, we can assume that the relationship between the three transmissions is known and precisely equal to the measured losses induced by the neutral density filters as in an ideal world. This can work reasonably well, but it is not the method that gave the best fit in this case. We believe the reason for this is that these data sets

were taken over several weeks. The variation in alignment between these sessions was enough to noticeably alter the fitted transmission. We will address this in later data sets with an altered experimental procedure. The results of these simultaneous fittings are shown in Table 5.2. The expected relationship can be seen, the more lossy fields have a lower transmission, and for the lower gain data, the measured losses and fitted transmissions are in reasonable agreement. However, the high gain data in Figure 5.4 very clearly diverges. We believe that this is primarily due to the effects of gain on the down converted near field, which we will consider in the next section.

5.2.2 An Extremely Lossy Field

We started the examination that led to Equation 5.6 from a desire to describe the result we observed. Now, we will attempt to use this result to quantify the key coefficients better. Equation 5.6 suggests that no measured value of the linear or second order eSFG coefficient is valid without appropriate characterisation of the transmittance of the system. Consider at what fluxes the efficacy of up conversion from two lossy down converted fields become equal and cross. Consider two different rates, R_1 and R_2, with transmission coefficients T_1 and T_2. The crossing point will occur when $R_1 = R_2$ and so the flux at the crossing point, ϕ_{cross}, will be:

$$\phi_{cross} = \frac{\delta(T_1 - T_2)}{2\sigma(T_2^2 - T_1^2 - T_2 + T_1)}. \tag{5.7}$$

If $|T_1 - T_2| >> |T_2^2 - T_1^2|$ (i.e. $T_1, T_2 << 1$, very lossy) this will reduce to an approximate constant and the crossing point will occur at:

$$\phi_{cross} \approx \frac{\delta}{2\sigma}. \tag{5.8}$$

The relationship in Equation 5.8 offers the possibility of determining the entangled coefficient, δ, without the need to quantify the losses present in the experimental set up. This could be useful to reduce ambiguity in the reported values of δ.

5.3 Probing the Higher Gain Regime

We have developed a model for the effects of losses in the down converted field on eSFG, and the overall structure appears to be adhered to. However, we only have two data points that show one key feature of this theory, that a more lossy field becomes more efficient than a less lossy one at sufficiently high energies. Furthermore, there are clear indications that the model is incomplete with our inability to reconcile the measured losses to the fitted transmissions, particularly at high energies and losses. We will address this in several ways. First, we will modify the experimental design to simplify and enhance consistency between datasets. This involved changing the neutral density filters from absorptive (Thorlabs NDK01) to UVSF reflective (Thorlabs NUK01) as we knew the material and could place a blank window of the same thickness for the no losses scans to ensure the dispersion was the same between each measurement. We placed all filters and the window into a filter wheel (Thorlabs FW102C) to remove the need for human interaction further and allow for greater automation. Finally, we removed the 70 nm filter. These changes mean the data presented in this Section will not be compatible with that in Section 5.1 as while the gain levels are similar, the measured PDC energy will be different. We will also include in the model the effects of gain on the PDC near field size (Section 3.4). Until now, we have treated the flux as proportional to energy. It is actually proportional to intensity; factoring this in will improve the model in the high gain regime.

5.3.1 Crossing Points

We will call the powers at which low loss field stimulate the same up conversion as a more lossy field, described in Section 5.2.2 by Equation 5.7, crossing points. As a practical matter, all down converted states will contain some amount of losses. Therefore, whilst the feature is not particularly beneficial, it should be present in all eSFG experimental designs and may provide a way to determine the linear coefficient independent of losses as attempted in Equation 5.8. In order to show that crossing points are a feature of entangled two photon interaction with losses, we will slightly alter the

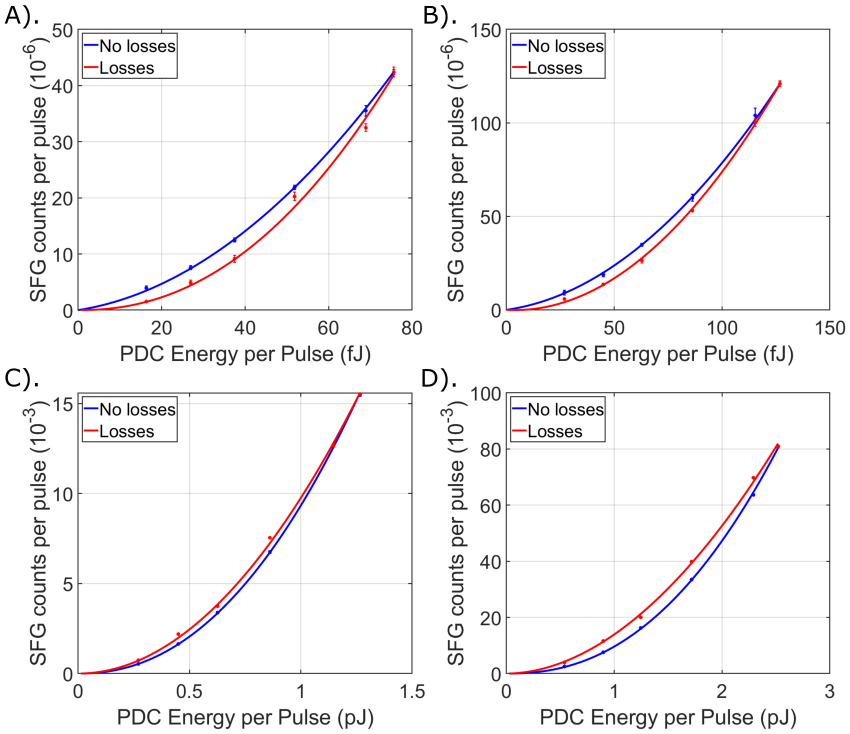

Figure 5.6: Power at the crystal reduced by the addition of more losses (red) vs by the reduction of gain (blue). As we progress A though to D, the initial gain is increased. For A and B, the gain is in the same range as Figure 5.4. For C and D, the gain is ∼2 and ∼2.5 times larger than Figure 5.4 respectively.

experimental procedure. For this data set, we will compare the SFG counts found from reducing the PDC energy by reducing the gain versus keeping the gain constant and reducing the PDC energy at the SFG crystal by adding losses into the far field of the PDC. This is the way that it has been done in literature previously; we will do this procedure in the non linear regime of eSFG. In particular, we will aim to match the energy at the SFG crystal with and without losses.

The result is shown in Figure 5.6. The blue data points and curves show the eSFG collected by reducing the PDC pump (PDC gain) and the red data is collected by increasing losses. One advantage of this method of investigating losses is that for the losses scan, the gain of the PDC is constant; therefore, we do not need to consider the changing properties of the PDC near field during analysis. Plots A to D are taken by increasing the initial gain level. These plots display the expected behaviour for the

model described by Equation 5.6. I think this procedure leads to confusion, so I will try to spell out some features explicitly. When doing this, the two curves meeting is not surprising or interesting; it is inevitable because the first data point for both the loss curve and the no loss curve is the same data point. This is made more confusing because the previous data I have presented, when I refer to a scan with losses in the down converted field, they had static losses, and the PDC energy was reduced by changing the gain. This time, losses are increased to reduce the PDC energy for the losses scans. Therefore, the first point is meaningless; it is simply the down converted field with no losses. Instead of looking for the point where they intersect, we need to examine the difference between each loss (red) and no loss (blue) data point. If at any energy, the loss data is higher than the no loss data, that means a more lossy field has stimulated more SFG with the same energy at the down converted crystal, the key feature of the crossing points introduced in Section 5.2.2.

My conclusions for this set of data are as follows: in the low gain, it is always more desirable to have a purer quantum state, but as we increase the gain, adding losses into the down converted field becomes advantageous. This can be seen as the data collected by reducing the PDC pump (blue data points) starts as more efficient (above in Figure 5.6 A and B) but as gain is increased, the data collected by increasing the losses (red data points) becomes more efficient in Figure 5.6 C and D. As previously stated, this may only occur because we already have losses in our down converted field. In the case considered here, quite a large number of losses, as all of the intentionally more lossy data points gave a brighter response at finite powers.

5.3.2 The Effects of Gain on eSFG

With the slightly altered experimental setting detailed at the start of this section, we can repeat the same experimental procedure as in Section 5.1, measuring the PDC energy at the SFG crystal and recording the resultant SFG counts from the PMT detector. We did this procedure for all the energy available to us for three different ND filters and the blank window of the same material and thickness, and the results are shown in Figure 5.7. This data is over a large range of energies, and therefore, it

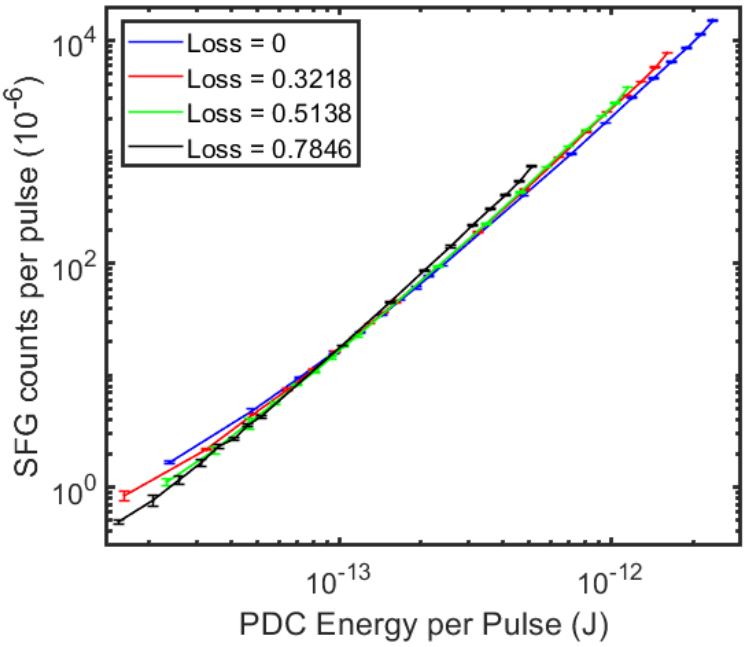

Figure 5.7: Repeating scan of power with the addition of static losses in the far field as in Figures 5.2, 5.3 and 5.4 with the filters and setting used for Figure 5.6.

is convenient to present it in log-log space. The general shape of the data is precisely as expected for very lossy fields. The fields with the most losses, black and green data points, begin by stimulating the least SFG. However, as the gain is increased, these stimulate the most, just as the black line in Figure 5.5 is predicted to stimulate a brighter response than the less lossy, green field. Whilst the structure is captured, we are unable to fit this data simultaneously with Equation 5.6 as was done in Figures 5.3 and 5.4 in Section 5.2.1. At the gain levels we have pumped the down conversion in this data set, we can no longer ignore the effects gain has on the physical properties of the down converted field. We therefore need to modify our model to account for the effects of gain.

5.3.3 Modified Model

Begin by considering classical sum frequency generation. We will assume that all scaling will relax to the classical case as $E \to \infty$. The classical limit on the up converted intensity, I_f, is related to the pump intensities, I_s and I_i, via [40]:

$$I_f = \sigma_{int} I_s I_i, \tag{5.9}$$

where we have placed all of the dependence on phase matching and crystal properties into the coefficient σ_{int}. We do not measure intensity, we instead measure pulse energy. This would not be a problem if the pulse shape and duration did not change. However, in the down converted field, they do (Section 3.4). We can explicitly write Equation 5.9 in terms of energy:

$$\frac{E_f}{\Delta t_f \Delta x_f^2} = \sigma_{int} \frac{E_s E_i}{\Delta t_s \Delta x_s^2 \Delta t_i \Delta x_i^2}, \tag{5.10}$$

E_n, Δt_n, and Δx_n are the energy, pulse duration and beam waist, respectively, of the n^{th} field (assuming a Gaussian pump). For classical SFG pumped with a Gaussian pump, the beam size and pulse duration are related by a constant factor, $\sqrt{2}$, which can be seen by substituting the Gaussian pulse shape into Equation 5.9. For the case we are considering, the two pump fields have the same pulse duration and beam size therefore we can make the substitutions $\Delta t_s = \Delta t_i = \Delta t$, $\Delta x_s = \Delta x_i = \Delta x$, $\Delta t_f = \Delta t/\sqrt{2}$ and, $\Delta x_f = \Delta x/\sqrt{2}$:

$$E_f = \frac{\sigma_{int}}{2\sqrt{2}} \frac{E_s E_i}{\Delta t \Delta x^2}. \tag{5.11}$$

The same argument for the linear term in the low gain results in no dependence on the pulse duration or beam size. Substituting this into Equation 5.6 results in an alteration to the second order term:

$$R_{tot}(T, E) = T\delta E + \frac{\sigma E^2}{\Delta t \Delta x^2}(2T^2 - 2T + 1). \tag{5.12}$$

When pumped with PDC, the beam size, pulse duration, and energy depend on gain. As we measure the energy at the up conversion crystal, we will treat the beam

size and pulse duration as if they were directly dependent on the measured pulse energy:

$$\Delta t = \Delta t(E),$$
$$\Delta x = \Delta x(E).$$

As we have previously done, we will take the ansatz derived from [49]:

$$\Delta i = \sqrt{\frac{\tanh(g)}{4g}}\Delta i_0. \tag{5.13}$$

$i = x$ or t, Δi_0 is the pump's i^{th} property and g is the gain. The energy of the down converted state can be written as:

$$E_{PDC} = n \sinh^2(g). \tag{5.14}$$

The energy in the equation above is the down converted energy produced at the down conversion crystal. This relates to the energy measured at the up conversion crystal, E, via the relationship:

$$E_{PDC} = \frac{E}{T},$$

where T is the transmission of the system as in Equation 5.12. Substituting these definitions into Equation 5.12:

$$R_{tot}(T,E) = T\delta E + \frac{8\sigma \operatorname{asinh}^{3/2}\left(\sqrt{E/nT}\right)}{\Delta t_0 \Delta x_0^2 \tanh^{3/2}\left[\operatorname{asinh}\left(\sqrt{E/nT}\right)\right]} E^2(2T^2 - 2T + 1). \tag{5.15}$$

5.3.4 Fitting with the New Model

Equation 5.15 assumes that the second order term scales with the average intensity of the down converted state and expresses the rate of up conversion in a quantity we can easily measure, the energy. These assumptions will allow us to fit the data in Figure

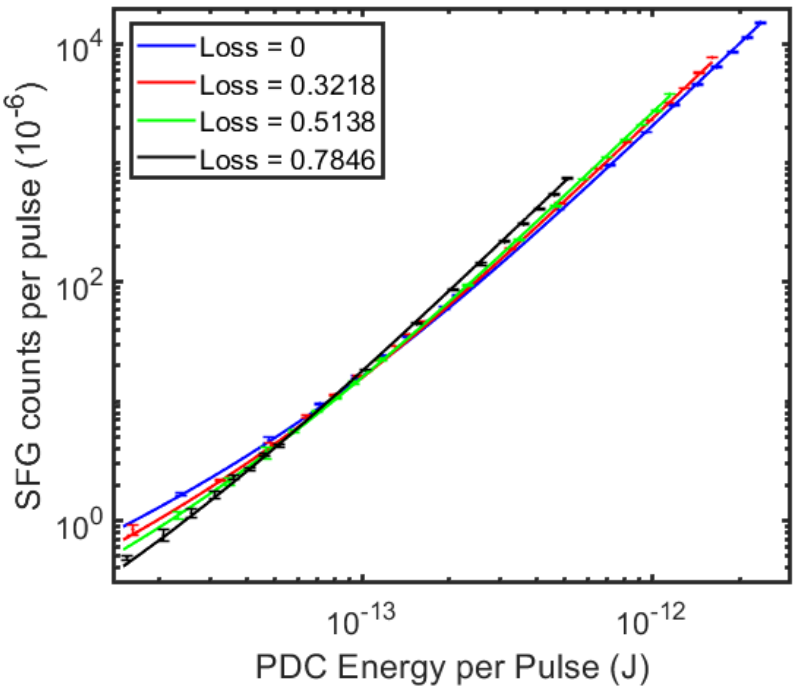

Figure 5.8: Data with UVSF filter attempted to fit with equation 5.15.

5.7. First, define a new second order coefficient:

$$\sigma' = \frac{8\sigma}{\Delta t_0 \Delta x_0^2},$$

We can carry out a similar procedure as in Section 5.2.1. We try fitting the 'no losses' case to Equation 5.15 and fit for δ, σ and n while trying different values of the initial transmission T using Matlab. We then take these, multiply the fitted transmission by the measured transmission for each data set to create the different curves and attempt to maximise the R^2 of all fits simultaneously. The result of this procedure is shown in Figure 5.8; all fits have R^2 values greater than 0.99. The fitted values of $\delta = 1.10 \times 10^9$ and $\sigma' = 1.10 \times 10^{21}$ with a transmission of the 'no losses' case of 0.0397. The fitted values of δ and σ are within one order of magnitude of the ones found when filtering (Section 5.2.1). As we have entirely changed the filtering of the down converted state, this is acceptable. However, this implies we have massive transmission losses even without any filters.

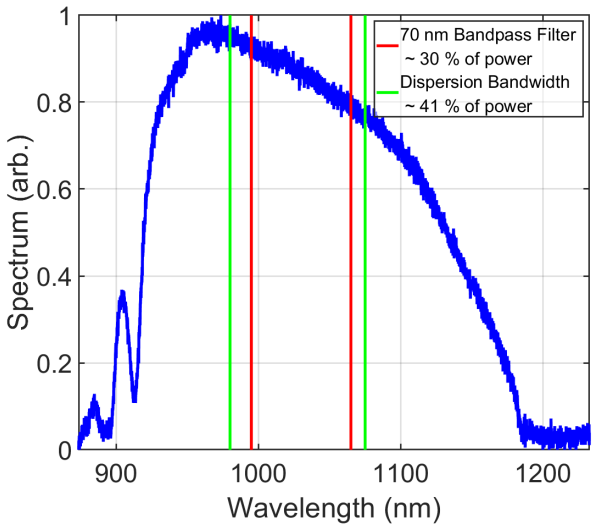

Figure 5.9: PDC measured spectrum showing the width of the 70 nm band pass filter (red) allowing transmission symmetrically around 1030 nm to maximise eSFG and the width of the spectrum transmitted with minimal additional dispersion from mirrors (green).

Removing the spectral filter supplies us with far more PDC photons and, therefore, a greater number of up converted photons. However, a large proportion of these PDC photons cannot undergo eSFG and, therefore, will count as part of the loss terms in Equation 5.15 as the modelled transmission reflects not simply the losses but really the percentage of the field we receive at the up converted crystal which can undergo entangled interactions. Figure 5.9 shows the full PDC spectrum with the bandwidth of the 70 nm filter, a bandwidth that we feel confident we can preserve entanglement well over, and the approximate bandwidth for which the Group Delay Dispersion (GDD) coefficient of the mirrors we use to filter the PDC pump remains below ~ 50 fs^2 which we will take as the bandwidth over which the dispersion of the optics is not so large as to destroy entanglement. With this assumption, a maximum of ~ 40 % of the measured down converted energy without the filter in place can coherently recombine. Therefore, we would expect the fitted value of T to be below this value; however, it is still an order of magnitude larger than the fit found. If the fitted transmission is accurate and the interpretation of the coefficients is correct, we will incur significant losses in our down converted field. Nevertheless, we still see an effect that is explained by the quantum

nature of the down converted state as its origins lay in the linear term of eSFG.

5.4 Discussion

As far as I am aware, this is the first systematic study of the effect that losses in the down converted field have on entangled sum frequency generation. For our convenience, we have introduced losses by randomly removing photons from the far field of the PDC. Doing this allowed us to quantify and control the losses easily. However, this is not the only form of loss. Any process which destroys the entanglement is a source of losses for the transmission coefficient T in Equations 5.6 and 5.15. T is not just a measurement of the transmission of the system but a measurement of the spatial-temporal losses of the system or, to put it another way, our inability to recombine the down converted state in both space and time. This is a stronger constraint than temporal losses that we can quantify by taking coincidence measurements. Without this quantity, we cannot appropriately calibrate the number of PDC photons we have available to undergo entangled SFG. Of particular importance, I believe, is re-imaging the down converted state inside of the sample we wish to undergo up conversion. By imaging the down converted state, we ensure that the field is reconstructed in intensity and give us the best chance of recombining the twin beam state in time and space. The ability, or quality, of imaging is a hard figure to quantify. However, I believe that failure to control for it adequately has been a significant problem in previous studies and can account for much of the reported inconsistencies.

Now that we have some conclusions of our own, I will return to some previous studies and attempt to comment on the results they have presented. What follows will be speculation and interpretation; we do not have any additional knowledge of these experiments than reported in the articles and supplementary materials. Furthermore, as we are proposing a novel interpretation, no data is directly applicable to our mechanism. It will, however, be an illuminating exercise, conveying the importance of the conclusions we have reached.

5.4.1 Reflective Review of the Literature

First, we should address the results of the two reports which have questioned previous investigations into this type of phenomena. Single-photon scattering [34] and hot-band absorption [39] have been shown to mimic the expected linear response at low photon fluxes and therefore can be confused for entangled two photon absorption. There is nothing that we have presented which disagrees with the point made in these reports. However, neither of these specific mechanisms can pertain to the results we have presented. Both of these criticisms rely on features that we do not have. In the case of single-photon scattering [34], this is only relevant when the up conversion process is inferred by measuring the down converted state; we, however, measure the up converted state directly. Hot-band absorption [39] is a molecular effect that can occur when high energy ground state electrons can be stimulated into their excited state by a single photon, which we have avoided by testing with sum frequency generation. Our conclusions, on the other hand, can be applied to all experiments in entangled two photon absorption as they rely on the nature of the field used to drive this interaction. We have to be careful and not speculate too much. However, several choices have been made in previous studies that, given what we have shown here, we may wish to question.

For instance, in both [34] and [39], they attempt to view entangled two photon absorption (eTPA) and present reasonable schemes. However, in both cases, we can question their ability to reconstruct the down converted state in space. In [39] (Supporting Information), they tell us the FWHM of the pump field inside of the down conversion crystal is $\approx 30\mu m$ whereas the SPDC beam width is $55.5\mu m$ in the sample cuvette. This means that they probably are not imaging the down conversion state one to one, which is the easiest way to ensure we can recombine the down converted state and interact deterministically. We cannot be sure that they are not trying to image the down converted state produced in the crystal at the sample partially because, unlike in our experimental design, they are focusing the PDC pump field into the down conversion crystal. This is not required to produce the state necessary to observe eTPA. It is usually done to increase the maximum intensity and thereby increase conversion effi-

ciency. However, in order to study the linear relationship between the number of pump photons and the number of up converted photons, we require spontaneous emission and higher intensities are not required. For the purpose of reconstructing the entangled pairs at the sample, focusing in the down conversion crystal should not matter. However, as in [39] they do not mention explicitly what lenses they are using to deliver the down converted state to the sample, nor do they state whether they attempt to keep the down converted state in its imaging plane, these do not seem to be properties that they believe are important. A similar problem arises in [34] where they focus the down converted state with a cylindrical lens. This will destroy many of the spatial correlations between individual photons. It should be noted that they do measure coincident counts between entangled photons after this lens however, temporal coincident counts are insufficient to determine whether a pair of photons can undergo eTPA. These possible issues do not detract from the reported result. The mechanisms they suggest for the linear scaling they see are still valid in the cases outlined and remain a concern for observing eTPA. However, we might question their ability to observe eTPA and therefore any strong conclusions about the relative magnitude of the observed effect versus eTPA.

Of particular interest to this discussion are the reports that study the same fluorophore. The articles [35], [36], and [37] all study Rhodamine 6G with conflicting results. In [36], they observe eTPA with approximately 8.7×10^{11} photons s^{-1}.

They observe the linear scaling between incoming photon flux and florescent signal by reducing the gain and measuring the fluorescence directly. They go on to show this linear relationship is due to entangled two photon absorption by also observing a second order relationship when they reduce the incoming photon flux by attenuating the down converted state directly. This is a robust method for showing that the linear scaling observed is due to entanglement and not a different single photon scattering process, such as hot band absorption. Studies [35] and [37] however, do not observe eTPA in Rhodamine 6G. All of these studies use varying crystals and lasers. [37] uses a pulsed, 110 fs laser with a central wavelength of 810 nm, frequency doubled to 405 nm, pumping a PPKTP crystal. [35] and [36] both use continuous wavelength lasers centred

on 532 nm pumping PPLN. The different crystal and beam properties will change the state somewhat; therefore, a direct comparison between studies is difficult. However, in [37], they fail to see any eTPA despite having approximately 1.2×10^{10} photons per second. Moreover, [35] shows a linear relationship between PDC pump power and SFG in a second PPLN crystal but then cannot see a linear scaling with the same set-up with eTPA in Rhodamine 6G with a maximum of approximately 5.4×10^{11} photons s^{-1} available to the sample. Both are lower than the energy used in the report, where they saw the linear scaling, and therefore, if their detectors are sensitive enough, they should have been able to see the linear scaling. What can be going on with these studies?

We will begin an attempt at explaining these discrepancies by outlining some assumptions. First, for this experiment, there is no fundamental difference between using a pulsed versus a continuous wave laser. The linear scaling that we try to observe will occur in the spontaneous regime of parametric down conversion where each twin beam state is independent of each other. Therefore, pumping with a pulse beam is equivalent to chopping the state produced by a CW pump, which both the cases that pump with a CW beam do in order to time gate the response (as in [35] and [36]). Second, the choice of crystal is not essential to the process. All we really care about is the energy-time, position-momentum entanglement present in the down converted state, which will be there no matter the crystal. The choice of one crystal versus the other may alter the efficiency of eTPA due to the dispersive effect of the crystal or the exact spectral response; however, the choice of PPKTP over PPLN should not be the difference between observing eTPA and not. Next, we will assume that all alignment is perfect. Much of the variation in reported results could be attributed to poor alignment; we have observed considerable swings in eSFG efficiency due to slight misalignment in our delivery system, which is hard to control, particularly when you do not realise you need to. However, we would do a disservice to our colleagues to assume this is the case. Finally, the most crucial aspect of the down converted state delivery system (how the down converted state is transmitted from the down converted crystal to the sample) is whether they are successful at recombining the down converted state in time and space. This can be reduced down to a maximum of three optics, the optic

projecting the beam into the far field of the down converted crystal, the optic projecting the beam into the near field of the down converted crystal or 're-imaging' the down converted field and, possibly, an optic focusing the pump driving into the down conversion crystal. All other optics between the down converted crystal and sample should not affect re-imaging process in these studies.

So far as we can determine, none of the studies mentioned ([35], [36], and [37]) recombine the down converted state in a one to one fashion as we do. This may not be essential to constructive recombination; however, there are reasons to suspect that it will be necessary. Returning to the equation derived for the rate of eSFG:

$$\hat{a}^{\dagger}_{SFG}(\omega_1, L)e^{i\omega_1 t}\hat{a}_{SFG}(\omega_2, L)e^{-i\omega_2 t} = L^2 \int_0^{\infty} d\omega \int_0^{\infty} d\omega_p \,\mathrm{sinc}^2\left[\Delta k(\omega_p, \omega)L/2\right] \beta^2(\omega_p, \omega)$$
$$\times \Big\{ |D(\omega, L')|^2 |C(\omega, L')|^2 |A_p(\omega_p)|^2 \hat{a}_i(\omega_p - \omega, 0)\hat{a}^{\dagger}_i(\omega_p - \omega, 0)\hat{a}_s(\omega, 0)\hat{a}^{\dagger}_s(\omega, 0)$$
$$+ |D(\omega, L')|^4 |A_p(\omega_p)|^4 \hat{a}_s(\omega, 0)\hat{a}_i(\omega_p - \omega, 0)\hat{a}^{\dagger}_i(\omega_p - \omega, 0)\hat{a}^{\dagger}_s(\omega, 0) \Big\}. \tag{5.16}$$

There are two terms which we have previously identified with the coherent and incoherent component. The second term proportional to:

$$\hat{a}_s(\omega, 0)\hat{a}_i(\omega_p - \omega, 0)\hat{a}^{\dagger}_i(\omega_p - \omega, 0)\hat{a}^{\dagger}_s(\omega, 0), \tag{5.17}$$

we have previously said describes interactions between non entangled pairs and is precisely a measurement of the second order correlation function, $G^{(2)}$:

$$G^{(2)}(\vec{r}_1, t_1; \vec{r}_2, t_2) = \langle E^*(\vec{r}_1, t_1)E^*(\vec{r}_2, t_2)E(\vec{r}_1, t_1)E(\vec{r}_2, t_2)\rangle. \tag{5.18}$$

The more important term is the first:

$$\hat{a}_i(\omega_p - \omega, 0)\hat{a}^{\dagger}_i(\omega_p - \omega, 0)\hat{a}_s(\omega, 0)\hat{a}^{\dagger}_s(\omega, 0), \tag{5.19}$$

this is the term that leads to linear scaling. This term refers to a process in which the single photon produced in down conversion is essentially instantly destroyed in

the up conversion process. In order to maximise this in the second up-conversion crystal, we need to reconstruct the real state, i.e. images one to one. The purpose of altering the field is generally to increase the intensity of the PDC as classical SFG scales with intensity. However, as stated in Section 5.3.3, we should not expect this intensity dependence to be mirrored in the linear regime. Therefore, focusing the down converted field into the sample for the sake of increasing intensity is needless if we want to study the linear relation between PDC and eSFG/eTPA. The analysis undertaken in Chapter 2 is for eSFG explicitly however, the same terms appear when eTPA is considered explicitly [21, 47–49, 69] with the same interpretations.

In [36], they observe the quantum effect but do not make any effort to match the state produced at the down converted crystal in the sample. They project the PDC into the far field with a 100 mm spherical lens and then focus with a 3 mm aspheric lens. This may be beneficial even without the one to one imaging as aspheric lenses are designed to correct for spherical aberrations and allow for smaller focal point. Therefore, they may bring all the photons they produce close enough in proximity to allow for linear scaling. They can do this because they only have, or are very close to only having, a single spatial mode and well below one photon per mode. Therefore, this study does not run the risk of overlapping modes and permitting the classical process to overwhelm the quantum. There are two other key choices made that may affect this observation. First, they have a smaller bandwidth when compared with the other two studies. A smaller bandwidth means the down converted state is emitted more symmetrically about the pump. Therefore, it is harder to meaningfully change the path length between the entangled photons when using such a simple design as in [36]. They also do not focus their pump into the down converted crystal but rather pump with a collimated beam. I cannot understand why this would alter the effect, however, the other two studies discussed here focus.

Provided we do not utterly destroy the spatial-temporal entanglement in our down converted state, we should always be able to see some remnant of the linear term. This is, I believe, the explanation for the result presented in [35] where they do not see the linear term from two photons absorption but do see it in sum frequency generation.

Entangled sum frequency generation is somewhat biased towards interactions between the entangled pairs due to the phase matching constraints placed on this process, particularly when the same crystal is used for up and down conversion. We cannot be sure that they are not imaging one to one as they do not state they are not or mention the lenses used. They do, however, mention that 'If focusing into the molecular sample is insufficiently tight ... there is a chance that the two photons within a pair will have poor spatial overlap', which implies they believe that the PDC beam waist is a property they can change after the down converted process. Therefore, they probably are not imaging one to one. I do not believe that the prism compressor they use for dispersion compensation contributes to spatial misalignment. A prism compressor can destroy the spatial properties of the beam used in it. However, they appear to deal with this appropriately by keeping all beams parallel. Therefore, we would expect aberrations to be at a minimum. It is reported in the thesis of Landes that this set up did eventually produce the expected linear response and curved towards a second-order term as they transitioned from below the single photon per mode to greater than one. Hence, this design cannot be too far from a working solution. I believe the primary problem will be the focusing and delivery of the down converted state into the sample. As they could observe a linear relationship in SFG, they cannot have eradicated the entanglement. Interestingly, they do mention and quantify the losses in a coincidence set up. When doing so, they even mention the necessity for a good spatial overlap. However, this method for determining losses can only quantify the temporal losses, so whilst I agree with their reasoning for attempting to quantify the losses, I do not believe this to be sufficient for quantifying the relevant losses inherent in this experiment.

The final study into eTPA of Rhodamine 6G we want to discuss [37] does not have any results showing a linear scaling between PDC and eSFG. This is a study of several common fluorophores, and in none is the linear term seen. Again, they do not image one to one; instead, they focus the pump and then collimate and refocus the PDC with a 200 mm and 50 mm lens, respectively. They quantify the losses by measuring the reduction of power from the up conversion crystal to the sample at 24 %. As mentioned in [35], this is not sufficient to quantify the relevant losses for entangled two photon

interactions. The losses they have are likely more extensive than this as they are not recombining the entangled state. One possible issue they face is that the PDC pump they use is centred on 405 nm. Therefore, the down converted state is centered at 810 nm. Classically, the two photon cross-section is relatively low around this wavelength. Hence, we would expect any eTPA to also be reduced relative to eTPA from a source centred on 1064 nm, as the other studies use.

All three studies have some potential issues, but the overarching issue is that none of them appropriately quantifies the losses in their converted state. However, this is mainly due to not having a mechanism that could describe this quantity appropriately. It is clear that without this, comparisons between these studies are nearly impossible despite the same, well established fluorophore used.

5.5 Conclusion

In this Chapter, we have shown the typical, expected linear relationship between the PDC energy and up conversion flux in eSFG. We have gone on to develop a model for the effects of losses in the down converted field as we transition into the high gain of parametric down conversion and shown that this has a good agreement with the experimental result. The characteristic outcome of this analysis suggested that a less entangled state/ more lossy state would stimulate more response at high photon fluxes. We went on to show this two times over and further developed the idea, factoring in the changing beam property. This result begins to place a limit on the achievable efficiency available to us from using entangled sources over a classical two photon process based on experimental design; we can start to understand what would make a good design versus a bad one. It also may help explain the varying reports in literature as we have previously failed to consider this aspect of the down converted state. We also implied a method to potentially quantify the losses. We may be able to determine independently the linear coefficient for a known crystal through a relationship such as 5.8 or by fitting the full Equation slightly above a single photon per mode. We can then use this to measure the effective losses in our down converted field by observing the linear regime and comparing the measured coefficient to the expected one. In attempting to observe

this phenomenon, there are a multitude of variables to consider. We have identified one of them, what we have termed the spatial-temporal losses. However, the phase matching of the down converted state will also affect the efficiency of up conversion in a way that these losses will not factor in. There are still challenges to be overcome with respect to comparative studies of this phenomenon. However, the introduction of spatial-temporal losses to this problem is a helpful starting point.

One final comment on the results presented in this chapter. While I am confident that the linear coefficient should depend linearly on the spatial-temporal losses and there should be a relationship between the linear and second order coefficient which depends on the spatial-temporal losses; I am not convinced that the crossing points observed (Sections 5.1.2, 5.3.1 and 5.3.2) are fundamental. Instead, I believe these are a consequence of the changing near field size and duration with gain and therefore a decoupling of the down converted near field intensity from down converted energy. When these studies were undertaken, we did not appreciate the magnitude of this effect. This will be addressed in the following chapter.

Chapter 6

eSFC Classical Comparison

It is appropriate to consider the correct comparison between classical and entangled sum frequency generation. We cannot show that driving sum frequency generation with a down converted field stimulates more up conversion than when driven by a classical field by adding losses in the entangled field, as previous studies have done, to show the quantum nature of the interactions. This is because the entangled state, even when spoiled by random losses, contains quantum correlations. However, the appropriate classical state to compare to is not apparent. In this chapter, we will consider this problem and present an investigation to place limits on the magnitude of any advantage. We will see that we can expect a slight improvement from the use of entangled photons in the stimulated regime of parametric down-conversion. However, this is lost at energies that are reasonable to drive sum frequency generation or two photon absorption experiments. I worked with a lab partner to mount these experiments, and I undertook the analysis of the results presented here myself.

6.1 Introduction

When considering which classical state we should compare with, there are several problems relating to the physical properties of the down converted state to consider. Specifically, we have a very broad spectrum and the pulse duration and near field size both change with the gain of the PDC. The simplest way of producing a 'classical' state (a

state without the quantum properties) while preserving all other properties of the PDC would be to destroy the entanglement in our down converted state. The PDC photons are emitted symmetrically about the pump beam propagation direction. Therefore, by removing photons symmetrically or asymmetrically in the PDC far field, we can preserve or destroy the entanglement whilst conserving the near field distribution. However, this in no way represents the field that is usually used to drive sum frequency generation. If we want to make a comparison with the classical field that is used in, for example, fluorescent microscopes, that would be the coherent laser field. The rate of classical sum frequency generation scales proportional to the intensity of the pump field. Therefore, the quantities we need to match are the energy per pulse, pulse duration and beam size. In parametric down-conversion, these properties are set by the gain of the PDC, and we will need to manually alter the beam size, pulse duration and energy of our coherent field simultaneously.

When we consider a comparison with a classical field, particularly in the high gain of PDC, we do not need to limit ourselves to the coherent contribution which recombines to form the pump. It remains the case that the only truly quantum interactions occur in this component. However, if this state is used to drive an imaging system, the whole up converted field would be selected as there is no advantage to only observing the coherent contribution. Whilst the additional contribution can only be classical in nature, it will not be a coherent state. Spontaneous Parametric Down Conversion is seeded from the background fluctuations, and therefore, its statistics are thermal. The rate of eSFG is proportional to two terms

$$\hat{a}_i(\omega_p - \omega, 0)\hat{a}_i^\dagger(\omega_p - \omega, 0)\hat{a}_s(\omega, 0)\hat{a}_s^\dagger(\omega, 0), \tag{6.1}$$

which describes entangled pairs interacting and

$$\hat{a}_s(\omega, 0)\hat{a}_i(\omega_p - \omega, 0)\hat{a}_i^\dagger(\omega_p - \omega, 0)\hat{a}_s^\dagger(\omega, 0), \tag{6.2}$$

which describes interactions between non entangled pairs. The second term is a mea-

surement of the classical second order correlation function $g^{(2)}$:

$$g^{(2)}(\vec{r}_1, t_1; \vec{r}_2, t_2) = \frac{\langle E^\dagger(\vec{r}_1, t_1) E^\dagger(\vec{r}_2, t_2) E(\vec{r}_1, t_1) E(\vec{r}_2, t_2) \rangle}{\langle |E(\vec{r}_1, t_1)|^2 \rangle \langle |E(\vec{r}_2, t_2)|^2 \rangle}. \tag{6.3}$$

This is essentially a measurement of how likely it is that two photons arrive at a specific position and time. For an ideal coherent state, this will always be 1. For a single mode thermal state, however, this will peak at $t_1 = t_2$ and $\vec{r}_1 = \vec{r}_2$ at a value of 2. Therefore, there is the possibility that pumping sum frequency generation with a thermal state may lead to a doubling of its efficiency [70–72]. Moreover, for entangled sum frequency generation, the first term described by Equation 6.1 remains. This contains a term that is also proportional to the square of the intensity. Therefore, one may conclude that pumping SFG in the high gain of parametric down conversion would, at worst, reach an equilibrium of three times the efficiency of a similarly intense classical coherent field [72]. When we compare eSFG to classical SFG directly, the result we see is not this clean cut. The remainder of this chapter will detail how the measurement was taken.

One last point of confusion we should address is that of terminology. We have been referring to the component of eSFG that contains the linear term as the coherent contribution, so named as it reconstructs the original PDC pump which is a coherent field. However, now we pump the SFG with a coherent field directly. To avoid this conflict, we will refer to the coherent pump as a classical field. This chapter will be formulated as such. The following section will use the entangled data shown in the previous chapter (with the 70 nm band pass filter in place) and compare this to classical SFG. It will, therefore, be a comparison between the coherent eSFG and the classical SFG. We will use this to place a limit on any entangled advantage we might expect to see from the down converted state. We will then consider the entire up converted field and show how the scaling in the high gain compares to a classical state. Finally, we will consider the effects that changing the length of the SFG crystal has on up conversion efficiency. This is a preliminary result, but the ideas it stimulates may be helpful when considering applications of this phenomenon.

6.2 Coherent eSFG Vs Classical SFG

The entangled data for this section was taken from Section 5.1 where the PDC is filtered with a 70 nm bandpass filter in the far field. This is done in an attempt to ensure the measured PDC can undergo entangled interactions in the up conversion process. We require the ability to change the duration of classical pulses and their beam size in accordance with their energy. This can be done with a pulse compressor used to chirp the field and a zoom beam expander. We will go into this in more detail in Section 6.2.2. First, we will detail an alternative method to determine the near field size and pulse duration at varying PDC powers.

6.2.1 Near field size and power

Throughout the previous Chapters of this thesis, we have used a model to fit the near field size versus PDC power data. When the measurement presented here was taken, we did not have this model. Therefore, a different technique was used, providing an alternative way to look at the problem similar to the formulation in Section 3.4.1 without taking the high gain limit. We relax the plane wave approximation in:

$$n_{PDC}(\Lambda, P) = n_0 \sinh^2(\Lambda\sqrt{P_{pump}}), \tag{6.4}$$

and substitute in a Gaussian pump field for one spatial dimension, $P_{pump} = P_{pump}(x)$:

$$P_{pump}(x) = P_0 \exp\left(\frac{-x^2}{2\sigma^2}\right). \tag{6.5}$$

By doing this, we get an Equation which can describe the down converted state distribution with only one true unknown, Λ:

$$n_{PDC}(x) = n_0 \sinh^2\left(\Lambda\sqrt{P_0}\exp\left(\frac{-x^2}{4\sigma^2}\right)\right). \tag{6.6}$$

As we have seen previously in Section 3.4.1, in the high gain, this relaxes to a Gaussian with a variance of $\sigma/\sqrt{\Lambda\sqrt{P_0}}$. However, across the entire range of gain, we can approximate the result as a Gaussian. We can use the following procedure to find the

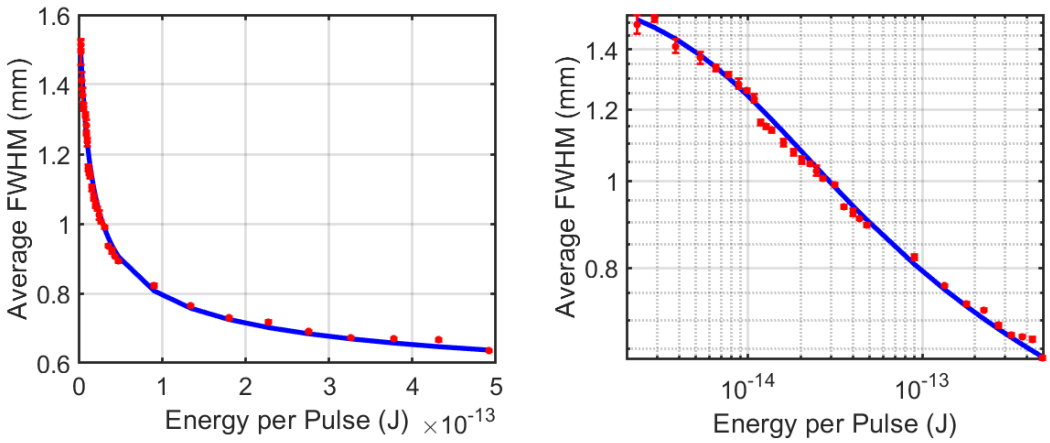

Figure 6.1: PDC near field size versus PDC energy modelled with the procedure described in main text. Presented in both linear and logarithmic scales.

value of Λ and thereby infer how the beam size and duration change with increased pump power:

1. Select a choice for Λ. We can also make selections for the beam size, σ, and PDC coefficient, n_0. However, both of these parameters can be separately determined and, therefore, need not necessarily be fitting parameters.

2. In our case, we measured the PDC power and therefore require a conversion between the PDC power and pump power given by:

$$P_0 = \left(\frac{\text{asinh}\left(\sqrt{n_{PDC}/n_0}\right)}{\Lambda} \right)^2 ,$$

   Where n_{PDC} is proportional to the measured PDC power. If we measured the pump power directly, we could ignore this step.

3. We then substitute these values into Equation 6.6, define a spatial dimension larger than the size of the pump field, $x >> \sigma$. Calculated the value of $n_{PDC}(x)$ along this dimension and fit the resultant to a Gaussian, reading off the expected variance.

4. These expected variances can be compared to the measured beam sizes and Λ

consequentially varied in order to better model the data and the procedure repeated.

This can be computationally expensive and slow; however, it is an effective method as shown in Figure 6.1. Once the parameter Λ is determined, we can determine the PDC pulse duration at varying power levels as well by simply replacing the spatial variance with the temporal one.

6.2.2 Changing the beam properties

We have an idea of how to model the beam properties with changing gain. Now, we need to be able to control a classical pump beam in order to mimic these properties. The main problem we face is that the down converted field is centred around 1030 nm and has a shorter duration than the field used to drive it, which is the second harmonic of the fundamental laser and has a duration of approximately 173 fs. The only classical field we have emitting at 1030 nm is this laser fundamental, which is naturally a longer pulse than its second harmonic. This field is also transform limited and, therefore, cannot be further compressed below its duration of 245 fs. The solution to this problem is to place the fundamental field into an optical parametric amplifier (OPA) and convert this field to 2060 nm. We can then up convert the field in a BBO crystal to once again be centered on 1030 nm. Both the down conversion in the OPA and up conversion result in shortening the pulse. In our case, the transform limited pulse should have a duration of about 50 fs determined by measuring the spectral bandwidth of the final field which had a full width half maximum of approximately 30 nm. However, we could not achieve this with our external pulse compressor and measuring the pulse duration with an autocorrelator. We instead achieved a minimum pulse duration of 60 fs, which is shorter than the required shortest pulse duration of around 80 fs and, as such, will suffice.

Figure 6.2 shows the experimental design. Note the flip mirrors at the exit port of the laser and just before the final SFG crystal. The lower path is the typical entangled design used previously. The upper path shows the components used to control the classical beam. The pulse is shortened as described above and then passes through

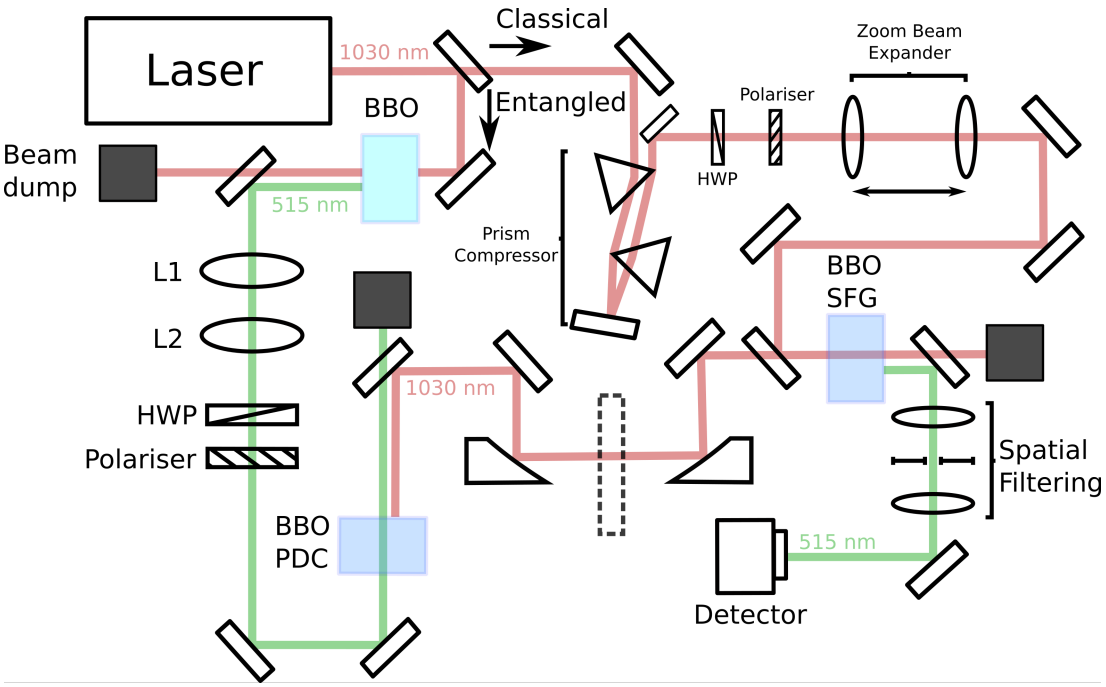

Figure 6.2: Experimental design. The lower path is the usual PDC production and eSFG set up, the upper path shows the beam manipulation to match the PDC properties. First is a pulse compressor for pulse duration control composed of two prisms and a flat metallic mirror. After this, the energy is controlled with a simple half wave plate and polariser and the beam size is controlled with a zoom beam expander. With these three elements, we can completely control the intensity of the classical pump.

a pulse compressor comprising of two UVSF prisms (Eksma 320-1218) and a folding mirror close to flat to reflect the beam through the two prisms. The dispersion in the prism leads to varying angles of refraction for the spectral components of the beam. They, therefore, propagate at varying angles between the two prisms and are brought back parallel by the second prism. By adjusting the prism's distances and positions, we can cause the shorter or longer wavelengths of the pulse to arrive at different times, thereby controlling the pulse duration [73]. The resultant beam is said to be chirped; we use this to achieve the required pulse duration as measured by an Autocorrelator (A.P.E Mini TPA/PE). The pulse durations were measured just before the beam entered the crystal to account for the dispersion added by the other optics.

After the pulse duration control, we have some spatial filtering comprised of a 50 mm aspheric lens (Thorlabs AL5040M-B), 100 micrometre pinhole and a 50 mm

plano-convex lens (Thorlabs LA1213-B) to ensure the beam profile remained Gaussian. Finally, the size of the collimated pump is controlled with a zoom beam expander (Thorlabs ZEB11). These comprise a minimum of three lenses with which we can control the beam size by varying the distance between the lenses. We then measured the beam size at the crystal position using a beam profiling camera (Gentec beamage 3.0).

6.2.3 Measurement

We want to make as close a comparison as possible to the entangled state and, therefore, need to vary the beam size and pulse duration for each power. We have, however, limited precision in the beam size and pulse duration we can achieve. Therefore, we selected a pulse duration and attempted to match it to the corresponding beam size. Then, we alter the energy of the pump in order to closely match the expected PDC energy for which the near field would have these properties. Instead of taking a single point, however, we took a scan around this value to ensure the expected second order relation and to determine the second order coefficient at this beam size and pulse duration. We repeated this for several values of power, beam size and pulse duration.

Because this is the first comparison where we consider the changing properties of the PDC near field properties, we wanted to make as direct of a comparison as possible and therefore have undertaken this procedure above. However, as we are investigating classical SHG we already know how the rate of up conversion changes with the pulse duration and beam size as:

$$I_{SHG} = \sigma_{int} I_{pump0}^2 \Rightarrow E_{SHG} = \frac{\sigma_{int}}{\sqrt{2}\Delta x_0^2 \Delta t_0} E_{pump}^2. \tag{6.7}$$

We therefore only need to take one measurement of the beam size and pulse duration, and we can use this to describe the up-converted power completely for all beam sizes and pulse durations.

The entangled sum frequency generation data used in this section is a combination of the data presented in Section 5.1 with no losses and a 70 nm bandpass in the PDC

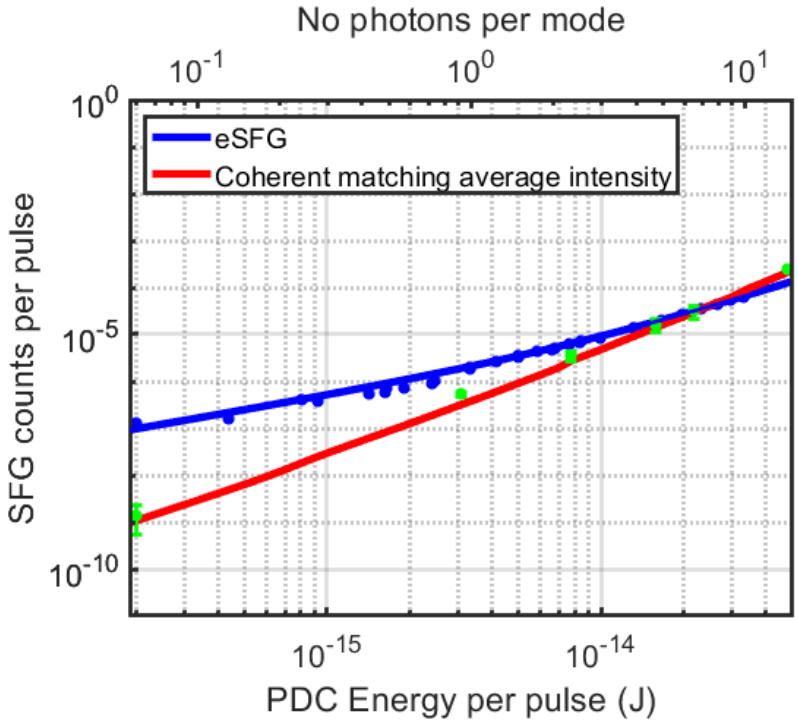

Figure 6.3: Classical SFG vs coherent eSFG. The eSFG is plotted in blue with a fit of the form $\delta x + \sigma x^2$. The green data points are the classical matching power, beam size and, duration. The red line is a projection using the expected values of beam size and pulse duration at a given power as in Equation 6.7.

far field. This consists of the data we have the most confidence in containing a strong quantum component however, as detailed in Chapter 5, we are fairly certain this is not optimised rather the best state that we could produce.

6.2.4 Result

The data is presented in Figure 6.3. Each green data point consists of a minimum of three scans taken around those pulse energies and with the properties of the near field PDC at that energy. The red curve is not fitted rather an average of the second order intensity coefficient for the classical field. This was determined by averaging the intensity coefficient (from Equation 6.7 this will be the intensity of the up converted field divided by the intensity of the pump field squared) found at each data point. I then estimated the expected up converted energy along the entire range of pump energies

using the changing beam size data presented in Figure 6.1 to calibrate the intensity at each energy. The blue entangled data is plotted with the fit found for the final no loss case to help understand the behaviour.

We can see that the coherent contribution for the entangled SFG becomes less efficient than the same intensity classical field, which occurs at approximately four photons per mode. Below this, the entangled case remains superior. This is the first evidence, to our knowledge, that displays a direct advantage in the stimulated regime of parametric down conversion in driving multi photon processes with down converted light when compared directly to a coherent field. It does however, place a limit on that advantage. Recently, there has been some suggestion that due to the persistent linear term, the entangled case should remain superior to the classical for all energies. We have already shown that if the down converted state has any losses, this may not be the case. The evidence here suggests that pumping SFG with a coherent state will also become more efficient than with a down converted state. However, we must remember that we are post selecting for the coherent contribution only in this data as to limit our consideration to just the quantum interaction. In the following section, we shall relax this and consider the entire up converted field.

6.3 Full eSFG Vs Classical SFG

We can consider the entire up converted eSFG by opening the iris in its far field (shown in Figure 6.2). Once done, we need to be careful to preserve both components. The coherent and incoherent components are emitted with different geometries. The incoherent component is emitted as a cone, and the coherent is a collimated beam. We, therefore, need to place a series of telescopes as if we just collimated the incoherent component, we lose the coherent, and if we just take the collimated coherent, we lose the incoherent. We placed a series of telescopes to ensure we maintain the near field of the eSFG and can image the SFG crystal at the position of the PMT detector with both of these components intact. When doing this, it is hard to keep the incoherent contribution as this component is very diffuse in the far field and cannot be seen directly. We believe that we may have losses in this component, possibly as much as

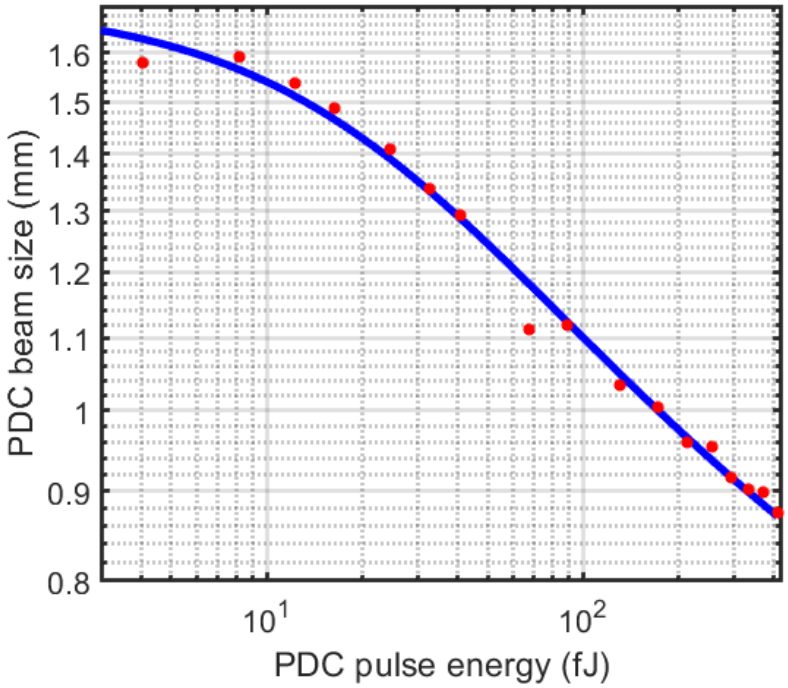

Figure 6.4: The near field size of the down converted state changing with PDC energy fitted with Equation 3.17. This data is the same as presented in Section 3.4.2.

50%, for this reason; however, we have not devised a way to measure these. If there are losses, these can, at worst, be systematic losses and, therefore, would be represented by a constant offset in the final data.

This comparison took place several months after our previous data was collected. When returning to this problem, the gain of our down converted state appeared to have changed. At the same pump energy, we got a lower PDC energy, but it appeared the number of modes had not changed. Believing this change was most probably due to a variance in our crystal due to damage or moisture infusion in the crystal, we retook the beam size versus PDC energy data (Figure 6.4) and used this to set the pulse duration and beam size of the classical field. Because of this change, I need to emphasise that the data presented in this section is not directly comparable to that in the previous sections, but the new comparison of eSFG (coherent plus incoherent) versus classical SFG is by itself valid.

The method for recording the eSFG is the same as before. We changed the PDC

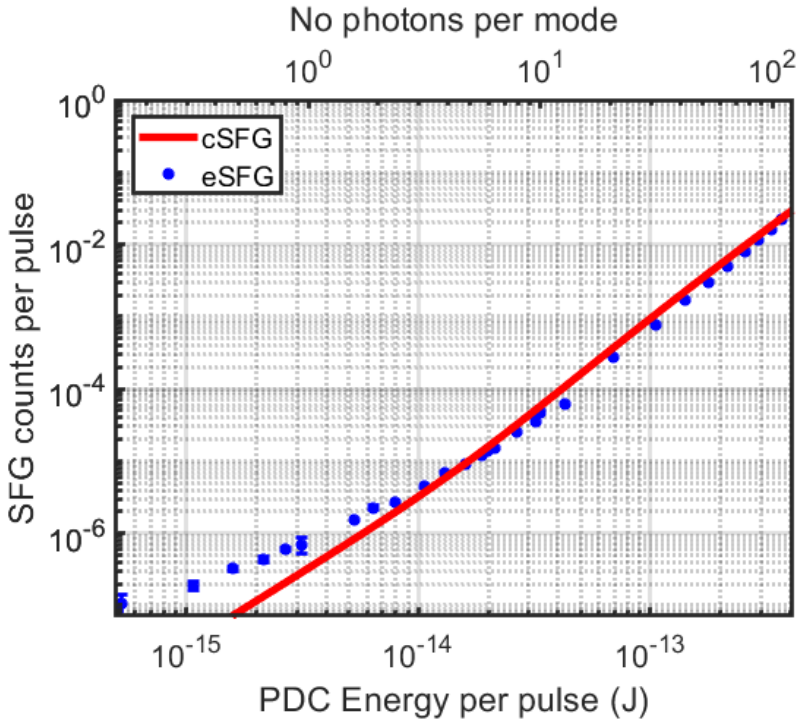

Figure 6.5: Classical vs all eSFG. The eSFG is plotted in blue. The red line is a projection using the expected values of beam size and pulse duration at a given power as in Equation 6.7.

pump power to reduce the PDC pump energy and measured the PDC power at the up conversion crystal, recording the eSFG response with a PMT. There is a 70 nm bandpass filter in the far field of the PDC, as with the previous data, and an 850 long pass filter to remove the scattering pump. For the classical data, we used the new calibration curves and projected the previous classical data using Equation 6.7 as there appeared to be no change in the up conversion crystal. The results are shown in Figure 6.5. We investigated higher pulse energies with this data. Therefore, we can more easily see the bending of the eSFG due to the linear contribution and the curve of the classical SFG due to the changing beam properties.

6.3.1 Full Vs Coherent Comparison

Figures 6.3 and 6.5 tell a very similar story. Below a certain point, the entangled case generates more SFG. By allowing the incoherent contribution to be measured, we have

increased the PDC energy, where we can claim more efficient up conversion from about four photons per mode to around six, which means a 50% increase in energy over which we see an improvement.

We should be careful about drawing too strong of a conclusion from this data. As previously stated, I am unsure about the amount of losses we have in the eSFG state. We have also not characterised the losses in our down converted state, and therefore, it may be possible to produce a state which could stimulate more eSFG. However, it appears that even with the incoherent component present, the entangled case becomes less efficient than the classical one. We can say that at the very worst, below approximately 6 photons per mode, using the state produced by parametric down conversion will stimulate more sum frequency generation than a classical coherent field. This is a ~ 6 times increase in the range of energies where we see an advantage from what is conventionally understood in literature, where the limit is placed at one photon per mode.

I have tried to emphasise that this is the first direct comparison between eSFG pumped with the state produced by parametric down conversion and a coherent field. Whilst, as far as I am aware, this is true, there are two studies I need to draw attention to that attempt something similar. The first is the article by Spasibko et al. [72] in which they make a comparison between a coherent source and the down converted state in the form of the bright squeezed vacuum (BSV), in the nomenclature that I have been using throughout, this is the high gain down converted state. However, instead of directly pumping with a coherent laser field, they create a 'pseudocoherent' source by post selecting the pulses of the BSV. To quote from the article, 'We register only pulses in which the number of photons in the BSV lies within certain boundaries. This way, we restrict the BSV fluctuations and mimic the generation of optical harmonics from coherent light' [72]. The light that they post select for has a second order correlation value of $g^{(2)} = 1.010 \pm 0.002$ ([72] supplementary materials), which is approximately that of a coherent field, and they have shown that the full BSV is more efficient at stimulating SHG then their pseudocoherent source by a factor of two. We have instead made a direct comparison to a true coherent field, the type that are currently used for

two photon processes.

The second report is from Tian et al. [74], where they compare classical two photon absorption driven by a coherent laser to two photon absorption driven by the state produced by four wave mixing. Four wave mixing also produces an entangled state with spatial-momentum, energy-time entanglement between pairs of photons. They say the reason they chose to use this process instead of PDC is because they can reach higher fluxes of entangled pairs of photons. In this report, they see a far higher flux when the entangled source drives TPA when compared to the classical source for two different fluorophores, Fluorescein and a DCM laser dye. I do not understand all of the details of this report. However, I have a reason to doubt this result. From what we have shown and my understanding of the process, the linear response between entangled energy and rate of absorption is fundamentally a property of the entangled state. If the state is below one photon per mode, there should be a dominant linear term; when above one photon per mode, there should always be a second-order term present. They observe a strong linear term when they pump Fluorescein with their entangled source at power levels of $>$ 1mw. However, when they attempt to pump their DCM dye, they observe a linear and second-order relation at a lower pump power of $\sim 100\mu$W. I believe this implies that at $\sim 100\mu$W, they are operating above one photon per mode; however, they see no second order term when they pump fluorescin at a higher power and, therefore, with even more photons per mode. They explain this difference by saying the classical two photon cross section of the DCM dye is larger than fluorescin, which is correct [75]. However, it is not the case that the entangled cross section is independent of this variable [24]. Therefore, we should be suspicious of the change from a dominant linear relation to a far weaker linear and a new second order relation with a reduction of power, even with a change of fluorophore without additional explanations.

Ultimately, the studies presented in this section remain the first investigation comparing the efficiency of entangled sum frequency generation to classical sum frequency generation induced by a true coherent field in the high gain of parametric down conversion.

6.4 Changing the SFG crystal length

The final investigation I will present regarding the differences between classical and entangled sum frequency generation is into how the crystal length of the up conversion crystal changes the efficiency of SFG. For the classical sum frequency generation, the rate of SFG depends on the crystal length, L, according to the equation:

$$R_{SFG}^{\text{Classical}} \propto L^2. \tag{6.8}$$

We can infer how we expect entangled sum frequency generation to scale with the crystal length. In an ideal world, we recombine all of the entangled photons. Each entangled pair has a finite but definite chance of up converting. Therefore, by reducing the crystal length, all we do is prevent the photons produced in the corresponding section of the down conversion crystal from up converting. Because of this, in the low gain, if the up conversion crystal is shorter than the down conversion crystal, we should expect a linear relationship between eSFG efficiency and crystal length. This already suggests a further enhancement when compared with the classical case, which is easy, in principle, to test. We just do the same experiment with a shorter crystal in the final SFG position.

The result of using a shorter up conversion crystal is shown in Figure 6.6. The left hand (Figure 6.6a) displays two scans, both with the 2 mm long BBO down conversion crystal we have used throughout. The upper diagram data was collected with a 2 mm up conversion crystal as we have used throughout this work; the lower was collected with a shorter 1.5 mm up conversion crystal. Both of these sets of data were taken over the same range of PDC energy to facilitate comparison. The classical comparison has been adjusted according to Equation 6.8 and is shown as a red line in the plots.

The most apparent takeaway is that it appears having a shorter up conversion crystal allows for the entangled sum frequency generation to stimulate more up conversion than the classical SFG over a larger range of energies. We expected this because the linear term should scale linearly with crystal length. However, that isn't quite happening, which is tricky to see without a more complete model.

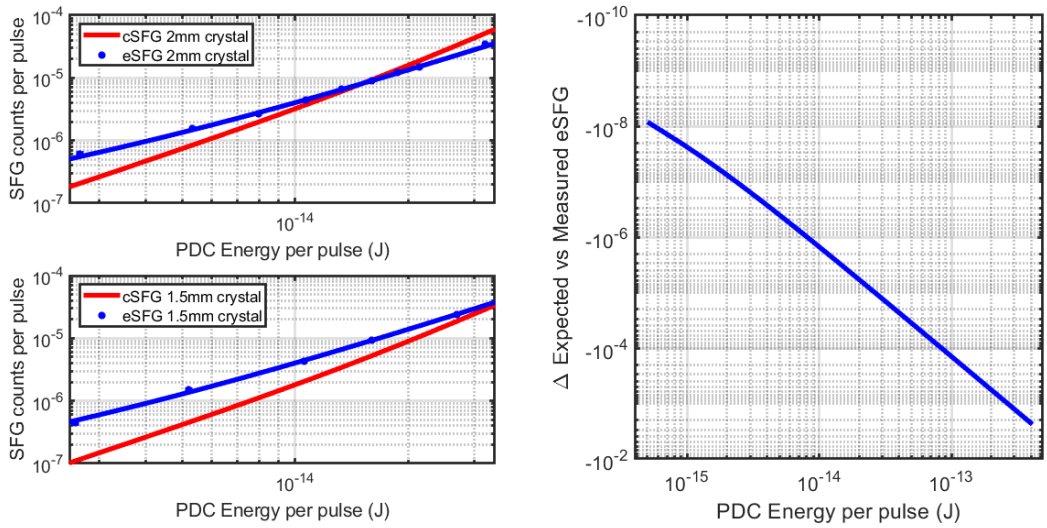

(a) (b)

Figure 6.6: The left hand diagram is a comparison between eSFG and classical SFG for two different SFG crystal lengths. The right shows the expected response of a shorter crystal based on the fit for the longer crystal minus the measured response. This shows that we measure more eSFG than we would expect—details in text.

In order to better understand the relationship, we need to write down what we expect to see. The eSFG scales as:

$$R_{eSFG} = \delta\phi + \sigma\phi^2. \tag{6.9}$$

Both coefficient, δ and σ, have a dependence on the crystal length, $\delta = \delta(L)$ and $\sigma = \sigma(L)$. Specifically, if successful in recombining the down converted state, for a crystal of length L we would expect:

$$\delta = L \times \delta_0 \tag{6.10}$$

$$\sigma = L^2 \times \sigma_0 \tag{6.11}$$

where δ_0 and σ_0 are the components of δ and σ respectively with no dependence on crystal length. Therefore the overall dependence of eSFG on crystal length is:

$$R_{eSFG}(L) = L\delta_0\phi + L^2\sigma_0\phi^2. \tag{6.12}$$

With this, we can fit the (entangled, blue) data in the upper diagram of Figure 6.6a to Equation 6.9 and use Equation 6.12 to rescale this data as if it were produced by a theoretical 1.5 mm crystal (times the linear coefficient by (1.5/2) and the second order coefficient by a factor of $1.5/2)^2$). We can then subtract the actual 1.5 mm data from this modeled data (the bottom diagram from Figure 6.6a), and we will see the difference between expected versus real results. This is shown in Figure 6.6b. In an ideal world, they would be equal and Figure 6.6b would be a flat line; however, this is not what we see. Instead, we see that the real result produced more up-conversion photons than the theoretical shorter crystal would as Figure 6.6b is negative for all PDC energies. Something is amiss. The 1.5 mm crystal is more efficient than it should be in stimulating eSFG.

6.4.1 Discussion

We do not have strong enough data or an experimental design to investigate this properly. However, there is a conclusion we might want to motivate: we are not fully reconstructing the down converted state along the entire crystal length. There are two possible causes for this, either a mismatch in the phase matching of the down conversion versus the up conversion crystal or a failure in delivering the down converted state to the sample. First, the phase matching. We could be struggling to match the crystal angle between the up and down conversion crystal and, therefore, do not maximise what we will term the phase overlap (the overlap between the phase matching curves of the down conversion and up conversion crystal). When a shorter crystal is used, the phase matching constraints are relaxed. Therefore, it is easier to maximise the phase overlap. This is unlikely as in both cases, at maximum gain the up conversion was bright enough to be able to optimise the response in real time.

The harder to understand and control is the imaging properties of the system. The purpose of imaging the down converted field is to maximise the chance of reproducing our state. However, ideal imaging only occurs on an infinitesimal plane, and states are produced along the entire length of the crystal. We can draw an analogy with conventional optics: photons that are transmitted on either side of the object plane

will arrive at the imaging plane slightly offset from the position they were emitted at, which leads to an overall blurring of the image until it is out of focus. The distance over which the image is in focus is called the depth of field. We do not have any tangible theory on this topic, but the idea is self sufficient. For entangled two photon interaction, the depth of field defines the length for which we can achieve coherent interactions (recombination of entangled pairs), and our depth of field is shorter than the length of our down conversion crystal. This would result in an effective crystal length that will alter the magnitude of both the first and second order coefficients of entangled sum frequency generation when compared to the classical coefficient.

Before mentioning possible ways of maximising this property, a quick aside: one wonders whether we want to increase the length over which the down converted field stimulates a response. What precise advantage does it bring us? It would be helpful in these measurements into the efficiency of eSFG/eTPA, particularly if we develop a method for determining the effective crystal length (length over which the down converted beam stimulates up conversion). However, for imaging applications, it is of no use. If what I propose is true, photons produced at the front face of the down conversion crystals and photons that are produced at the back face cannot stimulate a coherent response on the same plane. Therefore, by increasing the depth of field of our PDC delivery, all we would do is confuse where the photons were produced from, making the interpretation of the resultant image more complex. Nevertheless, if we want to increase the depth of field of our PDC, the general idea would be to increase the proportion of the state which arrives at the down conversion crystal along or close to the central ray axis of the focusing parabolic (or to think of it another way, the proportion of the state that is up converted which was produced at an angle to the PDC pump close to zero). We can do this by changing the phase matching (e.g. by altering the crystal angle, temperature or length), altering filtering to select for photons emitted only very close to the pump beam propagation direction or possibly decreasing the focal length of our parabolic mirrors. Trying most of these would involve a significant alteration of the down conversion properties that would make comparisons between studies hard, and great care would have to be taken to ensure all detailed reporting. This is beyond

the scope of the studies presented here but may be an essential idea when considering further work.

6.5 Conclusion

In this chapter, we have presented a comparative study of stimulating sum frequency generation with classical-coherent and entangled-parametrically down converted fields. We have seen that in the low gain, the entangled case stimulates a larger number of up converted photons. The region of advantage for the entangled case extends into the stimulated regime of parametric down conversion up to about six photons per mode. Above this, the entangled field behaves as a classical field with the same average intensity. This is a novel comparison. We then showed that the use of a shorter up conversion crystal was not as detrimental as a basic analysis may suggest. The shorter crystal allowed for a larger range of energies over which the entangled case stimulated more SFG than a classical coherent field. This raises further questions about how we can optimally deliver the down converted state and inside of what volume the down converted state can be considered entangled.

Chapter 7

Conclusion

This thesis aimed to study how the state produced by parametric down conversion affects the efficiency of entangle two photon process. It is clear that the principle properties of entangled two photon interactions are properties of the down converted field and not the up conversion process. Because of this, a more rigorous understanding of the down converted field must be sought. The discussions in Sections 5.4.1 and 6.4.1 imply a more significant constraint on the down converted field than can be quantified by taking coincident counts, which I have attempted to represent by introducing a transmission coefficient, T. Without quantifying the spatial-temporal loss (measurement of our ability to recombine the down converted state in space and time), we cannot have meaningful comparisons between studies. This idea ultimately apes the definition of the second order correlation function in the near field of the down converted field, which is an interpretation I have tried to motivate at the beginning of Chapter 6.

Our investigation has involved observing and describing the transition from the low gain to the high gain of parametric down conversion. We have shown how many of the physical properties of the down converted field change during this transition, and hopefully, I have provided some physically intuitive way of understanding how and why this occurs. This opens up a different regime of down conversion to consider, what I might call the 'mid' gain. In the low gain, all interactions are between single photons, and the properties of the down converted field (pulse duration, size, etc.) are static. In the high gain, generally, we talk about a squeezed states and single photon interactions

are not considered, but the properties of the down converted field will reach a steady state. In 'mid' gain, we still have single photon interactions, but the down converted field properties are not fixed. We have gone quite a long way in investigating this regime as it pertains to eSFG (i.e. its physical characteristics); however, it is not entirely clear what properties it may have. I would assume that it shares some characteristics of the low and high gain. Therefore, it may be the case that one could optimise a process or experiment by conducting it in this regime.

There are several directions in which this work could be furthered. First and foremost, there is the question of whether it is directly applicable to eTPA. I have presented the argument that it must be, but an experiment with eTPA directly would confirm this. Then, we could try to develop a method to independently or systematically quantify the spatio-temporal losses of a system and, thus, perhaps, optimise an experimental design. There is, of course, a possibility to directly use the knowledge we have developed to attempt to image a sample. Finally, we could attempt to compare eSFG to SFG from the state produced by PDC when we destroy entanglement (by for instance, filtering in such a way to remove just one of each entangle pair). Equation 2.33 tells us that the entangled properties of the down converted state lead to both a first and second order coefficient. Therefore, by comparing eSFG to SFG produced by the same field without entanglement, we might be able to better understand the effect the entangled component has and this may let us calculate properties of our entangled field such as spatial temporal losses and the effective crystal length.

Appendix A

The Down Converted State as a Squeezed Thermal State

In the main text, we have created a toy model aiming to explain the effect that losses in the down converted field have on the efficiency of entangled sum frequency generation. This analysis starts from the conclusion of Chapter 2 and essentially pretends that the interaction takes place between two independent classical fields. We should, however, be able to derive this relationship directly through a quantum analysis.

A squeezed vacuum field, the pump field we have been using throughout this work, is seeded from the thermal vacuum field. When we introduce losses into this field, a portion of the field is unaffected, and a portion of the field loses its entangled partner, and this component will behave as the input thermal field. Therefore, a lossy squeezed vacuum field is simply a squeezed thermal field [76].

The density matrix of a squeezed thermal field is:

$$\rho_{th} = (1+\bar{n})^{-1} \sum_{n=0}^{\inf} \left\{ \frac{\bar{n}}{1+\bar{n}} \right\}^n \hat{S}(r) \left|n\right\rangle \left\langle n\right| \hat{S}^{\dagger}(r), \tag{A.1}$$

where $\bar{n}$ is the average number of thermal photons, and $\hat{S}(r)$ the squeezing operator defined as:

$$\hat{S}(r) = \exp\left(\frac{1}{2} \left(r\hat{a}^2 - r\hat{a}^{\dagger 2} \right) \right), \tag{A.2}$$

where $\hat{a}^{\dagger}$ and $\hat{a}$ are the usual photon creation and annihilation operators, and r is

known as the squeezing parameter.

The rate of sum frequency generation and two photon absorption will always be proportional to the second order correlation function:

$$g^{(2)} = \frac{\hat{a}^\dagger \hat{a}^\dagger \hat{a}\hat{a}}{\langle \hat{a}^\dagger \hat{a} \rangle \langle \hat{a}^\dagger \hat{a} \rangle}. \tag{A.3}$$

More specifically, it will be proportional to the number of photons squared times the second order correlation function:

$$\langle \hat{n} \rangle^2 \times g^{(2)} = \hat{a}^\dagger \hat{a}^\dagger \hat{a}\hat{a}. \tag{A.4}$$

For a single mode squeezed thermal state, the second order correlation function takes the value [77]:

$$\left\langle g^{(2)} \right\rangle = 2 + \frac{(2\bar{n}+1)^2}{\langle \hat{n} \rangle^2} \sinh^2(r) \cosh^2(r). \tag{A.5}$$

where the expected number of photons is given by the expression:

$$\langle \hat{n} \rangle = \bar{n} \cosh(2r) + \sinh^2(r). \tag{A.6}$$

The crux of my argument is that there will exist a squeezed thermal field which behaves as a lossy squeezed vacuum field. In order to define this squeezed thermal field, we cannot preserve the interpretation of all of the variables in Equation A.5. In particular, we need to define a reduced squeezing parameter, r', and make the substitution in Equations A.5 and A.6:

$$r \to r'. \tag{A.7}$$

We will assume that the squeezed vacuum field is produced by transmitting the field through a system of transmittance T. The expected number of photons is then:

$$\langle \hat{n} \rangle = T \sinh^2(r). \tag{A.8}$$

Note, r in Equation A.8 is the original squeezing parameter of the down converted field before any losses. This related to the reduced squeezing parameter through the relationship:

$$\bar{n}\cosh\left(2r'\right) + \sinh^2(r') = T\sinh^2(r). \tag{A.9}$$

From the double angle relationship, $\cosh(2r') = \cosh^2(r') + \sinh^2(r')$, we can rewrite the above equation:

$$\bar{n} + (2\bar{n}+1)\sinh^2(r') = T\sinh^2(r). \tag{A.10}$$

$\bar{n}$ is the total number of thermal photons. If the squeezed thermal field is formed by transmitted a squeezed vacuum field with random losses through a system of transmission, T, then the total number of thermal photons (photons that have lost their entangled partner) will be $(1-T)\times\langle\hat{n}\rangle$ or:

$$\bar{n} = T(1-T)\sinh^2(r). \tag{A.11}$$

Substituting this into Equation A.10 and rearranging, we can get an expression for the reduced squeezing parameter in terms of physically measurable quantities:

$$\sinh^2(r') = \frac{T^2\sinh^2(r)}{(2T(1-T)\sinh^2(r)+1)}. \tag{A.12}$$

We can now substitute these relationships into the second order correlation function:

$$\begin{aligned}
\left\langle g^{(2)}\right\rangle =& 2 + \frac{(2T(1-T)\sinh^2(r)+1)^2}{T^2\sinh^4(r)}\sinh^2(r')\cosh^2(r') \\
=& 2 + \frac{(2T(1-T)\sinh^2(r)+1)^2}{T^2\sinh^4(r)}(\sinh^2(r') + \sinh^4(r')) \\
=& 2 + \frac{(2T(1-T)\sinh^2(r)+1)^2}{T^2\sinh^4(r)}\left[\frac{T^2\sinh^2(r)}{(2T(1-T)\sinh^2(r)+1)} + \frac{T^4\sinh^4(r)}{(2T(1-T)\sinh^2(r)+1)^2}\right] \\
=& 2 + \frac{1}{T^2\sinh^4(r)}\left[T^2\sinh^2(r)(2T(1-T)\sinh^2(r)+1) + T^4\sinh^4(r)\right].
\end{aligned} \tag{A.13}$$

The rate of SFG will be proportional to $\langle\hat{n}\rangle^2\left\langle g^{(2)}\right\rangle$:

$$\begin{aligned}\langle\hat{n}\rangle^2\left\langle g^{(2)}\right\rangle &= 2T^2\sinh^4(r)+T^2\sinh^2(r)(2T(1-T)\sinh^2(r)+1)+T^4\sinh^4(r)\\ &= T^2\sinh^2(r)+T^2\left(2+2T-T^2\right)\sinh^4(r)\end{aligned} \tag{A.14}$$

and finally, substituting for the measured number of photons $\langle\hat{n}\rangle = T\sinh^2(r)$:

$$\langle\hat{n}\rangle^2\left\langle g^{(2)}\right\rangle = T\langle\hat{n}\rangle+\left(2+2T-T^2\right)\langle\hat{n}\rangle^2. \tag{A.15}$$

This value of the second order correlation function does not agree with the previous model presented in the main text of this thesis, which I will call the semi-classical model as we treat the fields and independent classical fields. Before examining this difference (though I do not have an explanation of this difference, nor is it clear to me which is correct), we need to complement the result we have just reached. In the limit of $T \to 1$ we should reproduce the squeezed vacuum result which is [78]:

$$\left\langle g^{(2)}_{\text{Sqeezed Vacuum}}\right\rangle = 3+\frac{1}{\langle\hat{n}\rangle}, \tag{A.16}$$

and Equation A.15 reproduces this result when $T = 1$. Similarly, in the limit $T \to 0$ we should reproduce a pure thermal response for which the second order correlation function takes the value:

$$\left\langle g^{(2)}_{\text{Thermal}}\right\rangle = 2, \tag{A.17}$$

and Equation A.15 reproduces this result when $T = 0$ as expected.

Equation A.15 does not, however, natively show the crossing points which we have seen in the semi-classical model (Chapter 5). This is because, unlike the semi-classical model, there is no value that the transmission can take for which a smaller transmission results in a larger second order coefficient. As a reminder, the result derived in Chapter 5 (Equation 5.6) was:

$$R_{\text{Semi-Classical}}(T,\phi) = T\delta\phi+\sigma\phi^2(2T^2-2T+1). \tag{A.18}$$

And the rate of SFG the new 'Quantum' model gives will be:

$$R_{\text{Quantum}}(T,\phi) = T\delta\phi + \sigma\phi^2(2 + 2T - T^2). \tag{A.19}$$

We can recoup the crossing points by considering the changing property of the near field size and duration of the down converted state with increasing gain as outlined in Section 3.4 and applied to the previous model in Section 5.3.3 (see Figure A.1). This property on its own is sufficient to explain these features. If the 'Quantum' model is correct, then the crossing points are merely a consequence of the changing physical property of the down converted state. Equation A.19, in fact, suggests that a squeezed state should be more efficient for stimulating multi photon processes than a thermal state, no matter the transmission of the system. We should not be surprised by this, as all the squeezed should do is introduce pairs of photons that can undergo coherent recombination and have no detrimental effect on the thermal state. The 'semi-classical' model does not support this hypothesis.

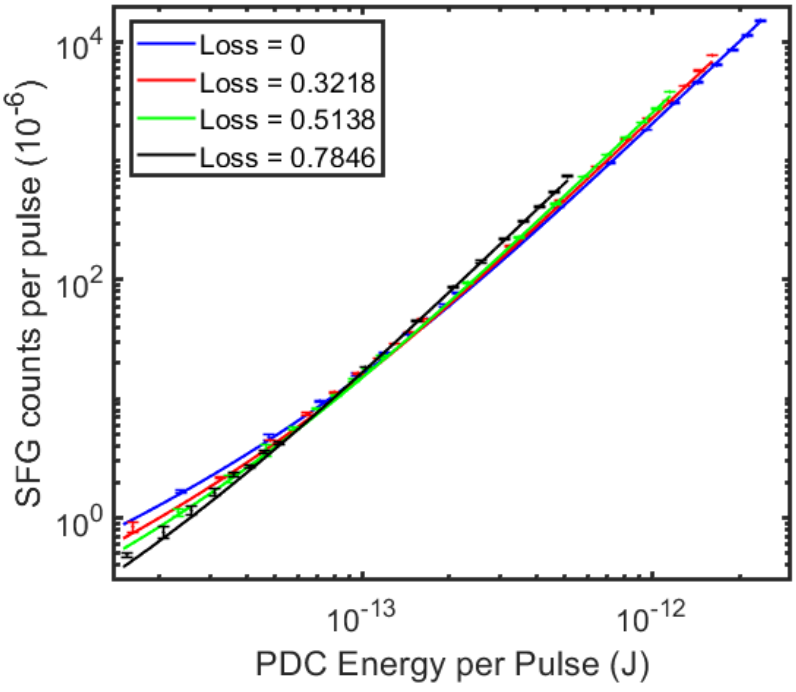

Figure A.1: The data from Section 5.3 fitted with Equation A.19 with he same procedure as outlines in Section 5.3.

We will note that the fact that this result suggests a lossy squeezed vacuum field should stimulate more than a thermal field does not suggest quantum supremacy as a thermal state, whilst being classical, is not the optimum state to pump two photon processes. I believe that a coherent state will be a more efficient state to drive two photon processes despite reports in the literature to the contrary ([70] for two photon absorption and [71] for second harmonic generation). The basis of both of these reports is the fact the second order correlation function for chaotic thermal light peaks at 2 (Equation A.17) whereas for a coherent field, it takes the value of 1:

$$\left\langle g^{(2)}_{\text{Coherent}} \right\rangle = 1. \tag{A.20}$$

Therefore, as two photon processes are proportional to the second order correlation function and as the thermal second order correlation function is twice that of the coherent, stimulating a two photon process with a thermal field should be twice as efficient as with a coherent field. This analysis, however, misses one key aspect of the thermal field: a thermal field is incoherent in phase. Two photons that arrive at an event will not generically be in phase. With apologies to theoreticians, I will consider this by attempting to factor in the phase in the number of photons. If we consider two frequency modes, ω_1 and ω_2, it can be shown that the rate of two photon processes (TPP) is proportional to:

$$R_{\text{TPP}}(\omega_1, \omega_1) \propto \langle \hat{n}_1 \rangle \langle \hat{n}_2 \rangle \left\langle g^{(2)}(\omega_1, \omega_2) \right\rangle, \tag{A.21}$$

where $\hat{n}_i$ is the number of photons of the i^{th} field. We introduce the phase factor into the operators so that:

$$\langle \hat{n}_i \rangle \propto \left| \int d\phi_i \; e^{i\omega_i t + i\phi_i} \right|^2, \tag{A.22}$$

where ϕ is the phase factor. The phase term in the rate of two photon processes will then be:

$$R_{\mathrm{TPP}}^{\text{Phase term}}(\omega_1,\omega_1) \propto \left| \int d\phi_1 \; e^{i\omega_1 t + i\phi_1} \right|^2 \left| \int d\phi_2 \; e^{i\omega_2 t + i\phi_2} \right|^2. \tag{A.23}$$

Without loss of generality, we can set $\phi_2 = 0$ and $\phi_1 = \phi$ where ϕ is the difference in phase between the two fields and set the limits of the integral from 0 to π; doing this takes the fields from perfectly in phase to perfectly out of phase. The phase dependence on the rate of two photon processes is then just:

$$R_{\mathrm{TPP}}^{\text{Phase term}} \propto \left| \int_0^{\pi} d\phi \; e^{i\phi} \right|^2. \tag{A.24}$$

For a coherent beam, $\phi = 0$, therefore:

$$R_{\mathrm{TPP}}^{\text{Phase term}}(\text{Coherent}) \propto \left| \int_0^{\pi} d\phi \; \right|^2 = \pi^2, \tag{A.25}$$

where as for an incoherent field:

$$R_{\mathrm{TPP}}^{\text{Phase term}}(\text{Incoherent}) \propto \left| \int_0^{\pi} d\phi \; e^{i\phi} \right|^2 = 4. \tag{A.26}$$

The ratio of the rate of two photon processes for a thermal vs a coherent field will thus be:

$$\frac{R_{\mathrm{TPP}}(\text{Thermal})}{R_{\mathrm{TPP}}(\text{Coherent})} = \frac{4 \times \left\langle g^{(2)}_{\text{Thermal}} \right\rangle}{\pi^2 \times \left\langle g^{(2)}_{\text{Coherent}} \right\rangle} = \frac{8}{\pi^2} < 1, \tag{A.27}$$

therefore, a thermal state stimulating a two photon process should be less efficient than an appropriately constructed coherent state. As a squeezed vacuum state peaks at 3, however, it should be more efficient as:

$$\begin{aligned} \frac{R_{\mathrm{TPP}}(\text{Squeezed Vacuum})}{R_{\mathrm{TPP}}(\text{Coherent})} = \frac{4 \times \left\langle g^{(2)}_{\text{Squeezed Vacuum}} \right\rangle}{\pi^2 \times \left\langle g^{(2)}_{\text{Coherent}} \right\rangle} &= \frac{4 \times \left[3 + \frac{1}{\langle \hat{n} \rangle}\right]}{\pi^2}, \\ &= \lim_{\langle \hat{n} \rangle \to \infty} \frac{12}{\pi^2} > 1. \end{aligned} \tag{A.28}$$

Our true field, the lossy squeezed vacuum field, should, therefore, be somewhere be-

tween these two extremes. The ratio of the rate of two photon processes for a lossy squeezed vacuum field vs a coherent field will be:

$$\begin{aligned}\frac{R_{\mathrm{TPP}}(\text{Lossy SV})}{R_{\mathrm{TPP}}(\text{Coherent})} = \frac{4 \times \left\langle g^{(2)}_{\text{Lossy SV}} \right\rangle}{\pi^2 \times \left\langle g^{(2)}_{\text{Coherent}} \right\rangle} &= \frac{4 \times \left[(2 + 2T - T^2) + \frac{T}{\langle \hat{n} \rangle}\right]}{\pi^2}, \\ &= \lim_{\langle \hat{n} \rangle \to \infty} \frac{4(2 + 2T - T^2)}{\pi^2}.\end{aligned} \tag{A.29}$$

Therefore, provided the transmission of the system is above:

$$T > 1 - \frac{\sqrt{12 - \pi^2}}{2} \sim 0.27, \tag{A.30}$$

then stimulating two photon processes with a lossy squeezed vacuum field will be more efficient than with a coherent state for all pulse energies.

The only data we have that are directly applicable to this result are in Section 6.3 in which we see an appropriately scaling coherent state become more efficient than the squeezed state; however, I do not believe that this data is strong enough to rebuke this analysis. My main trepidation pertains to whether we managed to collect the entire up converted state. The rest of the data presented considered only the coherent contribution of eSFG, which contains pure quantum interactions. These data sets have been well modelled by the semi-classical model in the low to mid gain regime of parametric down conversion. Ultimately, more experimental work needs to be conducted into the effect of losses in the down converted field no matter the model, as in both cases, the key linear term is linearly proportional to the transmission, T, of the and, therefore, the linear coefficient should not be quoted without a measurement of this transmission.

Bibliography

[1] A. Einstein, B. Podolsky, and N. Rosen. Can quantum-mechanical description of physical reality be considered complete? *Phys. Rev.*, 47:777–780, May 1935.

[2] Juha Javanainen and Phillip L. Gould. Linear intensity dependence of a two-photon transition rate. *Phys. Rev. A*, 41:5088–5091, May 1990.

[3] J. Gea-Banacloche. Two-photon absorption of nonclassical light. *Phys. Rev. Lett.*, 62:1603–1606, Apr 1989.

[4] Maria Göppert-Mayer. Über elementarakte mit zwei quantensprüngen. *Annalen der Physik*, 401(3):273–294, 1931.

[5] W. Kaiser and C. G. B. Garrett. Two-photon excitation in caf_2: eu^{2+}. *Phys. Rev. Lett.*, 7:229–231, Sep 1961.

[6] W. Martin McClain. Two-photon molecular spectroscopy. *Accounts of Chemical Research*, 7(5):129–135, 1974.

[7] C. J. R. Sheppard and R. Kompfner. Resonant scanning optical microscope. *Appl. Opt.*, 17(18):2879–2882, Sep 1978.

[8] Edward S. Barnard, Eric T. Hoke, Stephen T. Connor, James R. Groves, Tevye Kuykendall, Zewu Yan, Eric C. Samulon, Edith D. Bourret-Courchesne, Shaul Aloni, P. James Schuck, Craig H. Peters, and Brian E. Hardin. Probing carrier lifetimes in photovoltaic materials using subsurface two-photon microscopy. *Scientific Reports*, 3:2098, 2013.

[9] W. Denk, J. H. Strickler, and W. W. Webb. Two-photon laser scanning fluorescence microscopy. *Science (New York, N.Y.)*, 248(4951):73–76, April 1990.

[10] David R. Miller, Jeremy W. Jarrett, Ahmed M. Hassan, and Andrew K. Dunn. Deep Tissue Imaging with Multiphoton Fluorescence Microscopy. *Current Opinion in Biomedical Engineering*, 4:32–39, December 2017.

[11] Aleksandr A. Lanin, Artem S. Chebotarev, Matvei S. Pochechuev, Ilya V. Kelmanson, Daria A. Kotova, Dmitry S. Bilan, Yulia G. Ermakova, Andrei B. Fedotov, Anatoly A. Ivanov, Vsevolod V. Belousov, and Aleksei M. Zheltikov. Two- and three-photon absorption cross-section characterization for high-brightness, cell-specific multiphoton fluorescence brain imaging. *Journal of Biophotonics*, 13(3):e201900243, March 2020.

[12] Bernas T, Robinson Jp, Asem Ek, and Rajwa B. Loss of image quality in photobleaching during microscopic imaging of fluorescent probes bound to chromatin. *Journal of biomedical optics*, 10(6), December 2005.

[13] Ghauharali and Brakenhoff. Fluorescence photobleaching-based image standardization for fluorescence microscopy. *Journal of Microscopy*, 198(2):88–100, May 2000.

[14] Song L, Hennink Ej, Young It, and Tanke Hj. Photobleaching kinetics of fluorescein in quantitative fluorescence microscopy. *Biophysical journal*, 68(6), June 1995.

[15] Ghauharali, Hofstraat, and Brakenhoff. Fluorescence photobleaching-based shading correction for fluorescence microscopy. *Journal of Microscopy*, 192(2):99–113, November 1998.

[16] George H. Patterson and David W. Piston. Photobleaching in two-photon excitation microscopy. *Biophysical Journal*, 78:2159–2162, 4 2000.

[17] Jayne M. Squirrell, David L. Wokosin, John G. White, and Barry D. Bavister. Long-term two-photon fluorescence imaging of mammalian embryos without compromising viability. *Nature Biotechnology*, 17:763–767, 1999.

[18] K. König, T. W. Becker, P. Fischer, I. Riemann, and K.-J. Halbhuber. Pulse-length dependence of cellular response to intense near-infrared laser pulses in multiphoton microscopes. *Optics Letters*, 24:113, 1999.

[19] Jaroslav Icha, Michael Weber, Jennifer C. Waters, and Caren Norden. Phototoxicity in live fluorescence microscopy, and how to avoid it. *BioEssays*, 39:1–15, 2017.

[20] Malvin C. Teich and Bahaa E. A. Saleh. Entangled-photon microscopy. *Československỳ časopis pro fyziku*, 47:3–8, 1997.

[21] Frank Schlawin, Konstantin E. Dorfman, and Shaul Mukamel. Entangled two-photon absorption spectroscopy. *Accounts of Chemical Research*, 51(9):2207–2214, 2018.

[22] Carlos Sánchez Muñoz, Gaetano Frascella, and Frank Schlawin. Quantum metrology of two-photon absorption. *Phys. Rev. Res.*, 3:033250, Sep 2021.

[23] Yuanyuan Chen, Roberto de J. León-Montiel, and Lixiang Chen. Quantum interferometric two-photon excitation spectroscopy. *New Journal of Physics*, 24(11):113014, November 2022.

[24] Hong-Bing Fei, Bradley M. Jost, Sandu Popescu, Bahaa E. A. Saleh, and Malvin C. Teich. Entanglement-induced two-photon transparency. *Phys. Rev. Lett.*, 78:1679–1682, Mar 1997.

[25] B.N. Jagatap and William J. Meath. On the competition between permanent dipole and virtual state two-photon excitation mechanisms, and two-photon optical excitation pathways, in molecular excitation. *Chemical Physics Letters*, 258(1):293–300, 1996.

[26] L. Upton, M. Harpham, O. Suzer, M. Richter, S. Mukamel, and T. Goodson. Optically Excited Entangled States in Organic Molecules Illuminate the Dark. *The Journal of Physical Chemistry Letters*, 4(12):2046–2052, June 2013.

[27] N. Ph. Georgiades, E. S. Polzik, K. Edamatsu, H. J. Kimble, and A. S. Parkins. Nonclassical excitation for atoms in a squeezed vacuum. *Phys. Rev. Lett.*, 75:3426–3429, Nov 1995.

[28] Barak Dayan, Avi Pe'er, Asher A. Friesem, and Yaron Silberberg. Two photon absorption and coherent control with broadband down-converted light. *Physical Review Letters*, 93:023005, 7 2004.

[29] Dong Ik Lee and Theodore Goodson. Entangled photon absorption in an organic porphyrin dendrimer. *Journal of Physical Chemistry B*, 2006.

[30] Michael R. Harpham, Özgün Süzer, Chang-Qi Ma, Peter Bäuerle, and Theodore Goodson. Thiophene Dendrimers as Entangled Photon Sensor Materials. *Journal of the American Chemical Society*, 131(3):973–979, January 2009.

[31] Alica R. Guzman, Michael R. Harpham, Özgün Süzer, Michael M. Haley, and Theodore G. Goodson. Spatial Control of Entangled Two-Photon Absorption with Organic Chromophores. *Journal of the American Chemical Society*, 132(23):7840–7841, June 2010.

[32] Juan P. Villabona-Monsalve, Oleg Varnavski, Bruce A. Palfey, and Theodore Goodson. Two-Photon Excitation of Flavins and Flavoproteins with Classical and Quantum Light. *Journal of the American Chemical Society*, 140(44):14562–14566, November 2018.

[33] Juan P. Villabona-Monsalve, Omar Calderón-Losada, M. Nuñez Portela, and Alejandra Valencia. Entangled Two Photon Absorption Cross Section on the 808 nm Region for the Common Dyes Zinc Tetraphenylporphyrin and Rhodamine B. *The Journal of Physical Chemistry A*, 121(41):7869–7875, October 2017.

[34] Bryce P. Hickam, Manni He, Nathan Harper, Szilard Szoke, and Scott K. Cushing. Single-photon scattering can account for the discrepancies among entangled two-photon measurement techniques. *Journal of Physical Chemistry Letters*, 13:4934–4940, 6 2022.

[35] Tiemo Landes, Markus Allgaier, Sofiane Merkouche, Brian J. Smith, Andrew H. Marcus, and Michael G. Raymer. Experimental feasibility of molecular two-photon absorption with isolated time-frequency-entangled photon pairs. *Phys. Rev. Res.*, 3:033154, Aug 2021.

[36] D. Tabakaev, A. Djorović, L. La Volpe, G. Gaulier, S. Ghosh, L. Bonacina, J.-P. Wolf, H. Zbinden, and R. T. Thew. Spatial properties of entangled two-photon absorption. *Phys. Rev. Lett.*, 129:183601, Oct 2022.

[37] Kristen M. Parzuchowski, Alexander Mikhaylov, Michael D. Mazurek, Ryan N. Wilson, Daniel J. Lum, Thomas Gerrits, Charles H. Camp, Martin J. Stevens, and Ralph Jimenez. Setting bounds on entangled two-photon absorption cross sections in common fluorophores. *Phys. Rev. Appl.*, 15:044012, Apr 2021.

[38] Samuel Corona-Aquino, Omar Calderón-Losada, Mayte Y. Li-Gómez, Hector Cruz-Ramirez, Violeta Álvarez Venicio, María Del Pilar Carreón-Castro, Roberto De J. León-Montiel, and Alfred B. U'Ren. Experimental Study of the Validity of Entangled Two-Photon Absorption Measurements in Organic Compounds. *The Journal of Physical Chemistry A*, 126(14):2185–2195, April 2022.

[39] Alexander Mikhaylov, Ryan N. Wilson, Kristen M. Parzuchowski, Michael D. Mazurek, Charles H. Camp, Martin J. Stevens, and Ralph Jimenez. Hot-band absorption can mimic entangled two-photon absorption. *Journal of Physical Chemistry Letters*, 13:1489–1493, 2 2022.

[40] Robert W. Boyd. *Nonlinear optics*. Academic Press, an imprint of Elsevier, 2020.

[41] D. A. Kleinman. Nonlinear dielectric polarization in optical media. *Phys. Rev.*, 126:1977–1979, Jun 1962.

[42] Eugene Hecht. *Optics*. Pearson Education, Aug 2013.

[43] Gilbert Grynberg, Alain Aspect, and Claude Fabre. *Introduction to quantum optics: from the semi-classical approach to quantized light*. Cambridge university press, 2010.

[44] K. J. Blow, Rodney Loudon, Simon J. D. Phoenix, and T. J. Shepherd. Continuum fields in quantum optics. *Phys. Rev. A*, 42:4102–4114, Oct 1990.

[45] John Garrison and Raymond Chiao. *Quantum Optics*. Oxford University Press, June 2008.

[46] Mark Hillery. An introduction to the quantum theory of nonlinear optics. *Acta Physica Slovaca*, 59:1–80, Jan 2009.

[47] Michael G. Raymer and Tiemo Landes. Theory of two-photon absorption with broadband squeezed vacuum. *Phys. Rev. A*, 106:013717, Jul 2022.

[48] E. Brambilla, O. Jedrkiewicz, L. A. Lugiato, and A. Gatti. Disclosing the spatiotemporal structure of parametric down-conversion entanglement through frequency up-conversion. *Phys. Rev. A*, 85:063834, Jun 2012.

[49] A. Gatti, O. Jedrkiewicz, and E Brambilla. Modeling the space-time correlation of pulsed twin beams. *Scientific Reports*, 13, Oct 2023.

[50] Barak Dayan. Theory of two-photon interactions with broadband down-converted light and entangled photons. *Phys. Rev. A*, 76:043813, Oct 2007.

[51] A. Gatti, T. Corti, E. Brambilla, and D. B. Horoshko. Dimensionality of the spatiotemporal entanglement of parametric down-conversion photon pairs. *Phys. Rev. A*, 86:053803, Nov 2012.

[52] Y. R. Shen. Quantum statistics of nonlinear optics. *Phys. Rev.*, 155:921–931, Mar 1967.

[53] I. Abram. Quantum theory of light propagation: Linear medium. *Phys. Rev. A*, 35:4661–4672, Jun 1987.

[54] B. Huttner, S. Serulnik, and Y. Ben-Aryeh. Quantum analysis of light propagation in a parametric amplifier. *Phys. Rev. A*, 42:5594–5600, Nov 1990.

[55] Ivan N. Agafonov, Maria V. Chekhova, and Gerd Leuchs. Two-color bright squeezed vacuum. *Phys. Rev. A*, 82:011801, Jul 2010.

[56] Adel Joobeur, Bahaa E. A. Saleh, Todd S. Larchuk, and Malvin C. Teich. Coherence properties of entangled light beams generated by parametric down-conversion: Theory and experiment. *Phys. Rev. A*, 53:4360–4371, Jun 1996.

[57] N. Boeuf, David A. Branning, I. Chaperot, E. Dauler, S. Guerin, Gregg S. Jaeger, Antoine Muller, and Alan L. Migdall. Calculating characteristics of noncollinear phase matching in uniaxial and biaxial crystals. *Optical Engineering*, 39(4):1016 – 1024, 2000.

[58] David N. Nikogosyan. *Nonlinear Optical Crystals: A Complete Survey*. Springer, 2005.

[59] Valentin G. Dmitriev and David N. Nikogosyan. Effective nonlinearity coefficients for three-wave interactions in biaxial crystal of mm2 point group symmetry. *Optics Communications*, 95:173–182, 1993.

[60] Andreas Christ, Alessandro Fedrizzi, Hannes Hübel, Thomas Jennewein, and Christine Silberhorn. Chapter 11 - parametric down-conversion. In Alan Migdall, Sergey V. Polyakov, Jingyun Fan, and Joshua C. Bienfang, editors, *Single-Photon Generation and Detection*, volume 45 of *Experimental Methods in the Physical Sciences*, pages 351–410. Academic Press, 2013.

[61] F. Bréhat and Bruno Wyncke. Calculation of double-refraction walk-off angle along the phase-matching directions in non-linear biaxial crystals. *Journal of Physics B*, 22:1891–1898, 1989.

[62] Dongyue Liu and Bryan M. Hennelly. Improved wavelength calibration by modeling the spectrometer. *Applied Spectroscopy*, 76(11):1283–1299, 2022.

[63] M. Brida, G. Genovese and I. Ruo Berchera. Experimental realization of sub-shot-noise quantum imaging. *Nature Photon*, 4:227–230, 2010.

[64] E. Brambilla, A. Gatti, M. Bache, and L. A. Lugiato. Simultaneous near-field and far-field spatial quantum correlations in the high-gain regime of parametric down-conversion. *Phys. Rev. A*, 69:023802, Feb 2004.

[65] Orazio Svelto. *Principles of Lasers*. Springer, 2009.

[66] Barak Dayan, Avi Pe'er, Asher A. Friesem, and Yaron Silberberg. Nonlinear interactions with an ultrahigh flux of broadband entangled photons. *Phys. Rev. Lett.*, 94:043602, Feb 2005.

[67] S. Sensarn, Irfan Ali-Khan, G. Y. Yin, and S. E. Harris. Resonant sum frequency generation with time-energy entangled photons. *Phys. Rev. Lett.*, 102:053602, Feb 2009.

[68] Samuel Corona-Aquino, Omar Calderón-Losada, Mayte Y. Li-Gómez, Hector Cruz-Ramirez, Violeta Álvarez Venicio, María del Pilar Carreón-Castro, Roberto de J. León-Montiel, and Alfred B. U'Ren. Experimental study of the validity of entangled two-photon absorption measurements in organic compounds. *The Journal of Physical Chemistry A*, 126:2185–2195, 4 2022.

[69] Frank Schlawin. Two-photon absorption cross sections of pulsed entangled beams. *The Journal of Chemical Physics*, 160(14):144117, 04 2024.

[70] Andreas Jechow, Michael Seefeldt, Henning Kurzke, Axel Heuer, and Ralf Menzel. Enhanced two-photon excited fluorescence from imaging agents using true thermal light. *Nature Photonics*, 7(12):973–976, December 2013.

[71] Yujiang Qu and Surendra Singh. Photon correlation effects in second harmonic generation. *Optics Communications*, 90(1):111–114, 1992.

[72] Kirill Yu. Spasibko, Denis A. Kopylov, Victor L. Krutyanskiy, Tatiana V. Murzina, Gerd Leuchs, and Maria V. Chekhova. Multiphoton effects enhanced due to ultrafast photon-number fluctuations. *Phys. Rev. Lett.*, 119:223603, Nov 2017.

[73] R. L. Fork, O. E. Martinez, and J. P. Gordon. Negative dispersion using pairs of prisms. *Opt. Lett.*, 9(5):150–152, May 1984.

[74] Tian Li, Fu Li, Charles Altuzarra, Anton Classen, and Girish S. Agarwal. Squeezed light induced two-photon absorption fluorescence of fluorescein biomarkers. *Applied Physics Letters*, 116(25):254001, 06 2020.

[75] Sophie de Reguardati, Juri Pahapill, Alexander Mikhailov, Yuriy Stepanenko, and Aleksander Rebane. High-accuracy reference standards for two-photon absorption in the 680-1050 nm wavelength range. *Optics Express*, 24(8):9053–9066, Apr 2016.

[76] Takafumi Ono and Holger F. Hofmann. Effects of photon losses on phase estimation near the heisenberg limit using coherent light and squeezed vacuum. *Phys. Rev. A*, 81:033819, Mar 2010.

[77] M. S. Kim, F. A. M. de Oliveira, and P. L. Knight. Properties of squeezed number states and squeezed thermal states. *Phys. Rev. A*, 40:2494–2503, Sep 1989.

[78] R. Loudon. *The Quantum Theory of Light.* Clarendon Press, Oxford, second edition, 1983.